Physical Properties of Solids-

Structural and Electronic Structure Study of Semiconducting Alloys and Superlattices

A

THESIS

Submitted to the University of Allahabad
for the degree of

DOCTOR OF PHILOSOPHY
in
PHYSICS

by

REKHA SRIVASTAVA
M.Sc.

Under the Supervision of

Prof. Bal K. Agrawal
D.Sc., F. N. A.
Department of Physics
University of Allahabad, Allahabad

DEPARTMENT OF PHYSICS
UNIVERSITY OF ALLAHABAD
ALLAHABAD-211002 INDIA

JULY 2002

CERTIFICATE

This is to certify that the thesis entitled "***Physical Properties of Solids, Structural and Electronic Structure Study of Semiconducting Alloys and Superlattices",*** is a piece of research work done by Ms. Rekha Srivastava, under my guidance and supervision. The candidate ***Ms. Rekha Srivastava***, has fulfilled all the requirements for the ***Degree of Philosophy in Physics*** of the University of Allahabad, Allahabad, INDIA.

Bal Krishna Agrawal

(Prof. Bal K. Agrawal)

Supervisor 4.7.2002

Acknowledgements

It is with great pleasure and deep sense of gratitude that I take this opportunity to express my most sincere thanks to ***Prof. Bal K. Agrawal, D.Sc. F. N. A.*** for his able guidance and counsel and inspiring supervision through out the tenure of the present investigations. My research work is no doubt is the result of constant support and invaluable guidance of *my Guide* ***Prof. Bal K. Agrawal***. He always encouraged me all the time. I cannot forget his support which he gave me during my illness.

I am also grateful to ***Prof. G. K. Pandey,*** Head of the Physics Department for providing me necessary research facilities available in the department.

It is a special pleasure to thanks to ***Dr. S. Agrawal,*** Sineor Scientific Officer for her cheerful cooperation and assistance in developing the computer programme for the present investigation. I would remain grateful to ***Dr. P. S. Yadav*** for very helpful discussion. I am indebted to ***Dr. Pankaj Srivastava,*** a R. A. of our group for his cooperation in many ways in completion of the present work. My thanks are due to ***Mr. Sanjai Singh***, a Research Scholar of our group for his encouragement and suggestions. All the members of the ***Condensed Matter Physics Research Laboratory*** provided all possible help and cooperation during every stage of the research work which enabled me to complete this thesis.

The fellowship and financial assistance was provided to me by UGC, New Delhi for which I am grateful.

Thanks are also to ***Mrs. P. Chatterjee, Mr. L. Shukla , Mr. G. Singh*** and all the other members for their help in different ways.

I would remain ever grateful to my respected parents, my husband E***r. Ashish***, my brothers, ***Abhay & Amit*** along with other family members for their patience and constant encouragement to produce good result in my research work.

I shall always remain thankful to ***Almighty*** who inspired me and gave the strength to complete my research work.

Rekha Srivastava

(REKHA SRIVASTAVA)

Contents

List of Publications

[1]. ***Ab-initio*** **Study of anomalous band-gap bowing in $GaAs_{1-x}N_x$ alloys**

Bal K. Agrawal, P. S. Yadav, Rekha Srivastava, and Savitri Agrawal
Journal Of Physics: Condensed Matter, Vol. 10 (1998) p 4597.

[2] **Anomalous band gap bowing in $AlAs_{1-x}N_x$ alloys**

Rekha Srivastava, Bal K. Agrawal and P. S. Yadav, Solid State Communications 109 (1999) 383.

[3] **First –principles calculation of valence band offset and the interface sates in GaAs/GaN (001) superlattices**

Bal K. Agrawal, Savitri Agrawal and Rekha Srivastava, Surface Science 424(1999) 232.

[4] **Effect of atomic relaxation on the valence band offset and the interface states in ZnS/ZnSe (110) superlattices**

Bal K. Agrawal, Savitri Agrawal and Rekha Srivastava, Surface Science 431(1999) 84.

[5] **A First principles study of structural and electronic properties of $Ga_{1-x}Al_xAs$ alloys**

Rekha Srivastava, P. S. Yadav, S. Agrawal, Bal K. Agrawal and S. Kumar, Solid State Communications 118 (2001) 479.

[6] **Valence band offsets and interface states of polar GaN/SiC (001) 2X2 superlattices**

Bal K. Agrawal, Savitri Agrawal, Rekha Srivastava and Pankaj Srivastava
Physica E 11(1) 2001 , 27-34

Guide to Tables

Guide to Figures

Chapter-I

INTRODUCTION

INTRODUCTION

The electronics industry is the largest manufacturing industry in the world and by far the fastest growing one. It is currently estimated to be in the range of $900 billion industry. The semiconductor portion of the electronics industry is the backbone of a country. In order to have a fast industrial development and export capacity, a country need to have a vibrant semiconductor industry.

The semiconducting alloys have drawn the attention in the recent years for the study of their electronic and physical properties due to their potential applications in the opto-electronic devices. For example, III-V nitride semiconductors are potentially useful as high frequency microwave and short-wave length electroluminescent devices.

The recent surge of activity in wide band gap semiconductors has arisen from the need for electronic devices capable of operation at high power levels, high temperature and caustic environments and separately a need for optical materials, especially emitters, which are active in the blue and UV wave lengths. In the optical device arena, the ever-increasing need for higher density optical storage and full color display technologies are driving researchers to develop wide band gap semiconductors emitter technologies which are capable of shorter wavelength operations.

In the area of light communications using the facility of band gap engineering available in the semiconducting alloys, one can develop the necessary photodetectors and lasers suitable for light wave systems operating in the 1.3 - 1.6 μ wavelength region. The structural and electronic properties of semiconductors can be manipulated over wide ranges through the control of impurities and the alloys of semiconductors with different concentration of constituents and other imperfections.

Most of the electronic properties are controlled by the localized electronic states lying in and around the fundamental energy gap of a semiconductor. In general, there are three types of electronic localized/resonance states in a material; deep states and impurity states. Out of these tail states lie next to the electronic energy band edges and affect carrier mobilities. These states may originate either from the usual dopants or from the conformational variations like angular distortions of the network and similar other fluctuations.

Structural defects are believed to be always present in greater or lesser concentrations. The major defects are the dangling or broken bonds being incorporated in the network nearly of the order of one per 10 atoms leading to energy levels lying deep into the fundamental gap.

Semiconductor interfaces and surfaces are a fascinating research topic because it includes physics, chemistry as well as electronic device aspects during the recent past, this field experienced dramatic developments from both the experimental and theoretical side. New experimental tools, as well as advanced theoretical approaches provoked a more profound understanding of semiconductor interface properties.

The junction between dissimilar semiconductors has long attracted the attention of researchers in solid state physics and electronics. The additional degree of freedom provided by the two materials in the semiconductor heterojunction offers opportunities to pursue new phenomenon and applications not possible with homogeneous media.

If the characteristic width of the wells is comparable to the wavelength of the electrons, a series of quantum states will be formed in the wells, where the electrons tend to be confined. Three basic configurations are generally used: single quantum well sandwiched between two barriers, the multiple quantum well or the superlattice.

The investigation of Quantum Well Structures (QWS) and related interfacial problems is a unique field with profound implications for basic scientific study and the understanding of materials.

The Royal Swedish Academy of Sciences has awarded the 2000 Nobel Prize in Physics to *Zhores Alferov*, Director of the Ioffe Physico-Technical Institute in Saint Petersburg, Russia; *Herbert Krormer* of the University of California, Santa Barbara, "for developing semiconductor hetero-structures used in high speed and opto-electronics".

Intensive experimental and theoretical investigations of Quantum Well Structures and Superlattices are also being made to answer fundamental questions associated with possible effects of the breakdown of periodicity normal to the surface on the elementary excitations of the systems.

The electronic properties of contacts between two semiconductors are determined by an alignment of the band structures across the interface and the possible existence of space charge layers at abrupt interface. Band edge discontinuities are established within a few atomic layers while the regions of band bending depend on the doping profiles on both sides of the contact and will extend over a few Debye lengths.

The first model of the band structure alignment at semiconductor-semiconductor contacts neglected the existence of interface states at all. In *Gedanken* experiments, semiconductor interface may be formed by approaching two semiconductors until an intimate contact is reached. If no electronic surface and interface states are considered, the vacuums levels of both semiconductors will align. The conduction band discontinuity then results as the difference of the electron affinities of the semiconductors on the left and the right side of the contact.

Near infrared semiconductor lasers and LED's are now commonplace. The telecommunications industry has blossomed with the development of long wave length InGaAsP heterostructure lasers lattice matched to InP substrates, for use with

optical fibers. The recent development of AlGaInN devices has produced blue and violet heterostructure lasers and LEDs.

Heterostructures are also prevalent in transistors. In addition to heterojunction bipolar transistors (HBTs), field- effect devices with very high mobilities have been developed. For high electron – mobility transistors (HEMTs), these heterostructures which use dopants in high band gap materials to generate a high density two dimensional electron gas (2DEG) with low defects in quantum well, can operate at high frequencies and with low noise. Such devices, primarily of GaAs-GaAlAs and GaAs-InGaP but increasingly of Si-Ge alloys can be found in cell phones and satellite receivers.

The experimental determination of band offsets in semiconductor heterojunction continues is of great importance for a discussion of the relative merits of the various theoretical approaches in the approximation that these describe an ideal heterojunction which contributes to the band offset [1].

Considerable progress in the prediction of band offset has been obtained by theoretical models which are based on parameters of the bulk constituents e.g., a specific mid gap energy which serves as the lineup reference level. A more rigorous treatment of the electronic structure of a semiconductor heterojunction has been achieved through self -consistent band structure calculations for a crystal involving two slabs of the two constituents which form a sort of multiple quantum well by repeating the slabs in a supercell arrangement. The self -consistency takes into account the charge transfer across the heterojunction and possible interface dipoles. This is of particular importance since the inclusion of these interface dipoles has been a weak point in many models [2-4].

On the experimental side, photoemission experiments have provided in reliable data for the most important parameter of a heterojunction, the valence band offset (VBO) ΔE_v , and have also produced interesting data concerning the chemical reactions which take place upon interface. However, many comparisons between theory and experiment still refer to the data by *Katnani and Margaritondo*

[5] which are derived from the measurement performed on the heterojunctions. In 1974, *Dingle and co-workers* [6] measured the 2K infra red absorption spectra seen from a number of single, double and multiple quantum well heterostructures. Different spectroscopic methods have been used to measure the heterojunction offsets in the superlattices systems; photoelectron spectroscopy on single heterojunction [7] and IR absorption or photoluminesence excitation spectroscopy (PLE) on single and MQW heterostructures [6,8-10]. Valence band offset and interface formation in ZnTe/GaSb (110) and CdS/InP (110) are studied by photoemission using synchrotron radiation [11-12], Auger electron spectroscopy (AES) and low energy electron diffraction (LEED). *Chen et al* (1991) and *Leroux et al* (1993) measured the band offset of GaAs/InGaP under high pressure, low temperature photoluminescence performed on single and MQW grown by metal organic molecular beam epitaxy MBE [13-14]. The electronic structure of zinc blende – GaN films grown on GaAs (100) and (110) by plasma-assisted molecular beam epitaxy (MBE) [15-17], metal-organic vapour phase epitaxy [18] and similar techniques has been investigated.

On theoretical side, semiempirical tight binding calculations have predicted formation energies for various nonpolar AlN/SiC interfaces [19] unreconstructed hexagonal GaN/SiC (0001) interfaces [20] and for the reconstructed polar GaN/SiC (001) interface [21]. Empirical tight -binding approximation is used to calculate the transmission and reflection coefficients of carriers in GaAs /GaAlAs (100) interface [22]. Self -consistent calculation of the total energy, charge density and electronic states of Ge/GaAs(100) interface has been done by *Kunc and Martin* in 1981 [23]. Band offsets at semiconductor interfaces have been obtained by a self -consistent density functional calculation using ab-initio nonlocal pseudopotential [24]. Band structure of ultrathin layered superlattices $(GaAs)_n/(AlAs)_n$ [25] has been studied by the self -consistent pseudopotential method.

Christensen in 1988 [26] calculated the valence band offset in fifteen lattice matched semiconductor heterostructures by first principles self consistent relativistic LMTO method. The valence band offset at the zinc blende AlN/GaN (110) interface was calculated self consistently by means of LMTO method using

(5+5) layer supercell [27]. The full potential linearized augumented plane wave method was used to study the electronic and structural properties of strained (ZnTe) / (CdTe) (001) superlattices by *Continenza and Massidda* [28]. Ab initio local -density functional calculations of formation enthalpies and band discontinuites of polar interface between cubic SiC(001) substrate and lattice – matched, strained zinc blende GaN orAlN has been reported [29].

Most theoretical investigations have focussed on the cohesive and electronic properties of bulk nitrides [30 - 41] whereas much less publications have dealt with nitride heterostructures. Electronic structure calculations have been performed for short period GaN/AlN superlattices in the wurtize [42-43] as well as in the zinc blende [27, 42] structure. VBO have been predicted for pseudomorphic GaN/AlN, GaN/InN and AlN/InN zinc blende and wurtzite heterostructure [27, 41].

Electronic structure for various ordered structures of alloys has been investigated by using first principles total energy calculation by *Neugebauer and Van de Walle* [44]. *Rubio and Cohen* performed a quasiparticle study of the ordered alloys of III-V semiconductor [45]. Photoluminescence and absorption experiments on Ga $As_{1-x}N_x$ grown by plasma assisted metalorganic chemical vapor deposition, show a systematic redshift of the band edge luminescence with increasing N content [46].

We use a first-principles full-potential self-consistent linear-muffin-tin orbital (**FP-LMTO**) method to study the structural and electronic properties of complex systems. In **Part I**, we investigated the semiconducting alloys and in **Part II**, Superlattices or heterojunctions.

In **chapter II**, we discuss the theoretical aspects and the method used in the present work. The various experimental techniques, which are used for the measurement of electronic structure, are discussed in **chapter III**. In chapters **IV, V and VI** of Part **I** we present our results of the electronic structure of semiconducting alloys. **Part II** contains the chapters **VII, VIII** and **IX** where we

study the electronic and structural properties of Superlattices. Finally, the main conclusions are included in **chapter X**.

All the calculations in the present thesis were performed on **HP-735** and **HP-MPS-10 Cluster** computer systems available in our **Condensed Matter Physics Research Laboratory.**

Chapter-II

Method

METHOD

2.1 ELECTRONIC STRUCTURE:

The theory of electronic states in infinite crystals has been of great value for a better understanding of the chemical and physical properties of solid state materials. The calculation of the electronic structure of a solid is fairly complicated as there are 10^{23} electrons all interacting with one another, and with the same number of ions. Electrons at the microscopic level govern the behavior of these materials, and that one may obtain a surprisingly good description of many macroscopic properties in terms of the stationary states of the electronic systems.

The present motivation in the solid state theory is to devise methods for calculating one-electron energies and wave functions with speed and accuracy. So the method should be applicable to solids having atoms from all parts of the periodic table. It should also have potentiability for its application to realistic structures like crystals with many atoms per unit cells, crystals with surfaces, interfaces, impurities, cluster of atoms, amorphous systems etc.

2.2 VARIOUS METHODS:

The applications of the pseudopotential calculations has its own limitations. The APW and KKR methods have proven highly accurate for Fermi surface calculations but they are numerically unwieldy and lack transparency. The linear combination of atomic orbitals (**LCAO**) method is cumbersome when used as a first-principles method and, when parametrized, it has either too many parameters or the wave functions are ill-defined. The LCAO schemes using Gaussian orbitals have some computational advantages but they need at least twice as many basis functions as the KKR method. The first-principles pseodopotential method meets the requirement but this method is limited to treating sp- like valence and conduction electrons. Computationally this can be remedied by the addition of localized orbitals to the plane wave basis set but such a hybrid scheme is neither

elegant nor in accord with chemical and physical intuition based up on the smooth trends observed for the band structures through the periodic table; s-, p-, d-, and f-electrons ought to be treated on the same footing. Moreover, about three quarter elements of the periodic table have quite strong pseudopotentials and the remaining one quarter of the atoms have weak pseudopotentials to permit expansion of the pseudo wave functions in plane waves. Even for these one quarter atoms, the problem of slow convergence of the plane wave basis limits the choice of the number of atoms in the supercell.

The Linear Muffin Tin Orbital (LMTO) method is only one of many techniques which may be used to solve the one – electron problem in crystalline solids. However, the method does combine a certain number of very convenient features which makes it one of the most desirable techniques currently available.

The LMTO method is cast in the form of a standard algebraic eigenvalue problem and therefore has the speed needed in the self-consistent calculations. Although the method is an approximately one, it still has the accuracy required. LMTO method employs the same type of basis functions for all the elements and is physically transparent and may be used at several levels of approximation. Hence the LMTO technique may be applied to problem ranging from complicated self-consistent calculations in crystals with many atoms per unit cell.

The electrons are light particles which in their motion immediately follow the much heavier nuclei. This means that the nuclei and the electrons to a good approximation may be treated separately. One may first solve for the electronic structure and then , at the later stage , use the energy of the electronic ground state obtained as a function of nuclear positions as a potential energy for the motion of nuclei. The one electron approximation describes each electron as an independent particle moving in the mean field of other electrons plus the field of nuclei.

The mean field is made up of the electrostatic field from the electron charge cloud plus the corrections for the exchange correlation. The full many-body

Schrodinger equation is replaced by an effective one-particle equation `*Kohn and Sham* [47], *Lang* [48];

$$-\frac{1}{2}\nabla^2\varphi_i(\vec{r})+\left(\sum V_{ion}(\vec{r}-\vec{r}_1)+V_H(\vec{r})+V_{xc}(\vec{r})\right)\varphi_i(\vec{r}) = \varphi(\vec{r})\varepsilon_i(\vec{r}) \qquad \text{(i)}$$

The electron feels the potential due to the ions V_{ion}, the **Hartree potential** $V_H(\vec{r})$ which is the electrostatic potential due to the smeared-out charge density of all the other electrons, and the exchange-correlation potential $V_{xc}(\vec{r})$ to allow for the fact that the electrons actually move in a correlated way. The ground state charge density is given by a sum over occupied states;

$$\rho_0(\vec{r}) = 2\sum_{\substack{occupied\\ i}} |\varphi_i(\vec{r})|^2 \qquad \text{(ii)}$$

The ground state energy is

$$E_0 = 2\sum_{\substack{occupied\\ i}} \varepsilon_i - \frac{1}{2}\int d\vec{r}\, V_H(\vec{r})\,\rho_0(\vec{r}) - \int d\vec{r}\, V_{XC}(\vec{r})\,\rho_0(\vec{r}) + E_{XC} \qquad \text{(iii)}$$

The first term is the sum of one-electron energy levels; the second one is the electrostatic Hartree interaction subtracted to avoid double counting and the exchange-correlation energy E_{XC} explicitly added. The charge density and effective potentials must be determined self-consistently. The Hartree potential is given by;

$$V_H(\vec{r}) = \int d\vec{r}'\, V(\vec{r}-\vec{r}')\,\rho_0(\vec{r}') \qquad \text{(iv)}$$

The exchange-correlation potential depends on all the details of the charge density, and it is the functional derivative of E_{XC} with respect to ρ_0;

$$V_{xc}(\vec{r}) = \frac{\delta E_{xc}\left[\rho_0(\vec{r})\right]}{\delta\rho_0(\vec{r})} \qquad \text{(v)}$$

One employs the **local density approximation** *Hohenberg and Kohn* [49]. In a Hartree-Fock calculation one neglects correlation and also the method is very laborious because the exchange field depends in a complicated way on the one electron states in question.

In solids the mean field is much simpler and is a state dependent potential which can be constructed only from the electron density alone and which includes also the important effects of both exchange and correlation through the use of accurate many body calculations for a simple model systems. This is the Jellium model whose nuclei are smeared out to a uniform background.

Assuming the contributions from exchange and correlation to the total energy as ε_{xc} (ρ) per electron in a jellium of density n, the contribution in the real system is expressed as

$$E_{xc} \approx \int d\vec{r}\ \rho_0(\vec{r})\varepsilon_{xc}(\rho_0) \qquad \text{(vi)}$$

where $\varepsilon_{xc}(\rho_0)$ is the exchange-correlation energy per electron of an infinite homogeneous electron gas with local density ρ_0 . This is called the local approximation density functional theory. This local density approximation works surprisingly well even for isolated atoms and small molecules where the calculated energy of the ground state and the low lying excited state are found to be more accurate as compared to the Hartree-Fock method. Then V_{xc} becomes

$$V_{xc}(\vec{r}) = \frac{d}{d\rho}\left\{\rho\ \varepsilon_{xc}(\rho)\right\}\Big|_{\rho=\rho_0} \qquad \text{(vii)}$$

The effective single-particle approach can be rigorously justified for the ground state energy and the charge density using density functional theory *Hohenberg*

and Kohn [49]; the method is useful because the local density approximation for E_{xc} and V_{xc} works well, even when the electron density varies rapidly as in molecules *Gunnarsson et al* [50] and at a surface *Lang and Sham* [51], *Langreth and Perdew* [52].

In a self-consistent calculation, a new field is obtained by solving Poisson's equations for the nuclear point charges screened by the electronic charge density given by equation (ii) and adding to it the corrections for exchange correlation. After taking a weighted sum of the old and the new field, the calculation is repeated and iterated until the input and output fields are consistent.

The interpretation of the energy location of conduction band states is somewhat complicated because of the limitation of the LDA theory where the on-site correlation effects have been ignored and the calculated energies of the states above the valence band region are lower. A deficiency of the local density theory is that the calculated value of the fundamental energy gap is smaller than the experimental one. This arises from the fact that the excitation energies of these systems are not given by eigen values of the *Kohn-Sham equations* [53] and [54]. There are several attempts [55, 57] for calculating the electron self – energies Σ. In one of them namely, the GW approximation, the quasi-particle energies have been calculated which lead to wide band gaps somewhat nearer to the experimental values. This self-energy is seen to be a non-local energy dependent effective potential. This is beyond the scope of present work. *Hybertsen and Louie* [58] presented a first-principles theory of quasiparticle energies in semiconductors. They evaluated the self-energy operator in the GW approximation. The self-energy includes the effects of exchange and correlation on single-particle energies and is taken to be the first term in an expansion in terms of the screened Coulomb interaction and electron Green's function.

2.3 LINEAR METHODS:

The linear methods of band theory employ energy-independent basis functions derived from the partial waves and their first energy derivatives obtained

within the Muffin – Tin approximation to the potential. When applied to a MT potential they use logarithmic derivative parameters and provide solutions of arbitrary accuracy in a certain energy range. The linear methods thus combine the desirable features of the methods employing fixed basis functions with those of the partial-wave methods and they have none of the drawbacks. This is particularly true for the linear-muffin-tin orbitals (**LMTO**). Usually in the application of the standard LMTO method, an atomic sphere approximation (ASA) is used to make it efficient. However, this LMTO_ASA method suffers from several disadvantages. (i) It neglects the symmetry breaking terms by discarding the non-spherical parts of the electron density. (ii) The method discards the interstitial region by replacing the muffin-tin spheres by the space filling Wigner spheres. (iii) It uses spherical Hankel functions with vanishing kinetic energy only. The linear APW (LAPW) method is less transparent than the LMTO method because it is based on a plane wave representation and therefore needs more basis functions. Thus, the most economical basis functions are seen to be the linear-muffin-tin orbitals.

In the past, the linear-muffin-tin-orbital (LMTO) method *Anderson* [59], *Skriver* [60] for solving the one-particle Schrodinger equation self-consistently has become very popular for the calculation of the electronic structure of crystalline systems, and its modifications have been applied successfully to molecules *Gunnarsson & Harris* [50].

2.4 THE LMTO METHOD:

2.4(a) PARTIAL WAVES FOR A SINGLE MUFFIN-TIN:

An energy band structure calculation consists of the eigenvalues of the one-electron Schrodinger equation

$$\left[-\nabla^2 + V(\vec{r})\right] \Psi_j(k,\vec{r}) = E_j(k)\, \Psi_j(k,\vec{r}) \qquad (1)$$

for a single electron moving in the local potential $V(\vec{r})$. The form of the equation and its solution hinge on the symmetries of the Hamiltonian $\left[-\nabla^2 + V(\vec{r})\right]$, which in turn, is governed by $V(\vec{r})$.

The crystal potential $V(\vec{r})$ appearing in the Schrodinger equation is approximated by a so called muffin-tin potential which is defined to be spherically symmetric within spheres of radius S_{MT} and to have a constant value V_{MTZ} at S_{MT}. The muffin-tin is zero, in the interstitial region between the spheres as shown in Fig. 2.1. This kind of potential is designed to facilitate matching of wave functions from cell to cell through the assumption that the electrons propagate freely between spheres with a constant wave number $\kappa = \sqrt{E - V_{MTZ}}$. This assumption is valid only if the wavelength $2\pi/\kappa$ is large compared to the thickness of the interstitial region, i.e., the distance $S_{MT} - S_E$.

For simplicity we consider a crystal with one atom per primitive cell, and within a single muffin-tin well. We define the potential as

$$V_{MT}(\vec{r}) = \begin{cases} V(\vec{r}) - V_{MTZ} & \vec{r} \le S_{MT} \\ 0 & \vec{r} \ge S_{MT} \end{cases} \qquad (2)$$

Here $V(\vec{r})$ is the spherically symmetric part of the crystal potential. The Hamiltonian minus the energy for a system of superimposed muffin-tin wells is

$$H - E = -\nabla^2 + \sum_{\vec{R}} V_{MT}\left(\left|\vec{r} - \vec{R}\right|\right) - \kappa^2 \qquad (3)$$

where the sum extends over the crystal, and the kinetic energy κ^2 in the interstitial region is defined by

$$\kappa^2 \equiv E - V_{MTZ} \qquad (4)$$

We now seek the solutions of Schrodinger's differential equation

FIG. 2.1 The muffin-tin approximation:
(a) The unit cell, the muffin-tin sphere of radius S_{MT} and the escribed sphere of radius S_E.
(b) The radial wave function.
(c) The muffin-tin part of the crystal potential V(r).
(d) The muffin-tin potential $V_{MT}(r)$.

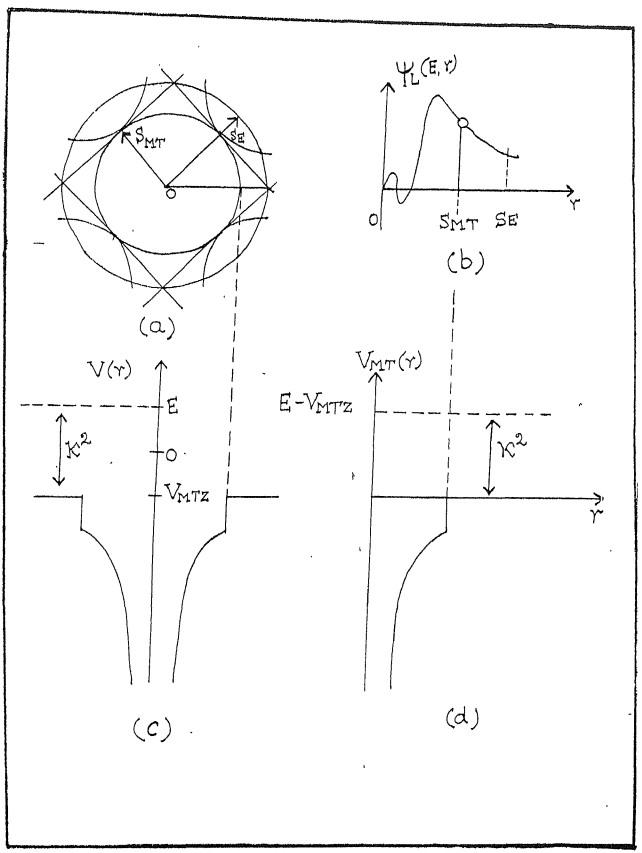
S_{MT}
SE
(a)
$\psi_L(E,r)$
0
S_{MT}
SE
r
(b)
V(r)
E
K^2
0
V_{MTZ}
(c)
$V_{MT}(r)$
$E-V_{MTZ}$
K^2
r
(d)

$$\left[-\nabla^2 + V_{MT}(\vec{r}) - \kappa^2\right] \Psi_L(E,\vec{r}) = 0 \qquad (5)$$

for all values of κ^2, i.e., both in the continuum and in the bound-state regime. In this case the spherical symmetry extends throughout all space and the wave functions are

$$\Psi_L(E,\vec{r}) = i^l Y_l^m(\vec{r}) \Psi_l(E,\vec{r}) \qquad (6)$$

where the l, m quantum numbers have been combined into one subscript L. For reasons of notation we have included a phase factor i^l, and the spherical harmonics $Y_l^m(\vec{r})$. Inside the muffin-tin well the radial part $\Psi_l(E,\vec{r})$ must be regular at the origin in order to be normalisable. It is obtained by numerical integration of the radial Schrodinger equation,

$$\left[-\frac{d^2}{d\vec{r}^2} + \frac{l(l+1)}{\vec{r}^2} + V_{MT}(\vec{r}) - \kappa^2\right] \vec{r}\, \Psi_l(E,\vec{r}) = 0 \qquad (7)$$

In the region of constant potential the solutions of equation (5) are spherical waves with wave number κ, and their radial parts satisfy equation (7) with $V_{MT}(\vec{r}) = 0$, i.e.

$$\left[-\frac{d^2}{d\vec{r}^2} + \frac{l(l+1)}{\vec{r}^2} - \kappa^2\right] \vec{r}\, Y_l(\kappa,\vec{r}) = 0 \qquad (8)$$

This well known **Helmholtz wave equation** has two linearly independent solutions which may be taken to be the *spherical Bessel* $j_l(\kappa,\vec{r})$ and *Neumann* $n_l(\kappa,\vec{r})$ functions, respectively.

2.4(b) MUFFIN-TIN ORBITALS:

In the interstitial region the potential is rather flat and the absolute value of the kinetic energy, $\left| E - V(\vec{r}) \right|$, is fairly small. If the interstitial region has a relatively small volume then it is reasonable to choose basis functions whose envelopes are solutions of the wave equation

$$\left[\nabla^2 + \kappa^2\right] \chi^i (\kappa,\vec{r}) = 0 \qquad (9)$$

with a constant numerically small kinetic energy, κ^2. We know that kappa must be independent of energy and hence, that the eigenvalue equation is linear in energy. This is not so in the KKR partial-wave method where the choice $\kappa^2 \equiv E - V_{MTZ}$ is made.

The muffin-tin orbitals (MTOs) are angular-momentum eigenfunctions centered at the sphere-sites R, i.e.,

$$\chi_{RL} (\vec{r}) = \chi_{Rl} (\vec{r})\, Y_L (\vec{r}) \qquad (10)$$

and the enevelope functions, χ^i_{RL} satisfy eqn. (9). The radial envelope function, χ^i_l is singular at the origin and well behaved at infinity. This means that for $\kappa^2 < 0$, chi must be that solution of eqn. (9) which decays asymptotically as $\vec{r}^{-1} \exp\left(-|\kappa|\vec{r}\right)$ and for $\kappa^2 = 0$, chi must be proportional to $\vec{r}^{-l-1}$. Finally for $\kappa^2 > 0$, *chi* can be any linear combination of *spherical Bessel* and *Neumann* functions and these decay asymptotically as $\vec{r}^{-1} \exp\left(i\kappa\vec{r} + in\right)$.

The linear MTO is obtained by augmenting the envelope function inside its own and from all other spheres. For the latter purpose we need to expand *chi* about the other sites. Since *chi* is regular, except at its own site R, it must have an expansion about site R′ of the form

$$\chi^{i}_{RL}\left(\kappa,\underline{r}_{R}\right) = \sum_{L'} j_{l'}\left(\kappa\ r_{R'}\right) i^{l'}\ Y_{L'}\left(\hat{r}_{R'}\right) S_{R'\ L',R\ L}\left(\kappa\right) \tag{11}$$

where j is that solution of the radial wave equation which is regular at the origin. The expansion is valid for $r_{R'} < \left|\underline{R} - \underline{R'}\right|$. The coefficients S are the so called KKR structure constants whose traditional normalization is such that eqn. (11) is correct when we choose

$$\chi^{i}_{RL}\left(\kappa,\vec{r}\right) = \kappa\ \eta_{l}\left(\kappa,\vec{r}\right) i^{l} \tag{12}$$

It may be shown that

$$S_{R'\ L',\ RL}\left(\kappa\right) = 4\pi \sum_{l''} C_{LL'L''}\ \kappa\ \eta_{l''}\left(\kappa\ R''\right) i^{-l''}\ Y^{*}_{L''}\left(\hat{R}''\right) \tag{13}$$

where

$$\underline{R''} = \underline{R} - \underline{R'}$$

and

$$C_{LL'L''} \equiv \int Y_{L}\left(\hat{r}\right)\ Y^{*}_{L'}\left(\hat{r}\right)\ Y_{L''}\left(\hat{r}\right)\ d^{2}\hat{r} \tag{14}$$

are the so called **Gaunt coefficients**. The matrix eqn.(13) is Hermitian. The major advantage of choosing the orbitals to be solutions of the translationally invariant wave equation (9) rather than the atomic orbitals is the simplicity of the expansion eqn. (11). The radial behaviour is $j_{l'}\left(\kappa,\vec{r}\right)$ regardless of the distance $\underline{R} - \underline{R'}$ and for a crystal one can perform the lattice-summations on the structure constants only as given below

$$S^{\underline{k}}_{Q'L',\ QL} = \sum_{T\neq 0} e^{i\underline{k}\underline{T}}\ S_{Q'L',\ (Q+T)L} \tag{15}$$

2.4(c) ENERGY-INDEPENDENT MUFFIN-TIN-ORBITALS:

In a solid their appears a contineous band states and therefore the entire energy dependence $\phi(E,\vec{r})$ should be supplied by the tails of the orbitals from the other atoms. This is achieved by augmenting the tails by the energy derivative function

$$\dot{\phi}(\vec{r}) \equiv \left[\partial\phi(E,\vec{r}) \Big/ \partial E \right]_{E=E_v} \tag{16}$$

evaluated at some arbitrary energy E_v . This works well because of the following Taylor series

$$\phi(E,\vec{r}) = \phi(\vec{r}) + (E-E_v)\,\dot{\phi}(\vec{r}) + o(E-E_v) \tag{17}$$

with

$$\phi(\vec{r}) \equiv \phi(E_v,\vec{r}) \text{ and } \dot{\phi}(\vec{r}) \equiv \partial\phi(E,\vec{r}) \Big/ \partial E \,|_{E_v} \tag{18}$$

is well converged in the energy range of interest after the two first, linear terms.

The linear LCMTO equations, which refer to as the LMTO equations may be written in the basis of the energy-independent muffin-tin orbitals. This involves some different integrals, which may be evaluated by means of the matrix elements. The LMTO secular matrix may be written in the form $\underline{\underline{H}} - E\underline{\underline{O}}$, which corresponds to the generalised eigenvalue problem

$$\sum_{L} \left(H^{k}_{L'L} - E^{jk} O^{k}_{L'L} \right) \alpha^{jk}_{L} = 0$$

and which may be solved by efficient numerical techniques to give the eigen values and eigenvectors. Although we use the LMTO method in conjunction with a

cellular potential which is spherically symmetric inside the atomic sphere but not flat in any region. In connection with a muffin-tin potential the simplest procedure is to fix κ^2 at zero and to integrate the Schrodinger equation out to the boundary of the atomic sphere.

2.5 FP-LMTO METHOD:

In full- potential linear muffin tin orbital (FP-LMTO) method, the interstitial-potential matrix elements are expressed as,

$$V^{I}_{vL,v'L'} = \int \chi^{*}_{vL}(x)\, V_I(x)\, \chi_{v'L'}(x)\, dx \qquad (19)$$

where I is the interstitial region, V_I is the interstitial potential and χ_{vL} is a LMTO envelope function centered at site v with angular momentum L.

A related problem is to bring into a tractable form the output charge density in the interstitial region, which is given as a linear combination of the products $\chi^{*}_{vL}\, \chi_{v'L'}$. It seems reasonable that the separate contributions can be represented in a similar way, with a higher angular-momentum cutoff because they vary more strongly. Thus, coefficients $A^{vL,v'L'}_{\mu K\alpha}$ are sought with the property that, throughout the interstitial region,

$$\chi^{*}_{vL}(x)\, \chi_{v'L'}(x) \approx \sum_{\mu,\, K,\, \alpha} A^{vL,v'L'}_{\mu K\alpha}\, H_{\mu K\alpha}(x) \qquad (20)$$

with

$$H_{\mu K\alpha}(x) = h_k\left(i\lambda_\alpha \left|x - R_\mu\right|\right) Y_K\left((x - R\mu)/\left|x - R_\mu\right|\right), \qquad (21)$$

i.e. the $H_{\mu K\alpha}$ are of the same general form as the LMTO envelope functions themselves. The latter are k-dependent Bloch sums of Hankel functions whose

kinetic energy is usually chosen to be zero and the $H_{\mu K\alpha}$ are replaced by periodic Bloch sums.

Equation (20) is the central relation of the present approach. When equation (20) is substituted in equation (19), the matrix element then reduces to a linear combination of integrals of the functions $H_{\mu K\alpha}$ times the interstitial potential. It is also assumed that the interstitial potential itself is expanded in functions of the type of equation (21). This is done for self-consistent molecular calculations because of the fact that the Poisson equation can be solved analytically in the Hankel-function basis. The interstitial integral has now been expressed as a linear combination of integrals of products of pairs of Hankel functions i.e. the three center integral has been reduced to a sum of two-center integrals. By using Gauss's theorem and the fact that the $H_{\mu K\alpha}$ are eigenfunctions of the Laplace operator, we express the two-center integrals as surface integrals over the spheres. Thus, they are easy to calculate by means of standard structure-constant expansions. Once an accurate enough expansion of the form (20) is available, the interstitial potential matrix elements can be evaluated.

One of the difficult step in this method is the determination of the coefficients in the expansion of equation (20). For the case that the interstitial region is not too large we can introduce extra empty spheres for the loosely packed systems. Then every point in the interstitial region lies close to one or more atomic spheres. This together with the fact that the products are smooth functions, suggests that a suitable representation can be obtained by interpolating between the surfaces of the spheres. This can be done by adjusting the coefficients in equation (20) until the best fit of the values and slopes of the right-hand side to the values and slopes of the product is obtained on all spheres simultaneously.

The one-center expansion near site μ is

$$\chi_{\nu L}(x) = \sum_{K} \left\{ a_{\mu K}^{\nu L} H_{\mu K}(x) + b_{\mu K}^{\nu L} J_{\mu K}(x) \right\} \qquad (22)$$

where $H_{\mu K'}$ is given as in equation (21) and $J_{\mu K'}$ is defined similarly for the spherical Bessel function, both at the same kinetic energy as $\chi_{\nu L}$. The final result for the interstitial matrix element then is

$$\int \chi^*_{\nu L}(x) V_I(x) \chi_{\nu' L'}(x)\, dx = \sum \Big\{ a^{\mu L^*}_{\mu K} D^{HH}_{\mu K K'} a^{\nu' L'}_{\mu K'} + a^{\mu L^*}_{\mu K} D^{HJ}_{\mu K K'} b^{\nu' L'}_{\mu K'} + b^{\mu L^*}_{\mu K} D^{JH}_{\mu K K'} a^{\nu' L'}_{\mu K'} + b^{\mu L^*}_{\mu K} D^{JJ}_{\mu K K'} b^{\nu}_{\mu}$$

(23)

The matrices $D_{\mu KK'}$ are all independent of k. The evaluation of the non-spherical potential terms inside the atomic spheres leads to an expression of the same form as in eqn.(22), with the $D_{\mu KK'}$ replaced by integrals which give the coupling between the augmented heads and tails on the μth sphere. Thus, once the matrices in eqn. (22) have been calculated, the corrections to the muffin-tin potential from inside the spheres and from the interstitial can be treated together. Now the full potential calculation has in this way been reduced to minimum, namely that of evaluating the effect of the non-spherical potential in the spheres. Therefore, this method for finding the coefficients in the expansion of equation (20) is suitable for self-consistent computations for fixed atomic positions.

2.6 ADVANTAGES OF LMTO METHOD:

The present method has several advantages. (i) Only a minimal basis set is required in the method, thus it enables its applications to large unit cells with high efficiency. (ii) The method treats all the elements of the periodic table in a similar manner. Thus, the atoms with a large number of core states and the metals having predominantly d- or f- character can be treated easily. (iii) As the augmentation procedure generates the correct shape of the wave function near the nuclei, it is quite accurate. (iv) The use of atom-centered basis functions belonging to the different values of the angular momentum in the method helps one to have a quite clear physical picture. (v) It fully includes the influence of the semicore states on the binding properties and the band structure of the material.

2.7 ADVANTAGES OF FP-LMTO METHOD:

It has been noted that quite reliable results could be obtained by employing a LMTO basis set if all the potential terms are determined accurately. For this, the sizes of the atomic spheres are shrunk so as to make them non-overlapping. The potential matrix elements are then split into two parts; one contribution coming from the atomic spheres and the other i.e. the atomic sphere one is easy to evaluate by expanding it in terms of the usual spherical harmonics. On the other hand, the evaluation of the interstitial contribution is quite difficult and very time consuming if done by standard techniques. Efforts have been made to find an efficient and quick way to determine the interstitial contribution. In the method used in the present work, the interstitial quantities were expanded in terms of the spherical Hankel functions. The involved three centre-integrals were expressed as the linear sum of two centre integrals. These two centre integrals involving Hankel functions can easily be evaluated analytically. The method does not employ the plane waves and is thus applicable to the periodic as well as the non-periodic systems which are so often need to be treated especially when there occur impurities, defects and the lattice distortions or atomic relaxations.

Chapter-III

Experimental Techniques

EXPERIMENTAL TECHNIQUES

The electronic structure of atoms can be studied by a number of experimental techniques. These experimental methods measuring or giving information about the electronic structure and electronic density of states may be broadly categorized as follows; methods studying (i) valence band region (ii) gap region and (iii) the conduction band region. We present below a brief description of some of the experimental techniques.

3.1 PHOTOEMISSION SPECTROSCOPY:

Photoemission spectroscopy (PES) is based on the phenomenon of photoemission, which was detected by *Hertz* in 1887. In 1905, *Einstein* proposed the concept of "photon" and explained the photoelectric effect using the following simple formula

$$E_k = h\nu - E_B - W_0,$$

where E_k is kinetic energy of photoelectron, $h\nu$ is the photon energy, E_B is binding energy of the electron, and W_0 is work function of the material. Though the main point of this formula is that the energy of light is quantized, in view of experiment, this also says that if we use this "photoelectron effect", we can know the electron energy state inside the material. That is, we can know the electronic structure of the matter. **Fig. 3.1** exhibits the ingredients of a modern PE experiment. The light source is either a gas discharge lamp, an X-Ray tube, or a synchrotron radiation source. The light (vector potential ($\vec{\mathbf{A}}$) impinges on the sample, which is a gas or the surface of a solid, and the electrons excited by the photoelectric effect are then analyzed with respect to their kinetic energy E_{kin} and their momentum $\mathbf{p}$ in an electrostatic analyzer. **Fig. 3.2** shows schematically how the energy-level diagram and the energy distribution of photoemitted electrons relate to each other. The solid sample has core levels and a valence band. In the present case of a metal, the Fermi energy E_F is at the top of the valence band and has a separation W_0 from the

vacuum level E_{vac}. If photoabsorption takes place in a core level with binding energy E_B ($E_B = 0$ at E_F), the photoelectrons can be detected with kinetic energy $E_{kin} = h\nu - W_0 - E_B$ in the vacuum. If the energy distribution of the emitted electron is plotted as in **Fig. 3.2**, their number per energy interval often gives a replica of the electron-energy distribution in the solid. This is an attractive feature of PES; it is able to provide us information on the electron energy distribution in a material.

But modern photoemission spectroscopy was available only in 1970's because we need the electron energy analyzer and ultra high vacuum (UHV) environment to get the undistorted data. One reason we need the UHV condition is the short escape depth of electron for study of solid surface, which is typically of the order of a few angstrom. This means that any spectroscopy of a solid suface involving electrons requires electrons from a very thin layer of the sample. Thus, if one wishes to learn about the bulk properties of the solid, one has to work with atomically clean surfaces. Surface contamination is another reason for UHV. Typically, the measure time for PES is of the order of ten minutes, so if the UHV condition is not satisfied, the signal come from not sample but contaminants. The required minimal pressure to experiment PES is around low 10^{-9} torr and the lower the better.

3.2. X-RAY PHOTOEMISSION SPECTROSCOPY (XPS) AND ULTRAVIOLET PHOTOEMISSION SPECTROSCOPY (UPS) :

The **UPS** and **XPS** measurements are the most powerful and universally applicable methods for obtaining direct information about the electron energy levels in the valence and atomic core regions, respectively. Photoemission is an excitation process. (Fig. 3.3).

XPS is photoemission spectroscopy using X-ray as a photon source. The energy range of X-ray in XPS is usually more than 1000 eV. X-ray of these energy range can be obtained by using characteristic X-ray line spectrum, which is due to transition of electron from high energy state to low one. When an atom is

bombarded by high energy electrons, some inner atomic electrons are sometimes knocked out, leaving vacancies in the inner shell. These vacancies are filled by electrons with outer high energy states, in which process the X-ray emits corresponding the energy difference between these two states. Most widely used targets to obtain X-ray in XPS are Al and Mg. The energy of Al K-alpha line is 1486.6 eV and Mg K-alpha 1253.6 eV.

A typical photoemission spectrum thus consists of peaks due to photoelectrons, which escape from various levels in the sample with no subsequent inelastic collisions, together with a continuous low background from electrons that undergo inelastic scattering before leaving the sample. The photoexcitation of core levels requires photons of relatively large energies, typically in the X-ray range. This type of spectroscopy is frequently referred to as X-ray photoemission spectroscopy (**XPS**). If one is interested in studying only the valence states, ultraviolet photons result in lower electron kinetic energies which generally allow both higher signal levels and greater resolution. Such studies are usually referred to as ultraviolet photoemission spectroscopy or UPS.

The UV sources used in the UPS have generally been rare-gas-discharge lamps. In recent years, synchrotron radiation from electron discharge rings has become useful as a light source for both X-ray and UV spectroscopic studies. UPS is one of the most useful tools to study the valence band structure of the condensed matters. It usually uses the He I line ($h\nu = 21.22$ eV) or He II line ($h\nu = 40.8$) as a photon source. Comparing with XPS, the resolution of the UPS is rather high (~MeV), so this is adequate for studying band structures though it is more surface sensitive than XPS. One useful feature of sources of polarized light is that polarized photons can provide information about the symmetry of the electronic states being probed.

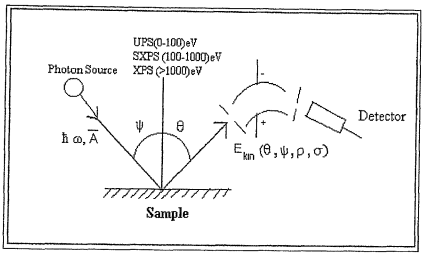
UPS(0-100)eV
SXPS (100-1000)eV
XPS (>1000)eV
Photon Source
ħ ω, A
ψ
θ
Detector
E kin (θ, ψ, ρ, σ)
Sample

Fig. 3.1

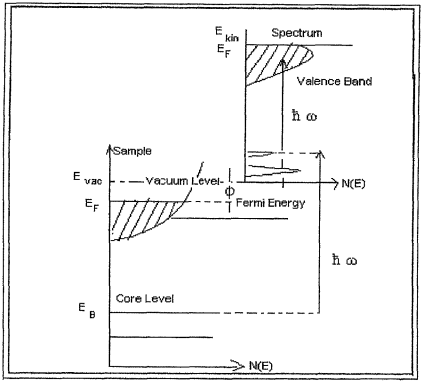
E kin
E F
Spectrum
Valence Band
ħ ω
Sample
E vac
Vacuum Level
Φ
N(E)
E F
Fermi Energy
ħ ω
Core Level
E B
N(E)

Fig. 3.2

FIG. 3.3 Energy level diagram for the electronic structure of a solid showing processes involved in **X-ray** and **UV - photoemission spectroscopy.**

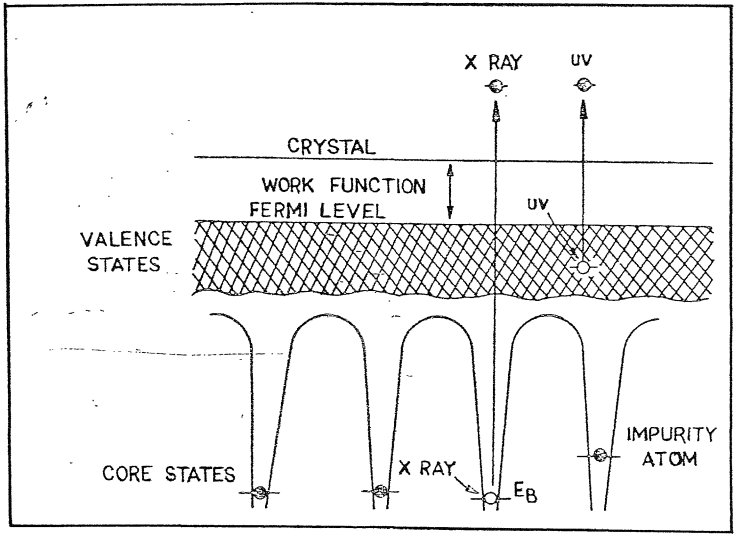
X RAY
UV
CRYSTAL
WORK FUNCTION
FERMI LEVEL
UV
VALENCE
STATES
CORE STATES
X RAY
E_B
IMPURITY
ATOM

3.3 ARUPS AND KRIPES:

Wave vector- or *k*-resolved band structures were eventually determined by using angle resolved ultraviolet photoemission spectroscopy (**ARUPS**) and angle- or *k*-resolved inverse photoemission spectroscopy (**ARIPES, KRIPES**). Photoemission spectroscopy was widely applied after new sources for ultraviolet light and soft X-rays became available. Differentially pumped, windowless discharge lamps equipped with monochromators are laboratory line-sources which may be routinely operated to yield photons between 16.8 and 40.8 eV while continuum of synchrotron radiation became accessible from electron storage rings.

3.4 AUGER ELECTRON SPECTROSCOPY (AES):

The Auger electron spectroscopy is a very powerful technique for the study of both the valence as well as conduction bands. (see Fig. 3.4). After an atomic core level is ionized by an energetic electron or photon, the hole in the inner shell can be filled by an electron from a less tightly bound level with the simultaneous emission of a photon or of a second electron that carries off the energy gained by the first. The latter non-radiative, decay process is referred to as an Auger process, after *Pierre Auger* who first identified the process back in 1925. The Auger electrons with the largest energy provide information about the initial core states and, like XPS spectra, can thus be used for elemental analysis. Because each element gives rise to many different Auger transitions, one must in most cases, consider several transitions for elemental analysis.

Changes in the valence electron densities will also markedly alter the energy distribution of the emitted Auger electrons, in other words, Auger chemical shifts are large. However, because Auger emission involves three different levels, these shifts are difficult to predict or interpret theoretically. One can, nevertheless, use the Auger spectra to provide important qualitative information.

FIG. 3.4 Energy level diagram for the electronic structure of a solid depicting **Auger processes.**

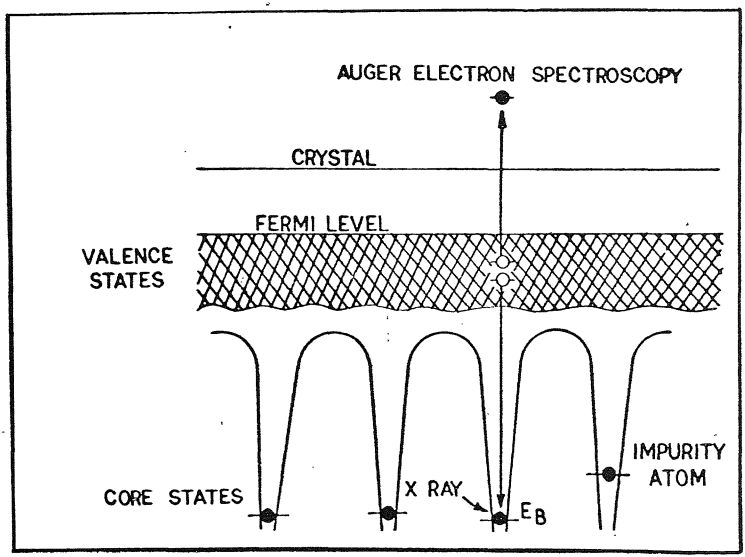
AUGER ELECTRON SPECTROSCOPY
CRYSTAL
FERMI LEVEL
VALENCE STATES
CORE STATES
X RAY
E_B
IMPURITY ATOM

3.5 LOW ENERGY ELECTRON DIFFRACTION (LEED)

There are essentially two types of **LEED** instruments; display-type systems and diffractometers. In display type systems as shown in Fig. 3.5(a), the electrons scattered into a large solid angle segment are observed simultaneously on a fluorescent screen. The inelastically scattered electrons and the secondary electrons generated by the incident beam are eliminated by a retarding field between the grids. In a diffractometer the electrons are scattered into a small solid angle are measured with a Faraday cup or channeltron after passing through a retarding field. (see Fig. 3.5(b)). Detector and crystal are rotated in a suitable manner so that all desired angles of incidence and diffraction may be covered. Diffractometers are far superior for quantitative intensity measurements but the display type of system has the advantage of speedy observation.

The electron gun usually produces a beam on the specimen with 0.1-10 μA current and a diameter from 10^{-4} to 10^{-3} m depending on electron energy (10-200 eV). The coherence of the beam is determined by the angular divergence. The scattered amplitudes have to be added only for the atoms within a coherence region and the total scattering is obtained by adding the scattered intensity of all coherence regions within the beam cross-section. Utmost surface perfection is essential for many quantitative studies but LEED patterns can be obtained easily from microscopically very rough and inhomogeneous surfaces. In order to keep the surface clean pressures below 10^{-9} Torr have to be maintained during observation.

FIG. 3.5 LEED Instruments

(a) Display-Type Systems

(b) Diffractometers

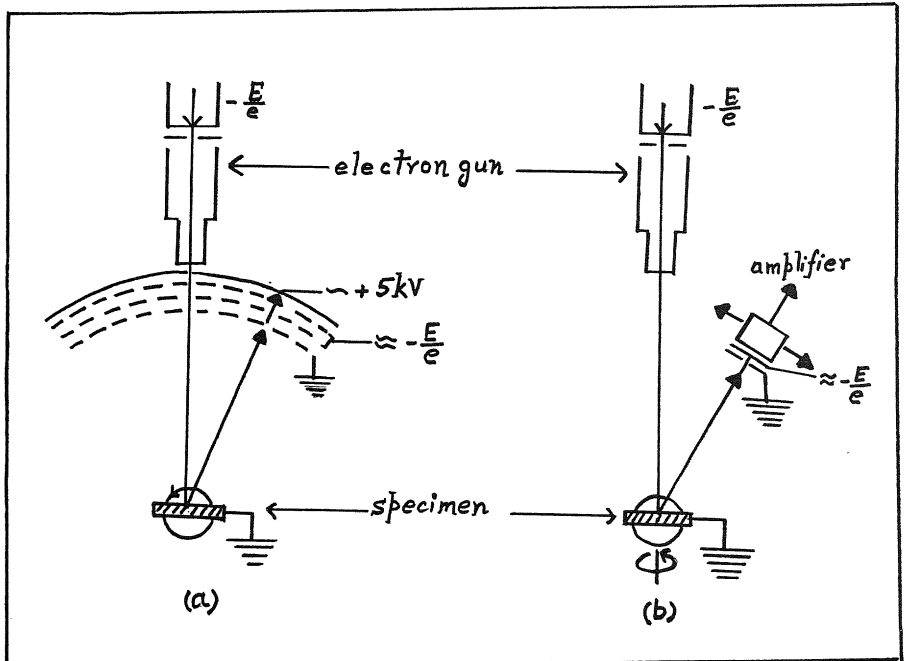
-E/e
electron gun
-E/e
+5kV
≈-E/e
amplifier
≈-E/e
specimen
(a)
(b)

Chapter-IV

$GaAs_{1-x}N_x$ ALLOYS

$GaAs_{1-x}N_x$ ALLOYS

4.1 INTRODUCTION:

In the past more than two decades, great attention has been devoted to the investigation of the electronic, excitonic and impurity properties of the semiconductor heterostructures, III – V semiconducting alloys etc. The interest for such investigations has been developed because of their wide range of potential device applications.

Recently, a new class of semiconductor alloys has been discovered in which one of the constituent elements is replaced by an element with highly dissimilar properties. The substitution of the group V element in group III-V compounds with small amount of nitrogen leads to drastic changes on the electronic properties. The most important effect is the reduction of the band gap.

GaAs, which has comparatively smaller band gap, plays an important role in semiconductor industry. GaAs is one of the most widely and extensively studied III-V group semi-conductor compound. This is true primarily due to extraordinary importance of GaAs as base material in solid state devices.. Among all the semi-conductor compounds, the gallium nitride (GaN) is emerging as one of the wonderful and the most promising material for the modern electronic and optoelectronic devices. It is mainly due to its wide direct band gap that would widely and extensively serve for applications in light-emitting devices operating in the blue and ultraviolet region. In fact GaN has many attracting properties such as stability at high temperature, considerable hardness and potential device applications. The alloys of III-V elements, which possess wide-energy gaps, are important for the development of the optoelectronic devices in the high frequency region. In the case of $GaAs_{1-x}N_x$ alloys, one expects to observe a variation of band gap from a value of 1.52 eV (GaAs) to a value of 3.3 eV (GaN). Thus a blue shift of the photoluminescence edge should have been observed experimently with the addition of N- atoms. On the contrary, a red shift of the photoluminescence edge

has been observed in these alloys [46]. In the alloys like $Al_xGa_{1-x}N$, where the lattice mismatch between the end components is about 2.9%, one observes a dominant role played by the cations in determining the electronic structure and the band gaps. On the other hand, in the $GaAs_{1-x}N_x$ alloys, the lattice mismatch is as large as 20% and the effects of various anion component concentrations are seen to be anomalous.

Compound semiconductor alloys of the type $A_xB_{1-x}C$ are often considered to consist of a regular arrangement of A and B atoms on a face centered cubic (fcc) sublattice. However, real alloys may, in general, be random. Deviations from randomness have been observed like phase separation i. e., formation of distinct AC and BC rich phases. Another case of deviation is the occurrence of order seen in both types of alloys $A_xB_{1-x}C$ and $AB_{1-x}C_x$. In extreme case of perfect order, one may observe alternating layers of pure AC and pure BC in cation variant systems $A_xB_{1-x}C$ or AB and AC pure layers in the anion variant systems $AB_{1-x}C_x$.

A full potential self consistent linear muffin tin orbital (FP-LMTO) method in the local density approximation (LDA) has been employed to investigate the electronic structure of the fourteen ordered $GaAs_{1-x}N_x$ alloys with x = 0.0, 0.037, 0.074, 0.111, 0.125, 0.25, 0.375, 0.407, 0.50, 0.625, 0.75, 0.875, 0.963 and 1.0 . In the local density approximation, we observe a near closure of the band gap in the concentration range x = 0.125 to x = 0.625 of the N atoms. It makes a possibility of the fabrication of the III-V light emitting devices covering the whole optical region. Earlier, *Rubio and Cohen* [45] have employed a psuedo-potential theory in the local density approximation to obtain a gap of 0.06 eV for one case only i.e., 25% concentration of N atoms. They have also performed a quasi-particle study and observed an opening of the band gap in LDA by about 0.7 eV.

Bellaiche et al [61] have discussed the electronic properties of some ordered alloys and quasirandom structures of Ga-As-N alloys by using local empirical pseudopotentials in the plane- wave pseudopotential approach. A fitting with the GW band structures, experimental band gaps and LDA deformation potentials was adopted to obtain the atomic potentials. For each composition,

results were averaged over a few randomly selected configurations. They considered a bimodal distribution of bond lengths.

In contrast to *Bellaiche et al* [61], we have investigated the electronic structure of the ordered and the random $GaAs_{1-x}N_x$ alloys by using a fully ab-initio LMTO method without adopting any fitting procedure. Although, we have adopted an unimodal distribution of bond lengths in major part of our calculations, the effects of bimodal distribution have been studied in a typical case and the results are not seen to be affected significantly.

4.2 CALCULATION AND RESULTS:

For the calculation of the charge density and the potential, the LMTO envelopes are expanded in terms of the Hankel-functions having the spherical harmonic components $l \leq 4$. Three values -0.01, -1.0 and -2.3 Ry for the decay factor in the Hankel functions are used in the construction of the muffin tin orbitals for real atoms. In the interstitial region two values -0.01 and -1.0 Ry of the decay factor have been employed. Each supercell contains an equal number of the real atomic muffin tin spheres (MTS) and the empty MTS's . The scalar relativistic effects have been considered in all the calculations. For the exchange correlation potential, the parametrization of *Hedin and Lundqvist* [62] has been chosen. In the present method, the wave functions of the core electrons of the atoms are relaxed and in the self consistent calculation in each iteration, the core electron charge density is recalculated.

We consider here a fcc lattice for all the alloys. A unit cell containing 8 molecular units (16 atom) has been employed for the different crystal structures of $Ga_8As_{8-n}N_n$ alloys for n = 0 – 8. For low concentrations of N or As atoms i. e., for x = 0.037, 0.074, 0.111, 0.407 and 0.963, a bigger unit cell or supercell containing 27 molecular units (54 atoms) has been employed.

The non-overlapping radii of muffin-tin spheres are chosen to be 2.17, 2.15 & 1.43 a. u. for Ga, As and N, respectively. We use muffin tin orbitals (MTO's) of 4s, 4p, 3d (4d) type for Ga (As) atoms and the 2s and 2p type MTO's for N. In a separate calculation, we have also considered Ga-4d states instead Ga-3d states as valence states at several N concentrations. However, the results are not significantly changed except for a small change in the magnitude of the band gap.

For the different structures of the ordered $GaAs_{1-x}N_x$ alloys, the lattice parameters have been calculated by minimizing the crystal energy for each system. We compare these calculated lattice parameters with the available experimental values and the others calculated values in Table 4.1 . The variation is shown in Fig 4.1. The variation is seen to be a nonlinear one. The departure from the linearity is appreciable. The presently calculated values for GaN is in excellent agreement with the experiment, whereas for GaAs the lattice parameter is seen to be well within 2% of the experimental value. Our calculated values are quite close to those reported for some alloys by other workers but are somewhat on higher side. The discrepancy may arise because of the use of correlation schemes by other workers which are different from the present one.

In all future calculations, the above calculated lattice parameters have been used. Further, for every ordered structure the bond lengths for the Ga-As and the Ga-N bonds are taken to be the same i. e., we assume an unimodal distribution of bond lengths. The effect of bimodal distribution of bond lengths is investigated in the later part of this article.

4.2(a) *Ordered Structures* :

The crystal lattices for all the considered ordered alloys have the zinc blende structure. In Figs. 4.2 & 4.3, the electronic structure is depicted for the 16 and 54 atom supercells, respectively. For brevity, we have not included the band structures for x = 0.625 and 0.875 in Fig. 4.2. The lengths of the primitive lattice vectors for the 16 and 54 atom supercell are, respectively doubled and tripled as compared to those of the two-atom unit cell. It results into the zone folding. Also,

TABLE 4.1 :

Variation of lattice constant with concentration of the constituent atoms in the ordered $GaAs_{1-x}N_x$ structures. All values are measured in Å .

SYSTEM (X)	PRESENT	OTHER CAL.	EXPT.
0.000	5.55	5.61[a]	5.65[b]
0.125	5.46		
0.250	5.36	5.30[c]	
0.375	5.26		
0.500	5.14	5.12[c]	
0.625	4.95		
0.750	4.83		
0.875	4.66		
1.000	4.50	4.42[d] , 4.48[e], 4.30[f]	4.50[g]

a Model dielectric function, *Zhu and Louie* 1991. [63]

b Numerical Data and Functional Relationships in Science and Technology 1982. [64]

c Pseudopotential, *Rubio and Cohen* 1995. [45]

d Pseudopotential, *Rubio et al* 1993. [34]

e LMTO - ASA, *Albanesi et al* 1993. [37]

f Pseudopotential, *Jenkins et al* 1994. [65]

g Optical absorption, *Lei et al 1992.* [66]

FIG. 4.1 Lattice constant variation in the ordered $GaAs_{1-x}N_x$ alloys. Experimental data is taken from "Numerical Data and Functional Relationships in Science and Technology 1982 [64]" and *Lei et al* 1992 [66]. The results of other calculations are taken from Refs. *Zhu and Louie* 1991 [63], *Rubio and Cohen* 1995 [45] and *Rubio et al.* 1993[34].

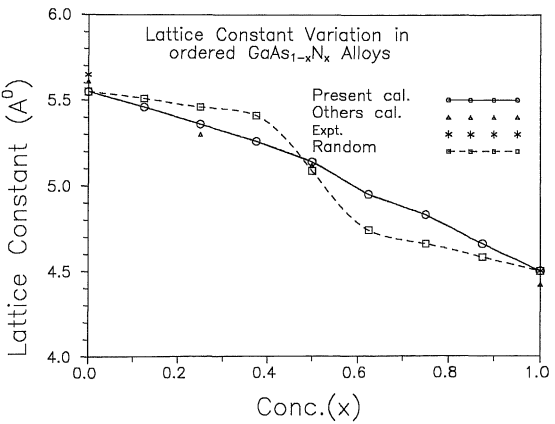
Lattice Constant Variation in
ordered GaAs1-xNx Alloys
Present cal.
Others cal.
Expt.
Random
Lattice Constant (A°)
Conc.(x)
6.0
5.5
5.0
4.5
4.0
0.0
0.2
0.4
0.6
0.8
1.0

the number of branches increase according to the larger number of molecular units in the supercell. The symmetry points of the bcc Brillouin zone are W (0.5, 0.25, 0), L (0.25, 0.25, 0.25), Γ (0, 0, 0), X (0.5, 0, 0) and K (0.375, 0.375, 0). In Figs. 4.2 & 4.3, the dispersion curves are shown only in the vicinity of the fundamental energy gap. In all future calculations, the origin of energy is chosen at the top of the valence band.

For the end component ordered structure, Ga_8As_8, the point group symmetry is T_d. A set of 19 special $\vec{k}$-points are selected in the irreducible part of the Brillouin zone for achieving the self- consistent results. The energy gap is a direct one equal to 0.61 eV. The states just above the bottom of the conduction band corresponds to the X-point of the Brillouin zone for the two atom unit cell. It happens because of the zone folding. The valence band maximum (VBM) is composed of As-p like states whereas the conduction band minimum (CBM) is composed of the s-like orbitals mainly of Ga having some contribution from As. It may be noted that the value of energy gap for this ordered structure in the GW approximation is 1.3 eV [45]. This value is again underestimated by 0.22 eV as compared to the experimental value of 1.52 eV.

For the most dilute ordered structure $Ga_{27}As_{26}N$ (3.7 % of N), the point group symmetry is again T_d. The N-atoms lying in the adjacent 54 atom supercells are sixth neighbours among themselves. The calculated electron structure in the neighbourhood of the energy gap is shown in Fig. 4.3. The band gap is 0.44 eV. The VBM is comprised of almost all the p-orbitals of the three constituent atoms N, Ga and As but the main contributions are from the N and As atoms. On the other hand, the main contributors to the CBM are the antibonding mixed states of N(s), Ga(s,p) and As (s,p) orbitals. For all the other alloy systems the main contributors are the s-like orbitals of N and Ga atoms with some contribution from the of As (s) orbitals.

For the next dilute ordered structure $Ga_{27}As_{25}N_2$ (7.4 % of N), two atomic configurations having different point group symmetries C_{2v} and C_{3v} were considered. In the C_{2v} symmetric configuration, two N-atoms are next nearest

neighbours among themselves whereas in the C_{3v} point group configuration, two N-atoms are fourth neighbours among themselves. For the C_{2v} and C_{3v} point group symmetries, the magnitudes of the band gap are seen to be different i.e., 0.283 and 0.350 eV, respectively. The variation of gap is seen to be small for the two different locations of the two N-atoms in the supercell. For brevity, we do not include the results obtained for C_{3v} -symmetry in the presentation of the results.

In the Ga_{27} As_{24} N_3 ordered structure, the three N atoms are second neighbours among themselves and the point group symmetry is C_{3v} . The magnitude of energy gap decreases to 0.11 eV. The orbital composition of the valence band maximum and that of the conduction band minimum are similar to the above discussed ordered alloys.

For the ordered $GaAs_{0.875}N_{0.125}$ system, the symmetry is T_d . There is one N-atom in 16-atom supercell and the N-atoms of the two adjacent supercells are fourth neighbours among themselves. A remarkable observation is that the band gap vanishes at this small concentration of N atoms. In LDA, the ordered alloy becomes metallic (zero band gap) at x = 0.125. The hybridized s - orbitals of all the atoms fill the energy gap completely. In fact, at the Γ- point where the closure of gap is seen, the states at VBM is comprised of the mixed As(p) and N(p) orbitals. Also, the charge inside the MT sphere of N has increased. We observe a localization of charge on N-atom.

For x = 0.25, again two different configurations of N atoms have been chosen. In C_{2v} symmetry, two N-atoms are next nearest neighbours among themselves, whereas in C_{3v} symmetry, the nearest two N-atoms are seen to be the third neighbours among themselves. For the C_{2v} and C_{3v} point group symmetries, the band gap is seen to be 0.064 and 0.0 eV, respectively. However, we have not included the results obtained for the C_{3v} symmetry in Table 4.2. The present value, 0.064 eV for energy gap obtained for C_{2v} - point group symmetry is in agreement with the value 0.06 eV reported by *Rubio and Cohen*, 1995. The inclusion of the many body effects such as considered in the GW approximation may reveal a finite

energy gap instead of the closure of the gap. *Rubio and Cohen* have calculated the GW value as 0.7 eV. The charge inside the MT sphere of N increases further.

For, x = 0.375, the three N-atoms are next nearest neighbours among themselves and the point group symmetry is C_{3v} . The lowest conduction states enter the valence band and the band gap is zero. The MT sphere for N atom acquires more charge.

For the next ordered structure, Ga_{27} As_{26} N_{11} supercell, the point group symmetry is chosen to be C_{3v} . There are two sets of clusters of N-atoms out of the total eleven N atoms. A cluster of four atoms is far separated from another set of 7 atoms. The N-atoms are second neighbours among themselves in each set. The minimum separation between the N-atoms in one set and the other set is equivalent to a separation between fourth neighbours. The seven atoms lying in the second set form a centered hexagonal normal to the <111> axis. The calculated energy gap is zero and we observe a closure of gap.

For the $GaAs_{0.50}N_{0.50}$ ordered alloy, again the two atomic configurations having different point group symmetries T_d and C_{2v} were considered. For C_{2v} symmetry, the nearest N-atoms lie in the second neighbouring lattice positions. For the T_d and C_{2v} point group symmetries, the magnitudes of the band gap are 0.00 and 0.16 eV, respectively. *Rubio and Cohen* [45] have obtained a band gap of 0.4 eV without including Ga-3d states in their calculation. Their reported GW value is 1.0 eV. We do not present the results obtained for the C_{2v} symmetry in Table 4.2. The charge in the MT sphere of N is large.

For x = 0.625, the point group symmetry is C_{3v} . The band gap is seen to be 0.011 eV. For the $GaAs_{0.25}N_{0.75}$ ordered alloy (x = 0.75), the point group symmetry is C_{2v} . The dispersion curves are similar to those of $GaAs_{0.50}N_{0.50}$ alloy except that the direct band gap is 0.34 eV. The ionic gap is wide (- 8 to - 11 eV). For an alloy containing 12.5 % of As atoms, i.e., $GaAs_{0.125}$ $N_{0.875}$ the point group symmetry is T_d in a 16 atom supercell. The band gap is seen to be 1.12 eV.

FIG. 4.2 Electronic dispersion curves for the ordered $GaAs_{1-x}N_x$ alloys (a) x = 0.00, (b) x = 0.125, (c) x = 0.25, (d) x = 0.375, (e) x = 0.50, (f) x = 0.75 and (g) x = 1.0 . The origin of energy has been chosen at the valence band maximum.

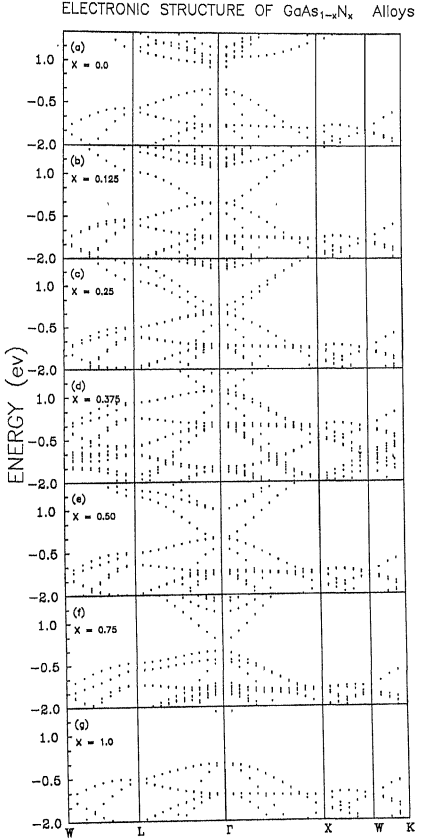
ELECTRONIC STRUCTURE OF $GaAs_{1-x}N_x$ Alloys
ENERGY (ev)
(a) X = 0.0
(b) X = 0.125
(c) X = 0.25
(d) X = 0.375
(e) X = 0.50
(f) X = 0.75
(g) X = 1.0
1.0
−0.5
−2.0
W
L
Γ
X
W
K

FIG. 4.3 Electronic dispersion curves for the ordered $GaAs_{1-x}N_x$ alloys (a) x = 0.037, (b) x = 0.074, (c) x = 0.111, (d) x = 0.407 and (e) x = 0.963. The origin of energy has been chosen at the valence band maximum.

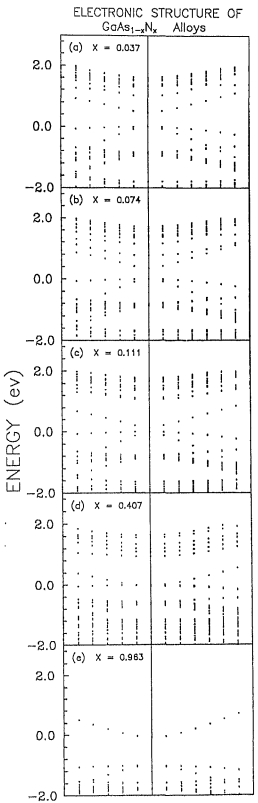
ELECTRONIC STRUCTURE OF
GaAs1−xNx Alloys
(a) X = 0.037
(b) X = 0.074
(c) X = 0.111
(d) X = 0.407
(e) X = 0.963
ENERGY (ev)
2.0
0.0
−2.0

On the other end of the alloy system, for one As atom in the 54 atom supercell ($Ga_{27}As\,N_{26}$) the point group symmetry is T_d . The electronic structure is depicted in Fig.4.3 (e). The band gap is smaller than that of pure GaN lattice and is equal to 1.66 eV.

For the Ga_8N_8 ordered structure, the other end component of alloys the direct band gap is 1.90 eV. The point group symmetry is T_d . The states lying just above the bottom of conduction band corresponds to the X-point of the Brillouin zone seen in the two-atom unit cell of GaN. The VBM originates from the N(p) states and the CBM from the antibonding mixed s-like states of N and Ga. This somewhat lower value of band gap in comparison to other results [34, 37, 65] may arise because of the use of different exchange - correlation potentials by other workers.

We observes an accumulation of charge or more localized charge around the N-atom in the concentration range 0.111 to 0.625 . The N-atoms behave more atomic like . The resulting fall in the potential energy leads to the lowering of N-2s states in the fundamental energy gap filling it partially or completely. Similar conclusion has been drawn by *Rubio and Cohen* [45].

In order to see the effects of bimodal distribution of bond lengths on the electronic structure as a typical case we perform a separate calculation for the ordered $Ga_8\,As_7N$ alloy. In this alloy the bond length for each GaAs and GaN bond is same and is equal to 2.38 Å in an unimodal distribution of bond lengths. In order to see the effect of the variation of bond length we have chosen a value of 2.02 Å for all the four neighbouring GaN bonds around the central N atom keeping the bond lengths of the GaAs bonds equal to 2.38 Å . The band gap is seen to be 0.035 eV against a zero value obtained for a Ga-N bond length of 2.38 Å. Thus, the zero band gap seen in a finite concentration range of N does not seem to be affected significantly in a bimodal distribution of bond lengths.

The direct band gap energy of the $GaAs_{1-x}N_x$ ordered alloys, is presented in Table 4.2. A closure of gap is observed from x = 0.125 to 0.625 . The calculated band gaps are compared with the available experimental data for x = 0.0 and 1.0 and the other calculated values available for x = 0.0, 0.25, 0.50 and 1.0. The variation of band gap energy with concentration x of N atoms is shown in Fig. 4.4.

4.2(b) *Random Alloys* :

In general, one may not expect occurrence of a particular ordered structure. A more probable situation is the occurrence of a number of various different local atomic configurations in different parts of an alloy. The alloy may be a disordered one depending upon the growth conditions. The properties of the disordered alloy may be simulated by considering the statistical mechanical distributions of the ordered structures. A cluster expansion method has been adopted [67-69] in the past for obtaining such a statistical mechanical description. It has been suggested that the coefficient of the cluster expansion method may be obtained by a first principle calculation of a set of ordered structures. This method which was first used for binary alloys can be extended to the ternary alloy in case the disorder is assumed to occur only on one type of sites say anion or cation as is the case for the presently discussed $AB_{1-x}C_x$ alloys. One simplifies the calculation by truncating the cluster expansion at the level of nearest neighbour interactions. For a tetrahedron structure one studies the five basic structures corresponding to the nearest neighbour tetrahedron $B_{4-n}C_n$ (n = 0 - 4) . The statistical mechanical property of the alloys may be considered as the property seen for the random alloys. Any statistical property F(x) at a particular concentration x may be expanded as

$$F(x) = \sum_n P_n(x)\, F_n \qquad \text{.....(1)}$$

where, F_n is the property for the anion tetrahedron and P_n (x) is the probability of the occurrence of cluster $B_{4-n}C_n$.

The probability of each cluster which is in general temperature dependent should be obtained at any given temperature by minimizing the free energy with respect to the probability P_n (x,T). However, we assume here a temperature independent random distribution function for the probability given by

$$P_n(x) = \binom{4}{n} x^n (1-x)^{4-n} \qquad \text{.....(2)}$$

A similar calculation has been done by earlier workers [37, 69, 70]. This is obviously a first approximation and may be expected to be valid for the case of frozen - in disorder of the gas or liquid phase from which the solid solutions are quenched.

Using eq.(1) we have calculated the band gap for the random alloys at different concentrations of N and have included the results in Fig 4.4. We observes a very large bowing in the energy gap curve with a minimum value of 0.114 eV at x = 0.375.

Our results compare very well with those obtained by *Bellachie et al* [61] for electronic structure. Similar to them, we observe a weak localization of the conduction band minimum wavefunctions around N atoms in the N- impurity region. (dilute N alloys) and a strong localization of valence band maximum wavefunctions around As atoms in the As impurity region (N- dominated alloys). For some of their " special quasirandom structures" which are different from our fixed zinc blende structures, they obtain a negative band gap in contrast to our zero band gap. These authors have obtained a minimum value of band gap equal to 0.4 eV for x = 0.50 random alloy in contrast to our value of 0.3 eV for the random alloy obtained here without using any fitting procedure.

Table 4.2 : Band Gap Variation in the ordered $GaAs_{1-x}N_x$ structures. All energies are measured in eV.

SYSTEM (X)	PRESENT CAL.	OTHER CALCULATION.		EXPT.
		LDA	GW	
0.000	0.61	0.60[a]	1.3[c]	1.52[b]
0.037	0.44			
0.074	0.28			
0.111	0.110			
0.125	0.000			
0.250	0.0640	0.06[c]	0.7[c]	
0.375	0.000			
0.407	0.000			
0.500	0.000	0.40[c]	1.0[c]	
0.625	0.011			
0.750	0.340			
0.875	1.120			
0.963	1.660			
1.000	1.900	2.10[d], 1.97[e], 2.32[f],	3.1[d]	3.20[g], 3.30[h], 3.52[i], 3.4[j]

a Model dielectric function, Zhu and Louie 1991. [63]

b Numerical Data and Functional Relationships in Science and Technology 1982. [64]

c Pseudopotential or quasi particle energy, *Rubio and Cohen* 1995. [45]

d Pseudopotential, *Rubio et al* 1993. [34]

e LMTO-ASA, *Albanesi et al* 1993. [37]

f Pseudopotential, *Jenkins et al* 1994. [65]

g Optical absorption, *Lei et al* 1992. [66]

h Photoluminescence and cathodoluminescence, *Paisely et al* 1989. [71]

i Cathodoluminescence at 53 K on epitaxial films, *Harrison* 1985. [72]

j Optical absorption, *Yoshida et al* 1982. [73]

FIG. 4.4 Variation of band gap with the concentration x for the ordered and random $GaAs_{1-x}N_x$ alloys. The results of other calculations are taken from Refs. *Zhu and Louie* 1991, *Rubio and Cohen* 1995 and *Rubio et al.* 1993.

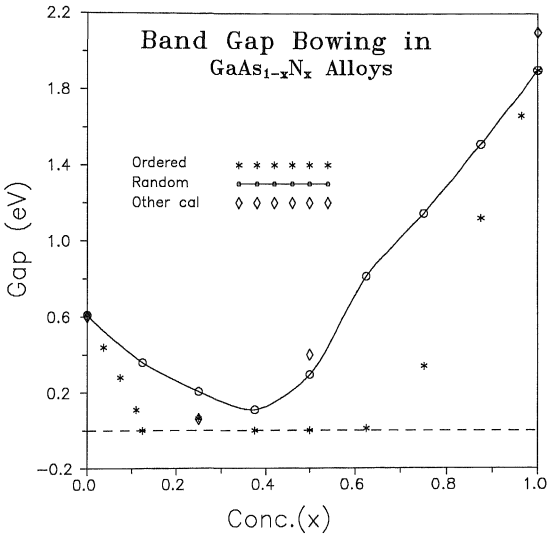
Band Gap Bowing in
GaAs1-xNx Alloys
Ordered
Random
Other cal
Gap (eV)
Conc.(x)
2.2
1.8
1.4
1.0
0.6
0.2
−0.2
0.0
0.2
0.4
0.6
0.8
1.0

Chapter-V

$AlAs_{1-x}N_x$ ALLOYS

$AlAs_{1-x}N_x$ ALLOYS

5.1 INTRODUCTION:

The semiconducting alloys of III-V elements exhibit very interesting electronic properties such as variation or lowering of energy band gap etc. Normally, the energy band gap variation is seen to be linear in III-V semiconducting alloys in which the concentration of cation component is varied as reported in $Ga_{1-x}Al_xN$ alloys [66, 70]. But, on the other hand, in some III-V alloys when the concentration of anion component is varied, the band gap reduces to a very small value or some times to zero (i.e. metallic behaviour) as has been seen in $GaAs_{1-x}N_x$ alloys at low concentrations. Thus, these mixed group V alloys such as $Al(Ga)As_{1-x}N_x$ can in principle allow one to close the band gap between the nitrides and the arsenides and will enable the fabrication of III-V light emitting devices covering the entire visible spectrum.

The III-V nitride semiconductors are potentially useful as high frequency, microwave and short-wavelength electroluminescent devices. The specific role of nitrogen is in the formation of short bonds which leads to smaller lattice constants than for other III-V semiconductors. At ambient conditions the AlN crystallizes in the hexagonal wurtzite structure, but the zinc blende structure is only slightly higher in energy [74]. These nitride compounds undergo a structural phase transformation to rocksalt structure under high pressure such as 12.9 GP for AlN [75]. Very few *ab initio* calculations of the electronic and physical properties of group III nitrides, arsenides and their alloys have been reported in the literature. *Christensen and Gorczyca* [32] have investigated the optical and structural properties of III-V nitrides by means of band structure and total energy calculations.

Experimental results for the electronic properties and the microscopic parameters of AlN and $AlAs_{1-x}N_x$ alloys have been scarce due to difficulties in growing high quality single crystals. More experimental work is required on these

compounds to understand the various physical properties. *Rubio and Cohen* [45] have performed a pseudopotential and quasiparticle study of the ordered $AlAs_{1-x}N_x$ alloys.

5.2 CALCULATION AND RESULTS:

For the calculation of electronic properties of ordered $AlAs_{1-x}N_x$ alloys, an unit cell having eight molecular units has been considered. The calculations for nine ordered systems of $AlAs_{1-x}N_x$ alloys (x= 0.0, 0.125, 0.25, 0.375, 0.50, 0.625, 0.75, 0.875 and 1.0) have been performed.

The radii of non overlapping spheres drawn around each real and empty atoms are properly chosen for each value of concentration (x) except for nitrogen atom for which the radius of atomic sphere is chosen to be the same and equal to 1.43 a. u. The radius of atomic sphere Al atom is varied from 2.30 to 1.92 a. u. The radius of As atomic sphere varies from 2.26 to 1.88 a. u.. Al (3s,3p, 3d), As (4s,4p, 4d) and N(2s,2p) states are considered as valence states.

5.2 (a) Ordered Structures:

The lattice parameters for different values of x in ordered $AlAs_{1-x}N_x$ alloys have been calculated by obtaining the minimum energy for each system and are plotted in Fig. 5.1. The calculated values are compared with other calculations and also with experimental values (see Table 5.1). The calculated values of lattice parameters for x = 0 and 1 are very close to the available experimental values. The variation of lattice parameter with x is seen to be non - linear. Our values are slightly at higher site than those reported by *Rubio and Cohen* [45] for some structures.

The calculated electronic dispersion curves are presented in Fig. 5.2.

FIG. 5.1 Lattice constant variation in the ordered and random $AlAs_{1-x}N_x$ alloys.

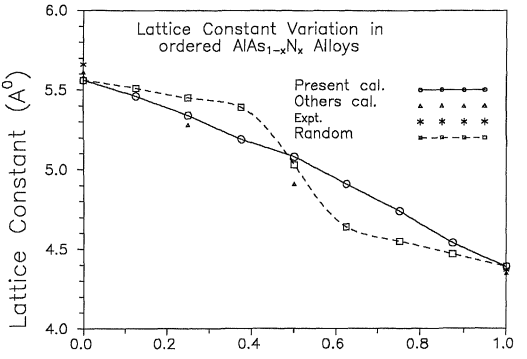
Lattice Constant Variation in
ordered $AlAs_{1-x}N_x$ Alloys
Present cal.
Others cal.
Expt.
Random
Lattice Constant (A^0)
Conc.(x)
6.0
5.5
5.0
4.5
4.0
0.0
0.2
0.4
0.6
0.8
1.0

3774-20
5863

Table 5.1:

Variation of lattice constant with concentration of the constituent atoms in the ordered $AlAs_{1-x}N_x$ structures. All values are measured in Å.

SYSTEM (X)	PRESENT	OTHER CAL.	EXPT.
0.000	5.56	5.61[a]	5.66[b]
0.125	5.46		
0.250	5.34	5.28[c]	
0.375	5.19		
0.500	5.08	4.91[c]	
0.625	4.91		
0.750	4.74		
0.875	4.54		
1.000	4.39	4.35[c,d]	4.37[e]

a (Ref. 63) **b** (Ref.64) **c** (Ref.45) **d** (Ref. 37) **e** (Ref. 76)

FIG. 5.2 Electronic dispersion curves for the ordered $AlAs_{1-x}N_x$ alloys (a) x = 0.00, (b) x = 0.125, (c) x = 0.25, (d) x = 0.375, (e) x = 0.50, (f) x = 0.75, (g)x = 0.875 and (h) x=1.0.

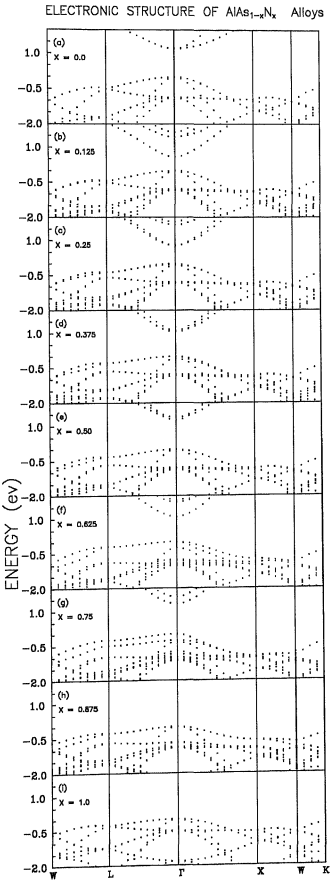
ELECTRONIC STRUCTURE OF $AlAs_{1-x}N_x$ Alloys
ENERGY (ev)
(a) x = 0.0
(b) x = 0.125
(c) x = 0.25
(d) x = 0.375
(e) x = 0.50
(f) x = 0.625
(g) x = 0.75
(h) x = 0.875
(i) x = 1.0
1.0
−0.5
−2.0
W
L
Γ
X
W
K

For Al_8 As_8 ordered system, the point group symmetry is T_d. The calculation were performed for 2-selected k-points in the irreducible part of Brillouin zone for achieving self consistent results. The energy gap is indirect and is equal to 1.21 eV. The main contributors to the valence band maximum (VBM) are As- p with some Al-p like states. On the other hand conduction band minimum (CBM) is comprised of mainly Al-p and some As-p like states.

For the dilute ordered Al $As_{0.875}N_{0.125}$ alloy, the point group symmetry is T_d. There is one N-atom in the 16-atom supercell and the N-atoms of the two adjacent supercells are fourth neighbours among themselves. The direct band gap is 0.59 eV. The lowest conduction state originating from the hybridization of s-orbitals of all the constituent atoms descends into the band gap of the AlAs. The remarkable observation is that the Al_8As_8 compound becomes a direct band gap material at a small value of x = 0.125.

For x = 0.25, the point group symmetry is C_{2v} . In this structure two N-atoms are next nearest neighbours among themselves. The band gap becomes a direct one and is equal to 0.77 eV. The VBM is composed of p- like state of As, Al and N atoms. On the other hand, the main contributors to the CBM are Al(s,p), N-s and As-s like states. For the $AlAs_{.625}N_{.375}$ ordered alloy, the point group symmetry is C_{3v} . The three N-atoms are next nearest neighbours among themselves. The direct band gap is 1.066 eV. For x = 0.50, the point group symmetry is T_d . The direct band gap is equal to 1.25 eV. For the $AlAs_{0.375}N_{0.625}$ ordered alloy, the point group symmetry is C_{3v} . The band gap changes to indirect one and is equal to 1.09 eV. For x = 0.75, $AlAs_{0.25}N_{0.75}$ ordered alloy, the point group symmetry is C_{2v} . The indirect band gap is 1.31 eV. For the $AlAs_{0.125}N_{0.875}$ ordered alloy, the point group symmetry is T_d . The indirect band gap is 2.13 eV. For the end component, Al_8N_8 ordered structure the point group symmetry is T_d . The indirect energy gap is 3.35 eV. There is a localization of charge on the N-atoms and the charge within the muffin tin spheres increases with the N-concentration.

The variation of the direct and indirect band gap energies with concentration of N-atoms for ordered systems $AlAs_{1-x}N_x$ are presented in Table 5.2

and Fig. 5.3. We observes that there is a crossover from indirect to direct band gap energy approximately at $x \approx 0.02$ and the alloys becomes direct up to $x \approx 0.56$. The alloy at high concentration ($x > 0.56$) again returns to an indirect one.

Unfortunately, no experimental data is available for comparison. On making comparison with the calculation of *Rubio and Cohen* our values for the direct and indirect band gaps, for the end components, AlAs and AlN, are quite close to (Table 5.2) their values. However for the alloys, there are quite large differences. For x=0.25, our value (0.77 eV) is higher than their values (0.45 eV), whereas reverse is the case for the indirect band gap. For $x = 0.50$ the present value (1.25 eV) is quite close to their value (1.13 eV). However, our indirect gap 3.92 eV is much higher than their corresponding value of 0.76 eV. Thus this alloy is direct band gap in our calculation in contrast to *Rubio and Cohen* who have seen it as an indirect band gap material in their pseudopotential calculation. It may be noted that *Rubio and Cohen* has employed a pseudopotential calculation for a smaller unit cell containing 8 atom.

5.2(b) ***Random Alloys*:**

The properties of the disordered alloys can be obtained by considering the statistical mechanical distribution of the ordered structures. For obtaining such a statistical mechanical properties a cluster expansion method has been used [67-69]. For details of the method please refer chapter-IV.

We have first calculated the lattice constant for random alloys using the theory which has been discussed in the previous chapter and the results are presented in Fig. 5.1. We find that the lattice constant for random alloys have greater (lesser) than that of the ordered alloys for $x < 0.50$ (>0.50).

For the random alloys the calculation has been made by taking the smaller value of band gaps (direct or indirect) for each alloy. There is a large band gap bowing in the energy gap curve with a minimum value of 0.82 eV at $x = 0.375$.

FIG. 5.3 Variation of band gap with the concentration x for the ordered and random $AlAs_{1-x}N_x$ alloys.

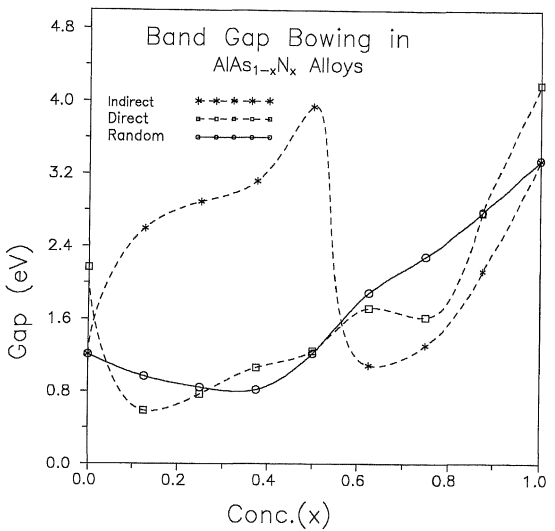
Band Gap Bowing in
AlAs1-xNx Alloys
Indirect
Direct
Random
Gap (eV)
Conc.(x)
4.8
4.0
3.2
2.4
1.6
0.8
0.0
0.0
0.2
0.4
0.6
0.8
1.0

Table 5.2:

Band Gap Variation in the ordered $AlAs_{1-x}N_x$ structures. All energies are measured in eV.

SYSTEM (X)	PRESENT CALCULATION		OTHERS CALCULATION		EXPT.
	INDIRECT	DIRECT	INDIRECT	DIRECT	
0.000	1.21	2.17	1.33[a]	2.07[a]	2.3[b]
0.125	2.61	0.59			
0.250	2.89	0.77	3.47[c]	0.45[c]	
0.375	3.12	1.066			
0.500	3.92	1.25	0.76[c]	1.13[c]	
0.625	1.09	1.72			
0.750	1.31	1.62			
0.875	2.13	2.77			
1.000	3.35	4.18	3.2[c]	4.2[c]	6.1[d], 6.28[e]

a (Ref. 63) **b** (Ref. 77) **c** (Ref. 45) **d** (Ref. 73) **e** (Ref. 78)

Chapter-VI

$Ga_{1-x}Al_xAs$ ALLOYS

$Ga_{1-x}Al_xAs$ ALLOYS

6.1 INTRODUCTION:

There has been tremendous interest in the development of opto-electronic devices, especially for obtaining solar cells, light emitting diodes and laser emitting devices. The GaAs which has a comparatively smaller band gap plays an important role in the semiconductor industry. The fact that GaAs is a direct band gap semiconductor makes it very useful for electro-optical devices. The almost perfect lattice match when combined with $Ga_{1-x}Al_xAs$ makes it possible to use $Ga_{1-x}Al_xAs$/GaAs heterojunctions and superlattices as light emitting devices like LED's, photo-detectors, semiconductor lasers etc. They find applications in high mobility transistors and in microelectronics.

We employ an unit cell containing eight molecular units for the different crystal structures of $Ga_{8-n}Al_nAs_8$ alloys for n = 0 – 8. The radii of the non-overlapping spheres are chosen to be 2.30, 2.25 and 2.28 a.u. for Ga, Al and As, respectively. Ga (4s,4p,3d), Al(3s,3p,3d) and As(4s,4p,4d) states are considered as the valence states.

For a detailed information of the method used, Please refer to Chapter –IV.

6.2 RESULTS AND DISCUSSION:

6.2(a) Ordered Structures:

The various unit cells chosen for the different concentrations of the Ga and Al atoms for x = 0.0 to 0.5 are presented in Fig. 6.1. The atomic configurations for x = 0.625 to 1.0 can be obtained from them by interchanging the Ga and Al sites. In choosing these different possible atomic configurations, it has been kept in mind that the point group symmetry of the unit cell should be at least C_{2v}. The lattice parameter for each system has been calculated by minimizing the crystal energy.

The calculated lattice parameters for the ordered and the random alloys are compared with the results of other calculations [63] and the available experimental data [64] in Table 6.1. The variation of lattice parameter with concentration x is seen to be linear for the ordered configurations as depicted in Fig. 6.2. The lattice parameters of the end components GaAs and AlAs are reproduced in the calculation within 2%.

The electronic structure for all the systems in the neighbourhood of the energy gap is presented in Fig. 6.3. For Ga_8As_8 , one of the end components, the unit cell is shown in Fig 6.1(a). The band gap is direct and is equal to 0.61 eV in LDA. The indirect band gap is 1.07 eV.

In some semiconductors like Si, a consideration of the first order effects of the many body interactions has shown that the resulting self energy correction in the fundamental energy gap is quite stationery. This prompted us to choose a constant value for self-energy correction (SEC) for each alloy to obtain realistic values for the band gaps which may be comparable to the experimental values. In the present case, the experimental data for the indirect band gap is available for the whole concentration range [79], we therefore use this data to obtain the underestimation of the band gap calculated here in LDA for each alloy.

We adopt the following procedure: we first determine the underestimation of the indirect band gap in the case of the end components of the alloys i.e., GaAs and AlAs. For GaAs and AlAs, the values for indirect band gaps in LDA are 1.07 and 1.21 eV, respectively whereas the reported experimental values are 2.01 and 2.25 eV, respectively. The many body effects cause, thus, an underestimation of band gap by 0.94 and 1.04 eV, in GaAs and AlAs, respectively and we adopt these values as self energy corrections for the end components of the alloys. As the values of SEC for the end components are quite near, we assume that for $Ga_{1-x}Al_xAs$ alloys , the self energy correction changes linearly from 0.94 to 1.04 eV for the full concentration range of x = 0 to 1. In our future calculation, we also assume this linear variation of SEC as wave vector-independent. For GaAs , the direct and indirect band gaps after including self energy correction are 1.55 and 2.01 eV, respectively.

FIG. 6.1 Different unit cells chosen for different concentrations of the Ga and Al atoms for x = 0.0 to 0.5 . The unit cells for x = 0.625 to 1.0 can be obtained from the above given unit cells by interchanging Al and Ga atoms.

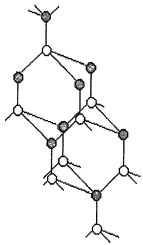

(a) Ga_8As_8

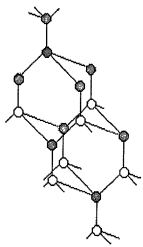

(b) $Ga_7Al_1As_8$

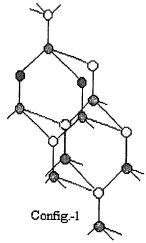

(c) $Ga_6Al_2As_8$

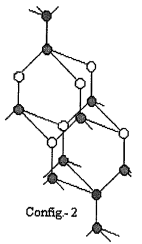

(d) $Ga_6Al_2As_8$

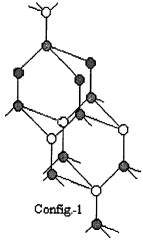

(e) $Ga_5Al_3As_8$

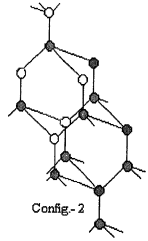

(f) $Ga_5Al_3As_8$

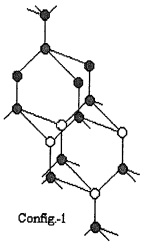

(g) $Ga_4Al_4As_8$

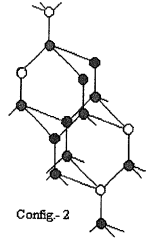

(h) $Ga_4Al_4As_8$

Table 6.1.

Variation of lattice constant with the concentrations of the constituent atoms in the $Ga_{1-x}Al_xAs$ structures. All values are measured in Å .

SYSTEM (X)	PRESENT CALCULATION		OTHER CAL.	EXPT.
	Ordered	Random		
0.000	5.554	5.554	5.61[a]	5.65[b]
0.125	5.556	5.556		
0.250	5.557	5.556		
0.375	5.558	5.556		
0.500	5.559	5.561		
0.625	5.560	5.562		
0.750	5.562	5.563		
0.875	5.563	5.565		
1.000	5.564	5.564	5.61[a]	5.66[b]

a. (Ref.63)

b. (Ref. 64)

FIG. 6.2 Lattice constant variation in the ordered and random $Ga_{1-x}Al_xAs$ alloys.

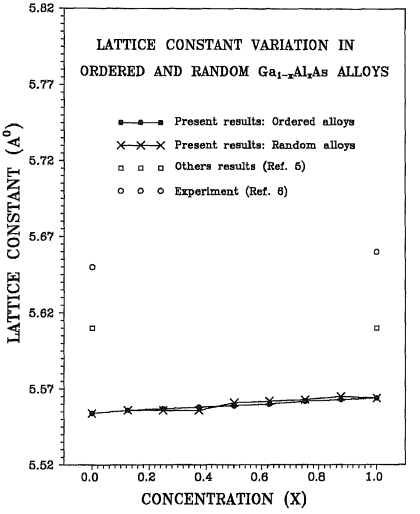
LATTICE CONSTANT VARIATION IN
ORDERED AND RANDOM $Ga_{1-x}Al_xAs$ ALLOYS
Present results: Ordered alloys
Present results: Random alloys
Others results (Ref. 5)
Experiment (Ref. 6)
LATTICE CONSTANT (A^0)
5.82
5.77
5.72
5.67
5.62
5.57
5.52
0.0
0.2
0.4
0.6
0.8
1.0
CONCENTRATION (X)

For the most dilute ordered $Ga_{0.875}Al_{0.125}As$ alloy, the point -group symmetry remains T_d as shown in Fig. 6.1b. There is one Al atom in the 16-atom supercell and the Al atoms of the two adjacent supercells are fourth neighbours among themselves. The calculated direct and indirect band gaps are 0.70 and 1.09 eV, respectively. Again, the states just above the bottom of the conduction band at the Γ point corresponds to the L-point of the Brillouin zone for the two atom unit cell because of the zone folding. There is splitting of states due to the interaction between the folded states e.g. interaction between L- and X- points states. An averaging has been done to determine the energies of the conduction states. At Γ-symmetry point, the VBM is mainly composed of the hybridized As-p and Ga-p like orbitals. The state at CBM is composed of the s-like orbitals of Al and Ga. For $x = 0.125$, the SEC turns out to be 0.95 eV and the self energy corrected direct and indirect band gaps are 1.65 and 2.04 eV, respectively.

For the next ordered $Ga_{0.75}Al_{0.25}As$ alloy, there are only two possible different configurations which may be considered . They possess C_{2v} - and C_{3v} - symmetries (Figs.6.1(c) & (d)) . In both the symmetry configurations, the two Al atoms of the unit cell are the next- nearest neighbours among themselves in C_{2v} symmetry in the same unit cell whereas in C_{3v} symmetry in the adjacent unit cells. The band gap is direct in both the configurations. The values of the direct and indirect band gaps for the C_{2v} - symmetric configuration are somewhat lower than those for the C_{3v} - configuration. The values of band gaps for C_{2v} are 0.79 and 0.97 eV and those for C_{3v} are 0.93 and 1.13 eV, respectively. Here, again the states just above the CBM at the Γ- point correspond to the L-point of the Brillouin zone for the two atom unit cell because of the zone folding. The states at VBM have contributions mainly from the p-like orbitals of As, whereas the states at CBM again have contributions from s-like orbitals of Ga and Al.

The extrapolated SEC is 0.97 eV and the values of the band gaps after the inclusion of SEC are 1.76 and 1.94 eV for C_{2v}. For C_{3v} configuration, these values are 1.90 and 2.10 eV, respectively. We look for the experimental data in the literature and find the absorption and the photoluminescence data of *Monemar et al* [79]. For a sample containing $x = 0.25$, they obtained the values of 1.92 and

2.07 eV for the direct and indirect band gaps. On making comparison with the present values obtained for C_{2v} and C_{3v} configurations in the unit cell, one finds that the experimental values are very close to the presently calculated values obtained for the C_{3v} configuration of atoms in this alloy.

For x = 0.375, again there are two possible different atomic configurations having the point group symmetries C_{3v} and C_{2v} as shown in Figs.1(e) and 1(f), respectively . In C_{3v}-symmetry, the three Al atoms are next-nearest neighbors among themselves whereas in C_{2v}-symmetry, Al atoms are again next-nearest neighbors, but they do not couple to the same As atom, instead form a linear chain. The VBM originates mainly from p-like orbitals of As atoms. The CBM comprises of the s-like orbitals of Ga and Al atoms. For $x < 0.375$, the state just above the bottom of the conduction band at the Γ- point corresponds to the L-point of the Brillouin zone for the two atom unit cell because of the zone-folding and the alloys possess direct band gap. For x = 0.375 , the values for the direct and indirect band gaps for the two atomic configurations are quite similar and are 1.1 and 1.02 eV, respectively. The behaviour of the alloy has now changed from a direct to an indirect band gap semiconductor. The SEC is 0.98 eV, making the values of the direct and indirect band gaps as 2.08 and 2.0 eV, respectively.

For the ordered $Ga_{0.50}Al_{0.50}As$ alloy, again there are two possible atomic configurations having point - group symmetries T_d - and C_{2v} {Figs. 6.1 (g) & (h)}. In T_d - symmetry, all the four Al atoms in the unit cell couples to the same As atom and are second neighbours among themselves. In the C_{2v} - symmetric configuration, there are two separated sets of two next nearest neighbouring Al atoms which are not coupled to the same As - atom. For both symmetries, the values of the band gap are slightly different . The CBM states at the Γ- point are the states of L- and X-points of a two-atom unit cell. The band gap becomes indirect. The VBM is composed of p- like orbitals of As atoms with some contributions from d-orbitals of Al. The CBM is comprised of s-like states of Al, Ga with some p-like contributions from Al. The SEC is 0.99 eV. The direct and indirect band gaps after including the SEC are 3.05 and 2.11 eV, respectively.

For x = 0.625, similar to the x = 0.375 case there are two atomic configurations having the point -group symmetries as C_{2v} and C_{3v} For all alloys having x > 0.625 at the Γ- point of CBM, one finds states appearing at X- point for a two-atom unit cell and the band gap is indirect , For x = 0.625 , the band gap is equal to 1.16 eV. The direct band gap is 2.09 eV. The VBM is composed of p-like orbitals of As, whereas the CBM is composed of s-like orbitals of As (central atom) and p-like orbitals of second neighbouring As atoms. The SEC is 1.0 eV. Thus, the self energy corrected direct and indirect band gaps are 3.09 and 2.16 eV, respectively.

For the ordered $Ga_{0.25}Al_{0.75}As$ alloy, the two atomic configurations possessing C_{2v} and C_{3v} point - group symmetries were considered. The values for the direct and indirect band gaps are quit similar for C_{2v} - and C_{3v} - symmetric configurations and are 2.10 and 1.18 eV, respectively. The VBM has contributions mainly from As-p like orbitals. The CBM is comprised of s-p mixed orbitals of As and Al atoms. The SEC is 1.02 eV and the self energy corrected values are 3.12 eV and 2.20 eV for the direct and indirect band gaps, respectively.

For x = 0.875, the point -group symmetry is T_d . The indirect and direct band gaps are equal to 1.21 eV and 2.12 eV respectively .The VBM is comprised of mixed As-p and Al-p like orbitals. The CBM has contributions mainly from p-like orbitals of Al and As alongwith some contributions from d-orbitals of As. The SEC is 1.03 eV and the self-energy corrected values for the direct and indirect band gaps are 3.15 and 2.24 eV, respectively.

For the other end component (x = 1.0) of the alloys, Al_8As_8 , the point group symmetry is T_d. The band gap is indirect and is equal to 1.21 eV whereas the direct band gap is 2.17 eV. The VBM is composed of p-like states of As and Al atoms and CBM is composed of p-like orbitals of Al and As and some d-like orbitals of As. The SEC necessary to achieve the experimental value of 2.3 eV for indirect band gap is 1.04 eV and the self-energy corrected value for direct band gap is 3.21 eV.

The total density of states for the ordered $Ga_{1-x}Al_xAs$ alloys for the whole concentration range of Al is shown in Fig. 6.4 . The electronic density of states has been obtained by employing 19 selected k-points in the irreducible part of the Brillouin zone with a Gaussian broadening of 0.015 Ry. The peak at the bottom of the valence band originates from the Ga-3d states.

6.2(b) Random Alloys :

In $Ga_{1-x}Al_xAs$ alloys , in some experimentally studied samples one may assume the occurrence of the disordered structures minimizing a random atomic configuration. Considering the statistical mechanical distributions of the disordered structures may simulate the properties of the disordered alloy. For a detailed information of the method used, please refer to chapter-IV.

We have calculated the lattice constants and the band gaps for the random alloys at different concentrations of Al which are shown in Table 6.1 and Table 6.2 (and Fig. 6.5), respectively. The calculated lattice constant for the random $Ga_{1-x}Al_xAs$ alloys shows an irregular behaviour with the concentration of Al in contrast to a regular linear behavior seen earlier for the ordered alloys.

6.2(c) Band Gap:

The band gap energies of the ordered and the random $Ga_{1-x}Al_xAs$ alloys after including SEC for different values of x are presented in Table 6.2 and in Fig. 6.5. For the random alloys, both the direct and indirect band gaps have been calculated . *Delgado et al* [80] have measured the indirect band gap of $Ga_{1-x}Al_xAs$ alloys in the concentration range, x = 0.48 to 0.90 and the direct band gap by observing low temperature photo-luminescence(PL). Their results are also included in Fig. 6.5. The other data is by *Monemar et al* [79] who have measured the band gaps for these alloys ; the direct band gap in very small concentration range of x = 0.24 to 0.40 and the indirect gap in the whole concentration range by observing the absorption and PL spectra . The measured values show a quite linear variation of the band gap with x alongwith a very small bowing. The calculated

values for both the direct and indirect band gaps also reveal small bowing. A crossover from the direct to indirect band gap is seen below x = 0.375 which is quite near to the measured value of 0.35. In the concentration range where the experimental data is available i.e., from x = 0.24 to 0.40, the calculated values for the direct band gap for the ordered alloys are in excellent agreement with the measured data. Similarly , the present values obtained for the indirect band gap for the ordered alloys in the full concentration range of x = 0.0 to 1.0 are also in very good agreement with the experimental data. Our results support the occurrence of the ordered structures in the grown up samples studied by different groups.

FIG. 6.3 Electronic dispersion curves for the ordered $Ga_{1-x}Al_xAs$ alloys for (a)x = 0.00, (b) x = 0.125, (c) x = 0.25, (d) x = 0.375, (e) x=0.50, (f) x = 0.625, (g) x= 0.75, (h) x= 0.875 and (I) x= 1.00.

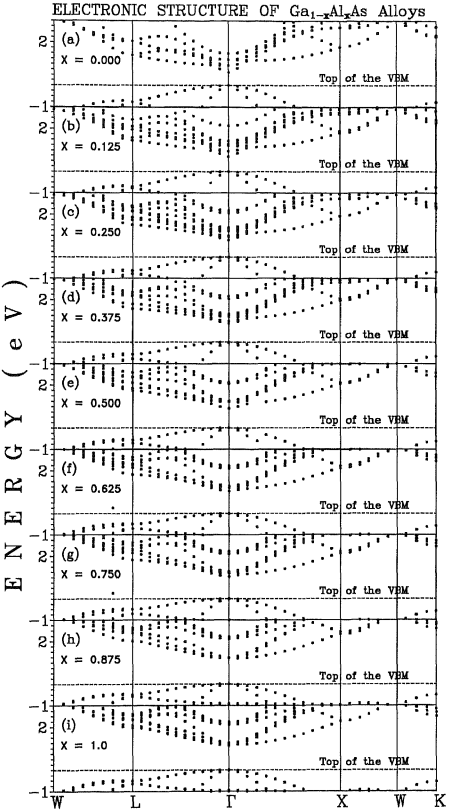
ELECTRONIC STRUCTURE OF $Ga_{1-x}Al_xAs$ Alloys
ENERGY (eV)
(a)
X = 0.000
(b)
X = 0.125
(c)
X = 0.250
(d)
X = 0.375
(e)
X = 0.500
(f)
X = 0.625
(g)
X = 0.750
(h)
X = 0.875
(i)
X = 1.0
Top of the VBM
2
−1
W
L
Γ
X
W
K

FIG. 6.4 The total density of states for the ordered $Ga_{1-x}Al_xAs$ alloys for (a) x = 0.00, (b) x = 0.125, (c) x = 0.25, (d) x = 0.375, (e) x = 0.50, (f) x = 0.625, (g) x = 0.75, (h) x = 0.875 and (I) x = 1.00.

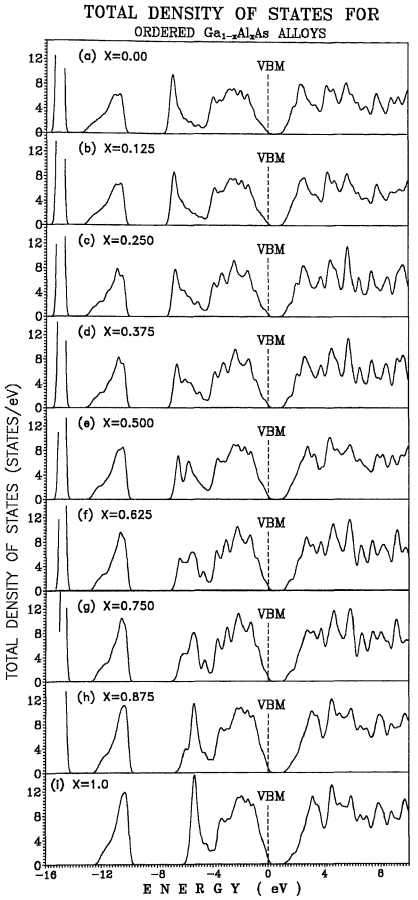
TOTAL DENSITY OF STATES FOR
ORDERED $Ga_{1-x}Al_xAs$ ALLOYS
(a) X=0.00
(b) X=0.125
(c) X=0.250
(d) X=0.375
(e) X=0.500
(f) X=0.625
(g) X=0.750
(h) X=0.875
(I) X=1.0
VBM
TOTAL DENSITY OF STATES (STATES/eV)
0
4
8
12
−16
−12
−8
−4
0
4
8
E N E R G Y (eV)

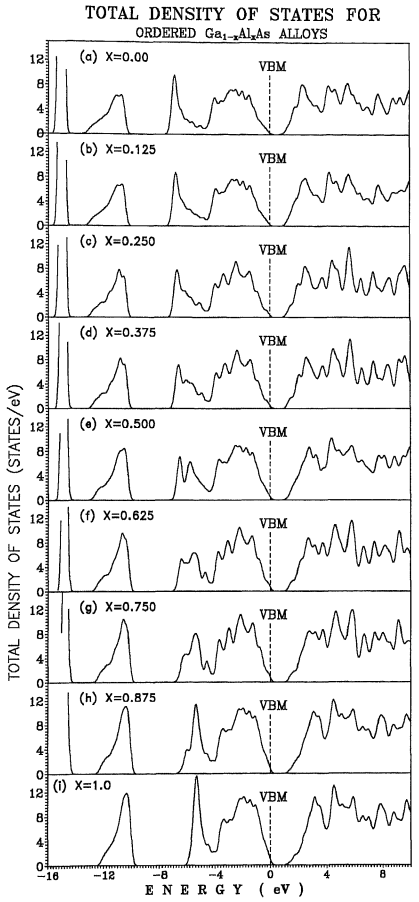
TOTAL DENSITY OF STATES FOR
ORDERED $Ga_{1-x}Al_xAs$ ALLOYS
(a) X=0.00
(b) X=0.125
(c) X=0.250
(d) X=0.375
(e) X=0.500
(f) X=0.625
(g) X=0.750
(h) X=0.875
(i) X=1.0
VBM
TOTAL DENSITY OF STATES (STATES/eV)
0
4
8
12
−16
−12
−8
−4
0
4
8
E N E R G Y (eV)

Table 6.2.

Variation of band gap including self-energy correction in the ordered and the random $Ga_{1-x}Al_xAs$ structures and comparison with the experimental data and other calculations. All energies are measured in eV.

SYSTEM (X)	PRESENT RESULTS WITH SELF ENERGY CORRECTION				OTHER CALCULATION (WITHOUT SELF-ENERGY CORRECTION)	EXPT.	GW
	Structures						
	Ordered		Random				
	Direct	Indirect	Direct	Indirect			
0.000	1.55	2.01	1.55	2.01	0.60 (direct)[a]	1.52[b] (direct) 2.01[c] (indirect)	1.3[d] (direct)
0.125	1.65	2.04	1.61	2.03			
0.250	1.90	2.10	1.70	2.04			
0.375	2.08	2.00	1.80	2.05			
0.500	3.05	2.11	2.50	2.13			
0.625	3.09	2.16	3.14	2.22			
0.750	3.12	2.20	3.16	2.23			
0.875	3.15	2.24	3.18	2.24			
1.000	3.21	2.25	3.21	2.25	2.07 (direct)[a] 1.33 (indirect)[a]	2.25[b] (indirect)	

a. *Zhu and Louie* 1991, (Model dielectric Function) [Ref. 63].

b. *Hellwege* 1982, [Ref. 64].

c. *Monemar* 1976, [Ref.79].

d. *Rubio and Cohen* 1995 (GW approximation), [Ref.45].

FIG. 6.5 Variation of energy band gap with concentration x for the direct and indirect gaps for the ordered and random $Ga_{1-x}Al_xAs$ alloys. The continuous curves are the extrapolated curves. The calculated direct and indirect band gaps for the ordered structures are shown by (●●●●●) and (▲▲▲▲▲), respectively. The calculated direct and indirect band gaps for the random alloys are denoted by (▪▪▪▪▪) and (×××××), respectively. The experimental data for the direct and the indirect band gaps by *Monemar et al* [79] are depicted by (□□□□□) , and (ΔΔΔΔΔ), respectively. The indirect band gaps measured by *Delgado et al* [80] are shown by (○○○○○) .

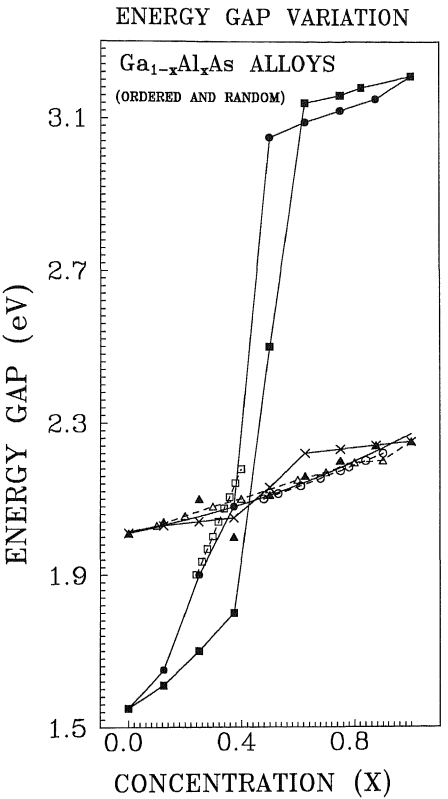
ENERGY GAP VARIATION
Ga1-xAlxAs ALLOYS
(ORDERED AND RANDOM)
3.1
2.7
2.3
1.9
1.5
ENERGY GAP (eV)
0.0
0.4
0.8
CONCENTRATION (X)

Chapter-VII

GaAs/GaN (001) SUPERLATTICE

GaAs/GaN (001) SUPERLATTICE

7.1 INTRODUCTION:

In the recent past, first-principles supercell calculations have been reported for the valence band offsets (VBO) for a number of superlattices [24, 81-89]. In most of the cases [90], the systems considered use the lattice-matched interfaces and the atomic positions in the interfacial region were assumed to retain their perfect three-dimensional lattice structures. This situation may be true for the interfaces formed from the chemically similar constituents. However, for interfaces built from the different types of the constituent semiconductors such as having different lattice parameters or chemical atoms (II-VI and III-V compounds), the interfacial atoms may relax and occupy positions different from the perfect lattice ones. It may result in appreciable changes in the values of the valence band offsets.

The III - V GaAs / GaN superlattices which have wide band gaps are very promising for the development of the opto-electronic devices in the visible and the ultraviolet regions of the electromagnetic spectrum with photon energies spreaded in a wide energy range. Band gap tuning is possible by forming alloys of the compounds with gaps of desired ranges. Quite recently *Ding et al* [91] have measured the valence band discontinuity at a cubic GaN/GaAs (001) heterojunction by using synchroton - radiation photoemission spectroscopy.

The lattice parameters of the pure GaAs and GaN differ by 20%. Epitaxial growth of a superlattice with alternating GaAs and GaN layers will contain built-in elastic strain which can be named as strained-layer superlattice. The strain may have two components: hydrostatic and shear. The shear components will lower the symmetry of the system and split the highly degenerate electronic levels which may cause drastic changes in the values of the energy gap. The strain dependence offers a convenient method for optimizing the electronic structure of the superlattices.

In the present chapter, we report the results for the valence band offsets for the GaAs / GaN superstructures with a (001) geometry and also the interface states after determining the atomic relaxations by minimization of the total energy for the supercells of (10+10) layers or (5+5) bilayers. Each bilayer is comprised of one set of cation and anion layers. For the details of the method, we refer to earlier papers [92 - 98].

7.2 CALCULATIONS

7.2(a) *Bulk GaAs And GaN* :

The LMTO basis functions for the atoms were chosen as Ga (4s,4p,4d), As (4s,4p,4d) and N(2s,2p,3d). Empty spheres were assumed to be present at the vacant sites and a set of appropriate (spd) states were chosen for them. The core electrons are not frozen but are relaxed in the sense that the core electron charge density is recalculated in each iteration in the self-consistent loop. We have not considered the spin-orbital coupling but have generated the self-consistent supercell potentials by considering the scalar relativistic effects. It has been observed [99-100] that spin orbit coupling to lowest order splits only the bands and does not change appreciably the relative positions of band centers. The cohesive properties are hardly affected.

7.2(b) *Superlattices* :

We have computed the electronic structure of the 20 layer superlattice (each layer contains one atom) by repeating a supercell containing 20 real atoms and 20 empty spheres on a fcc lattice.

The lattice mismatch between GaAs and GaN is about 20% and there is a possibility of achieving different types of strained superlattices (SSL) in their growth experiments. We consider the two geometries depending on the lattice

constant parallel to the interface (a) $a_{||}$ = 5.075 Å ("free- standing" interface) and (b) $a_{||}$ = 5.65 Å (i.e., GaAs unstrained).

We first perform calculations for the bulk compounds separately using the 40 atom supercell and determine the appropriate minimum energy interlayer distances for each compound. A value of the lattice constant parallel to the interface namely, the in-plane lattice constant $a_{||}$ is chosen in accordance with one of the above mentioned two geometries and the interlayer spacing of the (10+10) layer set was varied. The crystal energy is minimized to obtain an appropriate interlayer spacing to be used.

The valence band offset (VBO) is defined as the difference $\Delta E_v = E_v^R - E_v^L$, where E_v^L is the valence band maximum (VBM) of the compound on the left side (considered to be lying at lower energy) and that E_v^R as VBM of the compound on right side of the interface. The valence band maximum for each compound is determined for these layers in the superlattice which lie deep into the layer set of the compound.

The potentials at these middle layers on both sides of the interface should converge with the number of layers chosen in the supercell. This convergence has been tested by us by performing calculations for (7+7) bilayers. The results remain unchanged. *Christensen* [99] has also found that the (5+5) bicells yield almost the same VBO values as (7+7) bicells.

7.2(c) Atomic Relaxations And Valence Band Offset :

In the actual calculation of the valence band offset, for each compound, a bulk crystal is generated by repeating the two atom unit cell (containing cation and anion) on a fcc lattice which is later on distorted (if required) to have the appropriate planer lattice constant $a_{||}$ corresponding to the geometry of superlattice. A normal lattice constant $a_{\perp}$ is obtained by keeping the volume of unit cell unchanged. The crystal potential of the corresponding middle layer (assumed to be

having bulk like properties) of the 5 bilayer set of the superlattice is taken over to the above bulk crystal. A band structure calculation is then performed for each bulk crystal and the valence band maximum (VBM) is determined.

In a self-consistent calculation of the interface, the potentials of constituents are adjusted properly to each other and there exists, in general, a relative potential difference between the potentials of the middle layers of the two compounds. This difference in the potentials called the dipole contribution is added to the difference of the (VBM) obtained above for the bulk.

We determine two types of the VBO's (i) an averaged $\Delta E_{v,av}$ which is the difference for the constituent compounds obtained after taking weighted average of the VBM derived states for a compound that are split by the shear and (ii) ΔE_v , equal to the difference in the energies of the highest occupied VBM states.

7.2(d) Interface States :

The interface GaAs / GaN represents a two-dimensional defect when one moves from one material to another normal to the interface. The planar defect will thus induce some interface states; resonance and/or localized ones which would be characterized by the decay of the wavefunction either on both sides of the interface or on one side. The quantities like the valence band offset is not expected to be determined by the averaged bulk properties of the two different materials. It may be noted that all the model theories for estimating the valence band offsets which are based on the bulk properties of the constituents may no longer be true in real systems. A calculation is made for the interface states which are identified by extracting those states for which the values of the eigen vectors decrease away from the interface region.

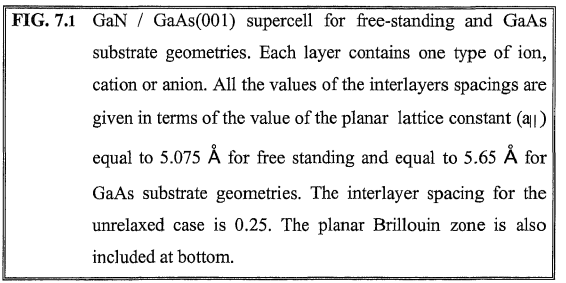

FIG. 7.1 GaN / GaAs(001) supercell for free-standing and GaAs substrate geometries. Each layer contains one type of ion, cation or anion. All the values of the interlayers spacings are given in terms of the value of the planar lattice constant ($a_{||}$) equal to 5.075 Å for free standing and equal to 5.65 Å for GaAs substrate geometries. The interlayer spacing for the unrelaxed case is 0.25. The planar Brillouin zone is also included at bottom.

GaAs/GaN Superlattice

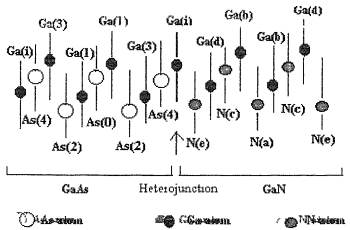

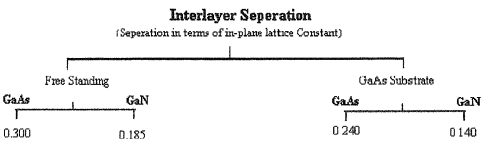

(b) Brillouin Zone for GaAs GaN Superlattice

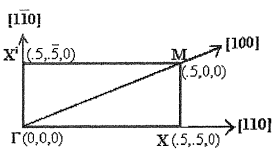

FIG. 7.2 Electronic structure for the (5+5) (001) bilayer slabs of pure (a) GaAs (b) GaN in the free- standing geometry and for (c) GaAs (d) GaN for the GaAs-substrate geometry.

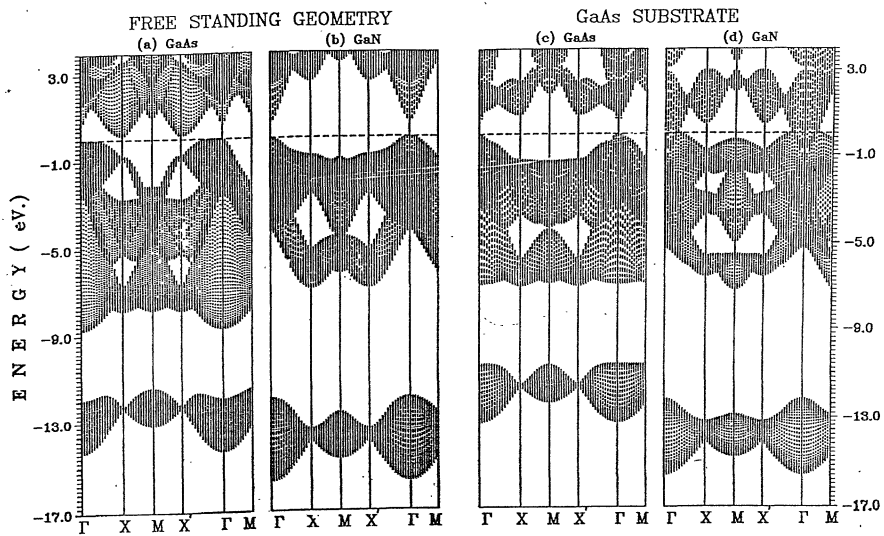
STRAINED PURE GaAs AND GaN (001) SLABS
FREE STANDING GEOMETRY
GaAs SUBSTRATE
(a) GaAs
(b) GaN
(c) GaAs
(d) GaN
ENERGY (eV.)
3.0
-1.0
-5.0
-9.0
-13.0
-17.0
Γ X M X' Γ M

FIG. 7.3 Electronic structure and interface states for the GaN / GaAs (001) superlattice for the (i) free-standing geometry [Figs. (a) & (b)] and (ii) GaAs - substrate geometry [Figs. (c) & (d)], respectively.

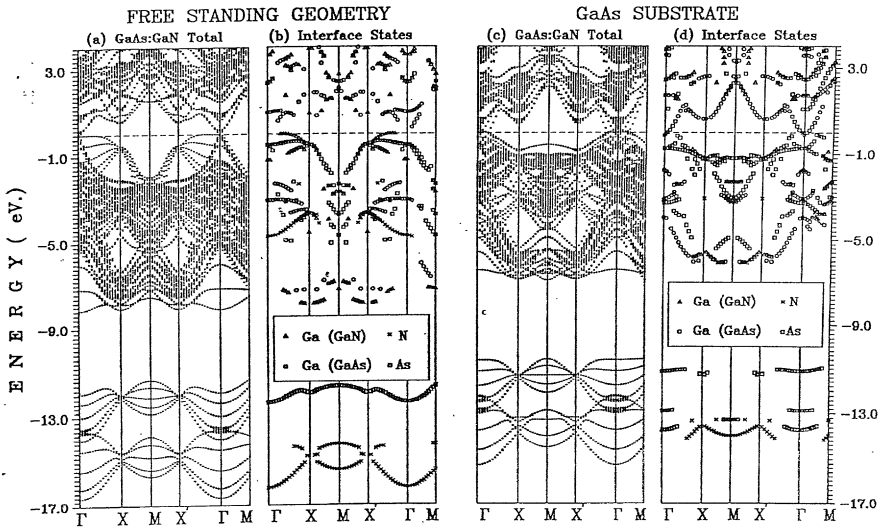
GaAs:GaN (001) HETEROJUNCTION
FREE STANDING GEOMETRY
GaAs SUBSTRATE
(a) GaAs:GaN Total
(b) Interface States
(c) GaAs:GaN Total
(d) Interface States
ENERGY (eV.)
3.0
−1.0
−5.0
−9.0
−13.0
−17.0
Γ X M X Γ M
Ga (GaN) N
Ga (GaAs) As

7.3 RESULTS

7.3(a). *Free Standing* GaAs / GaN (001) *Superlattice:*

For the free standing superlattice, $a_{||} = 5.075$ Å, for GaAs, the interlayer spacing increases by 0.05 in the units of lattice parameter ($a_{||}$) and in GaN, it decreases by 0.065. These spacings have been depicted in Fig. 7.1(a).

(i) *Electronic Structure*:

The planer Brillouin zone for the (001) interface is shown in Fig. 7.1(b). The symmetric points are Γ(0,0,0), X(0.5,0.5,0), X′ (0.5,-0.5,0) and M(0.5,0,0.5); all of them lie in the $\vec{k}$ -plane parallel to the interface (001).

The electronic structure for the pure strained GaAs and GaN slabs for the above obtained energy minimized interlayer spacings are depicted in Figs. 7.2(a) and 7.2(b), respectively. The total widths of the valence bands are 14.4 and 15.8 eV for GaAs and GaN, respectively. The ionic gap for GaN is much wider (-7 to -12 eV) than GaAs (-8.8 to -11.4 eV). Although, the bottom of the conduction band in both the semiconductors descend into the fundamental gap, they retain their semiconducting character ; there is no closure of energy gap. A notable feature in the case of strained GaAs is that the bottom of the conduction band appears now at the symmetry point X in contrast to the unstrained GaAs where it appears at Γ - point as may be seen in Fig.7.2(c).

In Fig. 7.3(a), we include the electronic structure of the free standing strained GaN/GaAs (001) superlattice. A comparison with Fig. 7.2 reveals some notable features. In the heterojunction, there is an overall downward shift of the electronic states in GaN by about 1.6 eV with respect to that of GaAs. The low lying s-like orbital states of GaAs and GaN are almost separated. The total width of the valence band for the heterojunction increases to about 17.0 eV . The width of the ionic gap is similar to that of pure strained GaAs slab and the upper part of the

ionic gap is composed mainly of the GaAs states. Also, the top of the valence band of the heterojunction originates mainly from the GaAs electron states. On the other hand, the GaN states descend into the fundamental gap filling it completely making it metallic. A similar closure of gap in local density approximation has been observed in the ordered $GaAs_{1-x}N_x$ alloys in the concentration range x = 0.125 to 0.625 by our group [101]. However, the many body effects such as considered in the GW approximation will raise the conduction states and may open the gap. The VBM's however, will remain unaffected.

(ii) *Electron Density Of States :*

Calculations for the electronic density of states were performed for the GaAs / GaN superlattice without relaxing the atoms of the heterojunction. The total density of states (DOS) is shown in Fig. 7.4(a) and the projected electronic density of states at the atoms of the different layers in Fig.7.5(a). The metallic behaviour of the GaN/GaAs(001) superlattice is evident from Fig.7.4 , where the fundamental gap contains a small density in the lower part of the gap. A perusal of Fig.7.5(a) reveals that there is enhanced Ga -s -induced density at the bottom of the CBM at the interface atom Ga_i. Dominant contributions from the As-p orbitals appear at VBM in the interfacial region. The projected density at the N- atoms is quite small in the vicinity of the energy gap. The projected density at the interfacial Ga atom has contributions from the hybridized As - s and the N-s orbitals at the bottom of the valence band.

(iii) *Valence Band Offsets:*

We allow all the atoms to relax by different magnitudes in accordance with the calculated forces and perform self-consistent calculations for the relaxed structures. We studied the variation of the total energy and obtained the energy minimum for a slight displacement of the interfacial Ga layer towards the As layer with 0.15% and -0.21% changes in the GaN and GaAs bond lengths, respectively.

The calculated values for the two types of VBO's as defined earlier are presented in Table 7.1 for different magnitudes of atomic displacements at the interface. It may be noted that the different magnitudes of atomic displacements give rise to different changes in the GaAs and GaN bond lengths. The values for ΔE_v are larger than those of $\Delta E_{v,av}$. This large difference occurs because of the occurrence of quite large shear strain in the heterojunction which splits the three -fold bulk VBM state significantly. For the minimum energy configuration the two values of band offsets are $\Delta E_{v,av} = 1.86$ eV and $\Delta E_v = 2.72$ eV.

We observe that the value of the offset increases with decrease (increase) in the interface GaN (GaAs) bond length. For a combined changes in the bond lengths of GaN and GaAs at the interface by 0. 54% and - 0.84% respectively. $\Delta E_{v,av8}$ or ΔE_v decreases by 0.11 eV i.e. by 6%.

In the minimum energy configuration of the relaxed atoms, we depict the levels at the VBM for GaAs and GaN on the two sides of the interface in Fig. 7.6(a). In order to investigate the effect of the interfacial GaN bond length change on the valence band offset, we have made a separate calculation. While keeping intact the GaAs bond length in the heterojunction, we shift all the layers lying on the GaN side except the interfacial Ga layer. We find that the VBO increases (decreases) with the shortening (lengthening) of the GaN bond length and these changes are doubled when the changes in both the GaAs and GaN bond lengths are considered .

(iv) *Interface States* :

The interface states have been calculated for the minimum energy GaAs / GaN superlattice. The states having the magnitude of eigen vector > 0.3 on the interface atoms and for a decay factor of 0.10 i.e. , the states for which the modulus of the eigen vector of one type of atoms decreases by 10% or more away from the interface, are shown in Fig. 7.3(b), along some symmetric directions in

the different energy regions. Most of the states show a bulk like behaviour in one of the host compounds but decay on the other side of the interface.

The decay behaviour of some interface states are depicted in Fig. 7.7(a) for the free standing interface. The conduction states in the vicinity of the energy gap originate from the sp-hybridized orbitals of Ga and N atoms and practically do not enter the GaAs layers but decay slowly to-wards GaN layers. The interface states at and near VBM are the mixed As-p and Ga - p orbitals decaying fast on both sides of interface. The Ga-p induced interface states appearing in the range - 1.0 eV – -5.0 eV decay only to-wards the GaAs layers. The interface states lying in the energy region -12.0 to -13.5 eV originate mainly from the As -s and N -s orbitals and decay only to-wards the GaAs side. The interface states lying at the bottom of the valence band (E = - 16.3 eV) originate mainly from the N-s orbitals and decay on both sides of the interface.

7.3(b) *GaAs Substrate GaN(001) Superlattice* :

Now, the GaN is deposited on the GaAs substrate so that the value of the lattice constant parallel to the interface is equal to that of the host GaAs i.e., $a_{||}$ = 5.65 Å. The two separate calculations for finding the energy minimum of the 10 bilayer unit cell each for GaAs and GaN give the interlayer spacings as 0.24 and 0.14 (in the units of $a_{||}$), respectively. A value of 0.24 smaller than the experimental value of 0.25 for the interlayer spacing in GaAs is obtained because of the occurrence of the energy minimum for the bulk GaAs at a smaller lattice volume.

For this geometry, the forces on the atoms are quite similar to those seen for the free-standing geometry both qualitatively and quantitatively. Similar to the free standing case, the atoms in the various layers are relaxed in the direction of the forces experienced by them by overall different magnitudes and self-consistent calculations are performed.

The electronic structure for the unstrained pure GaAs and the strained pure GaN slab is presented in Figs. 7.2(c) and 7.2(d), respectively. The states lying below the ionic gap remain unaffected with a change in the in - plane lattice constant. However, there are notable changes in the upper part of the valence band of the GaN. For a larger value of $a_{||}$, there occur more states in the vicinity of the VBM. Also, the Ga-induced states descend into the fundamental gap and enter the valence band.

The electronic structure for the GaN/GaAs (001) heterojunction in the GaAs- substrate geometry is shown in Fig. 7.3(c). The total density of states and the projected ones are presented in Figs. 7.4(b) and .7.5(b), respectively. The total density of states for the two different geometries are quite similar . There are states in the fundamental gap region.

The calculated values of the two types of VBO'S for the various atomic configurations are presented in Table 7.2. In general, the magnitude of $\Delta E_{v,av}$ are much larger then those for ΔE_v for the GaAs substrate geometry (GSG) in contrast to the free standing geometry (FSG) where the reverse is true. The values of the two types of VBO'S for the minimum energy configuration are $\Delta E_{v,av} = 1.32$ eV and $\Delta E_v = 0.67$ eV. The variation in the values of VBO'S is quite large and is strongly sensitive to the atomic displacements. For 0.199 % elongation and -0.442% contraction in the bond lengths of GaN and GaAs, respectively, the VBO decreases by -0.11eV i.e. by 8% . For the minimum energy configuration the positions of the energy levels at the interface are shown in Fig. 7.6(b).

The interface states for the GaAs substrate GaN (001) heterojunction has been depicted in Fig. 7.3(d). The interface states are quite similar to those seen for the free standing geometry. The lowest states decay to-wards the GaAs side of the interface and are bulk like in GaN. The interface states near -11 eV decay towards the GaAs layers and practically do not enter the GaN side. The states in the vicinity of the top of the ionic gap originate from Ga -s orbitals and decay towards the GaAs. The states near - 3.3 eV arise from the p- orbitals of anions and are bulk like in GaN and decay to-wards the GaAs side. In the energy region - 1.7 eV the

interface states are the mixed s - p orbitals which decay towards the GaN side but remain bulk like in GaAs layers.

7.4 Effect Of Atomic Relaxation On Valence Band offsets:

The VBO shows dependence on the position of the interfacial Ga atoms, Gai. The interatomic separation within the Ga_i layer is smaller in FSG as compared to that of GSG by about 9% and the value of VBO is enhanced by about 40%. In GSG, the in- plane shear strain in GaN layers is about 46% while the GaAs layers remain unstrained. On the other hand, in FSG, the in-plane shear strains are present both in the GaAs and GaN layers of the order of 23%. For contraction within GaAs layers and elongation within the GaN layers, the values of VBO'S are higher. The shear strains split the three- fold degenerate VBM of the bulk by a magnitude depending upon the amount of strain. The values of ΔE_v reveal (Tables 7.1& 7.2) very large changes with strain. These changes become subtle for the weighted average of the split VBM states.

The layers are polar, each layer containing one type of ions. The shift of the interface layer Ga_i to-wards (away) the GaAs (GaN) bulk layers decreases VBO'S. Small changes in the bond lengths caused by atomic displacements normal to the layer incur large changes in the values of VBO'S. The observed changes in VBO'S are seen to be greater in GSG than in FSG. For 0.2 to 0.4 % changes in bond length in GSG, the VBO changes by 8% whereas for 0.5 to 0.8% changes in bond lengths in FSG, VBO changes by 6% only.

In the experimental measurement GaN layers were deposited on the GaAs substrate our calculated value 1.32 eV for the GaAs substrate and 1.86 eV for the free standing geometry is quite near to the measured volume of 1.7 – 1.8 eV. The measured sample may have somewhat different atomic configuration than the ideal configuration considered in the present calculation. A change of bond length of the order of 1 to 2% may enhance the VBO approximately by 30 % – 40. *Bellaiche et al* [102] after using LAPW method have reported a value of 2.18 to 2.28 eV for the band offset for relaxed atoms which is on the higher side.

TABLE 7.1

VALENCE BAND OFFSET (in eV) FOR GaN/GaAs(001) SUPERLATTICE IN FREE STANDING GEOMETRY FOR DIFFERENT SETS OF CHANGES IN GaAs AND GaN BOND LENGTHS.

% change in bond length		Band Offsets	
GaAs	**GaN**	$\Delta E_{av,v}$	ΔE_v
0.84	- 0.55	1.98	2.83
0.00	0.00	1.89	2.75
*** -0.21**	**0.15**	**1.86**	**2.72**
-0.86	0.54	1.78	2.64

* Minimum energy of Superlattice

TABLE 7.2

VALENCE BAND OFFSET (in eV) FOR GaAs SUBSTRATE GaN/GaAs (001) SUPERLATTICE FOR DIFFERENT SETS OF CHANGES IN GaAs AND GaN BOND LENGTHS.

% change in bond length		Band Offsets	
GaAs	**GaN**	$\Delta E_{av,v}$	ΔE_v
0.446 -	-0.197	1.36	0.71
***0.000**	**0.000**	**1.32**	**0.67**
- 0.442	0.199	1.21	0.56

* Minimum energy of Superlattice

FIG. 7.4 Total electron-density of states for the GaN/GaAs(001) superlattice for the (a) free standing geometry and (b) GaAs - substrate geometry.

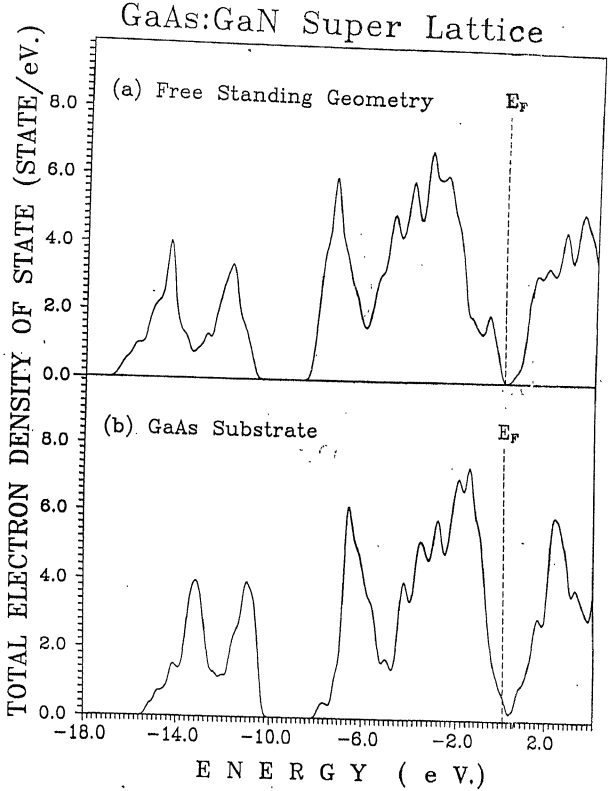
GaAs:GaN Super Lattice
(a) Free Standing Geometry
E_F
(b) GaAs Substrate
E_F
TOTAL ELECTRON DENSITY OF STATE (STATE/eV.)
0.0
2.0
4.0
6.0
8.0
−18.0
−14.0
−10.0
−6.0
−2.0
2.0
E N E R G Y (e V.)

FIG. 7.5 Projected electron density of states (PDOS) for the cation Ga and anions As and N lying in the different layers of the GaN/GaAs(001) superlattice for the (a) free standing geometry and (b) GaAs - substrate geometry.

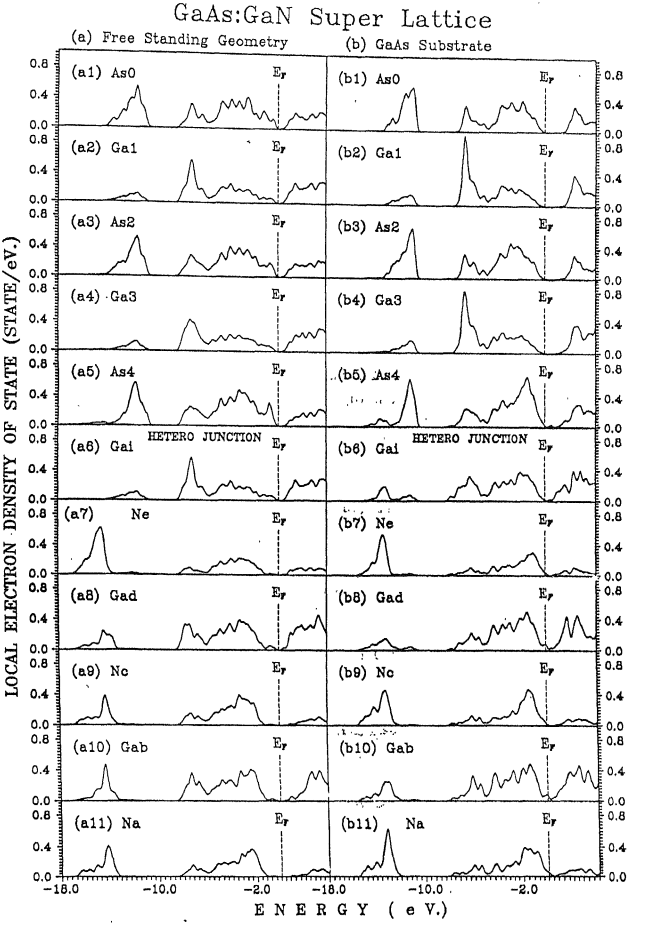
GaAs:GaN Super Lattice
(a) Free Standing Geometry
(b) GaAs Substrate
(a1) As0
(b1) As0
(a2) Ga1
(b2) Ga1
(a3) As2
(b3) As2
(a4) Ga3
(b4) Ga3
(a5) As4
(b5) As4
HETERO JUNCTION
(a6) Gai
(b6) Gai
(a7) Ne
(b7) Ne
(a8) Gad
(b8) Gad
(a9) Nc
(b9) Nc
(a10) Gab
(b10) Gab
(a11) Na
(b11) Na
E_F
LOCAL ELECTRON DENSITY OF STATE (STATE/eV.)
0.0
0.4
0.8
-18.0
-10.0
-2.0
E N E R G Y (e V.)

FIG. 7.6 Energy levels in eV for GaN and GaAs at the valence band maximum on the two sides of the interface for (a) the free standing geometry (b) GaAs as substrate.

GaN\GaAs SUPERLATTICE

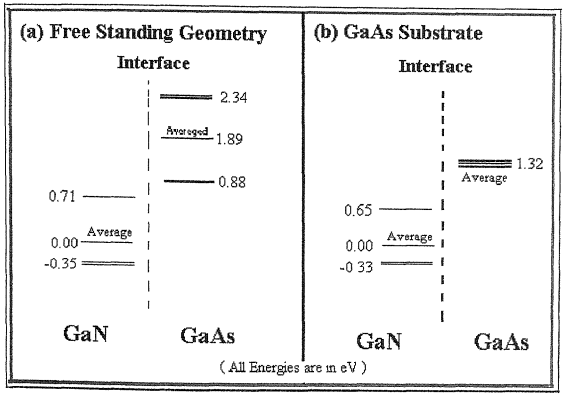

FIG. 7.7 Variation of magnitude of eigen vectors on the atoms lying on the various layers for (a) free standing geometry and (b) GaAs-substrate geometry.

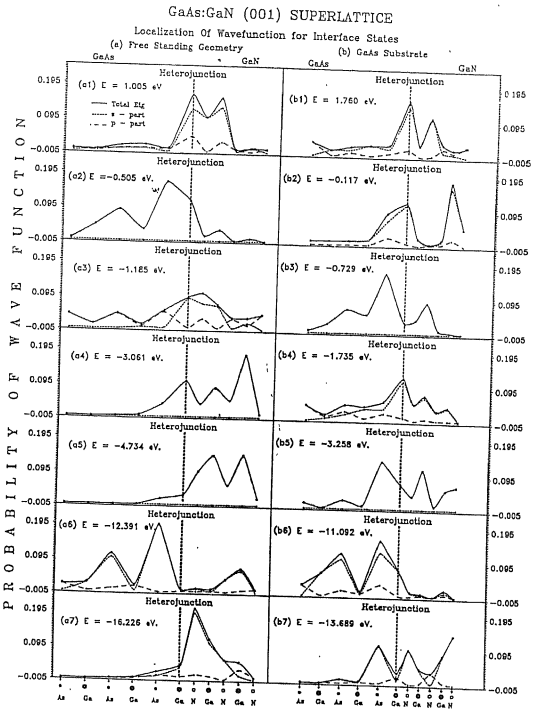
GaAs:GaN (001) SUPERLATTICE
Localization Of Wavefunction for Interface States
(a) Free Standing Geometry
(b) GaAs Substrate
GaAs
GaN
Heterojunction
(a1) E = 1.005 eV
Total Eig
s - part
p - part
(b1) E = 1.760 eV.
(a2) E =-0.505 eV.
(b2) E = -0.117 eV.
(a3) E = -1.185 eV.
(b3) E = -0.729 eV.
(a4) E = -3.061 eV.
(b4) E = -1.735 eV.
(a5) E = -4.734 eV.
(b5) E = -3.258 eV.
(a6) E = -12.391 eV.
(b6) E = -11.092 eV.
(a7) E = -16.226 eV.
(b7) E = -13.689 eV.
0.195
0.095
-0.005
PROBABILITY OF WAVE FUNCTION
As Ga As Ga As Ga N Ga N Ga N

Chapter-VIII

ZnS/ZnSe (110) SUPERLATTICES

ZnS/ZnSe (110) SUPERLATTICES

8.1 INTRODUCTION:

The II-VI superlattices, which have wide band gaps, are very promising for the development of the opto-electronic devices in the visible and the ultraviolet regions of the electromagnetic spectrum with photon energies spreaded in a wide energy range. Band gap tuning is possible by forming alloys of the compounds with gaps of desired ranges.

Multilayer systems formed from ZnS and ZnSe have been investigated. Multilayer structures containing alternate layers of ZnS_xSe_{1-x} and ZnSe compounds have potential applications in the development of blue-light emitting diodes and blue lasers. The lattice parameters of the pure ZnS and ZnSe differ by 4.5%. Epitaxial growth of a superlattice with alternating ZnSe and ZnS layers will contain built-in elastic strain which can be named as strained-layer superlattice. Further, a variation of the composition x in the ZnS_xSe_{1-x} alloys allows a chemical tuning of gaps as well as the elastic strain. The strain may have two components: hydrostatic and shear. The shear components will lower the symmetry of the system and split the highly degenerate electronic levels which may cause drastic changes in the values of the energy gap. The above strain dependence on x offers a convenient method for optimizing the electronic structure of the superlattices.

Yokagawa [103], have grown successfully the ZnS/ZnSe strained-layer superlattices by using a low pressure vapor-phase expitaxial method. More recently, *Shahzad*, [104] grew several ZnSe/ ZnS_xSe_{1-x} strained layer superlattices (SLSL) by employing molecular-beam epitaxy and performed photoluminescence experiments. For x = 0.19, they measured the valence band offset (ΔE_v) equal to 0.109 eV. Their prepared structure may be considered approaching to a free standing superlattice.

In an earlier paper, [92] *Agrawal et al.* investigated the influence of structural relaxation on the electronic and atomic structures and the valence band offset (VBO) of the semiconductor-semiconductor interfaces; lattice mismatched II-VI ZnS / ZnSe (001) and the lattice matched combination of II-VI and III-V ZnTe / GaSb (110) superlattices. In this calculation, the total energy was minimized for supercells of (3+3) layers and the resulting geometry was transferred to a (5+5) supercell to determine the VBO. In the case of polar Zn / ZnSe interface, the VBO changes significantly i.e., by about 0.35 eV as the interface layer Zn atom moves from unequal interface ZnS and ZnSe bonds to equal bond lengths. The Zn displacement for the minimum energy superlattice was about 0.8% of the in-plane lattice constant. The change in the averaged VBO with strain is determined entirely by the strain splitting of the valence band maximum. The calculated value of VBO for a particular geometry i. e., the free-standing one was 0.53 eV which is in an excellent agreement with the extrapolated measured value of 0.52 eV by *Sahzad et al* .

For the ZnTe / GaSb(110) superlattice, a value of 0.69 eV was obtained for the relaxed geometry in contrast to the measured value of 0.34 eV by *Wilke & Horn* [*11*]. The authors pointed out that the discrepancy might arise because of mixing and segregation at the experimentally studied interface.

Lambrecht et al [105] have calculated the band offsets for a number of heterojunctions by using a restricted treatment of self consistency in the LMTO method in atomic sphere approximation (ASA) . Also, these authors have not investigated the presently discussed ZnS/ZnSe heterojunctions. Further, the effect of the atomic relaxation of the atoms of the different layers on the band offsets which would be investigated in the present work, have not been considered by *Lambrecht et al.*

Calculated results for the effects of the detailed atomic structure on the band offsets of ZnSe/ZnS superlattices have been reported by *Christensen and Gorczyca* [99-100] after employing LMTO in atomic sphere approximation (ASA). In the ASA scheme, one can not optimize the lattice structure by minimization of

the total energy of the system and therefore, *Christensen* used the convenient Keating model for determining the forces and the positions of the relaxed atoms. This method may work well for the superlattices formed from the atoms, which are nonionic, like Si and Ge. However, for the superlattices containing the ionic atoms like Zn, Se, S, the above scheme may be questionable. Although in the Keating model, the above work considered the Coulombian interactions to the extent that the elastic properties of the constituent pure ZnS and ZnSe were well reproduced, but the Coulomb effects on the forces caused by the large atomic rearrangements in the interfacial region may not be very well accounted for.

Very recently, *Wei and Zunger* [106] have calculated band offsets for the chalcopyrites and Zn-based II-VI alloys by using the general potential relativistic all electron linearized augmented plane wave (LAPW) method alongwith the density functional theory. For the ZnS / ZnSe (001) superlattice, they have obtained a valence band offset of 0.53 eV which is equal to the value obtained in earlier calculation [92].

In this chapter, we report the results for the valence band offsets for the ZnS/ZnSe superstructures with a different geometry i.e., (011) and also the interface states after determining the atomic relaxations by the minimization of the total energy for the supercells of (5+5) layers in contrast to our earlier results for the (001) superlattices obtained after minimizing the energy for the supercells of (3+3) layers only. A preliminary account of the work has been reported earlier [107]

8.2 CALCULATIONS

8.2(a) Bulk ZnSe And ZnS :

The chosen LMTO basis functions in the valence energy region were Zn(4s,4p,3d), Se(4s,4p,4d) and S(3s,3p,3d). In order to account for the influence of semi-core 3d-states in Se, we made a separate calculation and thus a two panel self-consistent method was employed.

The energy minimum was seen to appear at the ratio V_{calc} / V_{exp}= 0.98 for ZnSe (a = 5.59 Å) and at 0.95 for ZnS (a = 5.34 Å) which are quite encouraging. The detailed results for the energy variation, the electronic structure, the elastic constants and the frozen phonon frequencies for the bulk ZnSe and ZnS compounds have been reported in another publication [108] .

8.2(b). Superlattices :

The lattice mismatch between ZnSe and ZnS is about 4.5% and there is a possibility of achieving different types of strained superlattices (SSL) in their growth experiments. We have obtained results for the three geometries depending on the lattice constant parallel to the interface (a) $a_{||}$ = 5.59 Å (i.e., ZnSe unstrained); (b) $a_{||}$ = 5.47 Å ("free- standing" interface) and (c) $a_{||}$= 5.34 Å (ZnS unstrained).

8.3 RESULTS

8.3(a) Free Standing ZnS/ZnSe (110) Superlattice :

For the free standing superlattice, the value of the lattice constant parallel to the interface of the ZnS and ZnSe layers was chosen as the average of the lattice constants of the two host lattices i.e., $a_{||}$ = 5.47 Å . For ZnSe, the minimum energy interlayer spacing increases by $0.0075\sqrt{2}$ in the units of planar lattice parameter ($a_{||}$) and for ZnS, it decreases by $0.0125\sqrt{2}$. At the interface, the separation between the ZnSe and ZnS layers was chosen to be the average of the obtained energy minimized interlayer spacing of the two components ZnS and ZnSe. These spacing have been depicted for the free standing geometry without atomic relaxation in Fig. 8.1. Here, the atoms of the various layers are numbered by 2, 1 and 0 on the ZnSe side and by C, B and A on the ZnS side as one move away from the interface.

(i) *Electron Density Of States* :

Calculations were performed for the ZnS/ZnSe superlattice first without relaxing the atoms. The total electron density of states (DOS) after selecting 18 k-points for the first panel i.e., after ignoring the density of the quite low lying 3d states of Se is shown in Fig. 8.2.

With a motivation to see the variation of local density of states at the atoms of the different layers, we present the local density of states at different atoms for the free standing geometry without atomic relaxation in Fig. 8.3. The local density of states at all the atoms Zn, S & Se for the superlattice is seen to be quite similar to their counter-parts in the host compounds. All the atoms possess DOS in the whole energy range of the valence band i.e. from -14 to 0.0 eV. However, the anions S and Se have dominant contributions of p-states in the upper part of the valence bands and the s-like states around -12 eV. The DOS at the cation Zn in both the host lattices ZnS and ZnSe contains dominant contributions from the d-orbitals in the limited energy range around -6.5 eV. It may be noted that, in general, the overall local density in most of the energy range at each atom is layer-independent i.e., the magnitude of local DOS at the interface layers are very much similar to those for the middle layer. However, a close observation of the figures reveals that there are extra states at the interface layer atoms specially in the lowest energy region.

(ii) *Valence Band Offsets*:

We allow all the atoms of the superlattice to relax by different magnitudes and perform self-consistent calculations for the relaxed structures and obtained the energy minimum.

FIG. 8.1 Free standing ZnS/ZnSe(110), (5,5) supercell. Each layer contains two dissimilar atoms. All the values of the interlayer spacing are given in terms of the value of the lattice constant in the plane which is 5.47 Å here. The interlayer spacing for the unrelaxed case is $0.25\sqrt{2}$ in terms of planer lattice constant.

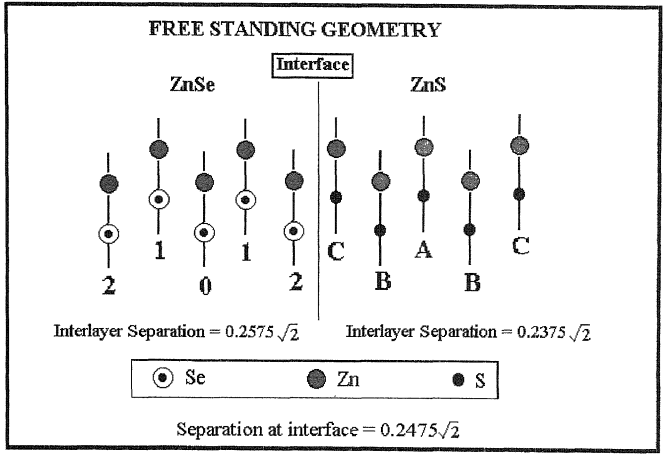
FREE STANDING GEOMETRY
Interface
ZnSe
ZnS
2
1
0
1
2
C
B
A
B
C
Interlayer Separation = 0.2575 √2
Interlayer Separation = 0.2375 √2
Se
Zn
S
Separation at interface = 0.2475√2

FIG. 8.2 Total electron-density of states for the ZnS/ZnSe (5,5) superlattice for the free standing geometry without any atomic relaxation.

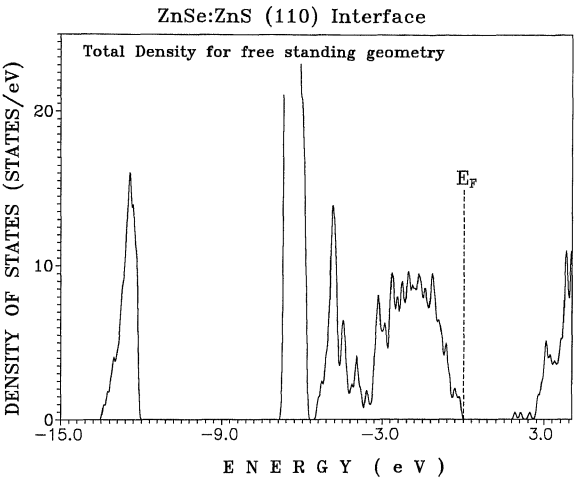
ZnSe:ZnS (110) Interface
Total Density for free standing geometry
DENSITY OF STATES (STATES/eV)
20
10
0
E_F
−15.0
−9.0
−3.0
3.0
E N E R G Y (e V)

FIG. 8.3 Projected electron density of states (PDOS) for the cation Zn and anions S and Se lying in the three different ZnS and ZnSe layers of the ZnS/ZnSe (110) superlattice for the free standing geometry without atomic relaxation. A, B and C for ZnS and 0, 1 and 2 for ZnSe denote, respectively the middle layer, the next layer and the layer forming the interface.

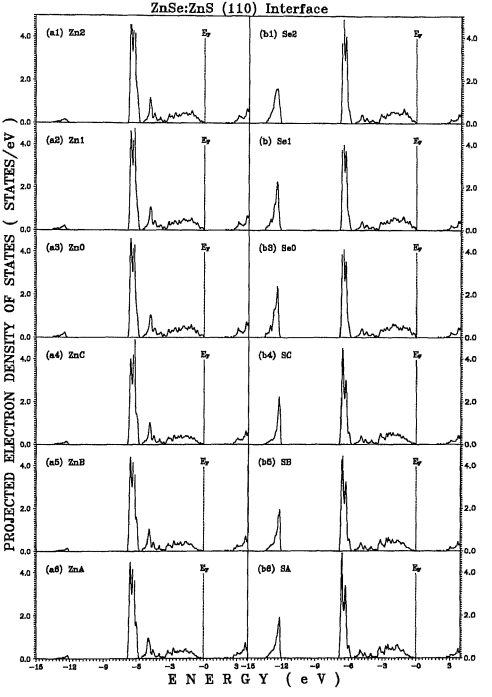
ZnSe:ZnS (110) Interface
(a1) Zn2
(b1) Se2
(a2) Zn1
(b) Se1
(a3) Zn0
(b3) Se0
(a4) ZnC
(b4) SC
(a5) ZnB
(b5) SB
(a6) ZnA
(b6) SA
E_F
PROJECTED ELECTRON DENSITY OF STATES (STATES/eV)
ENERGY (eV)

TABLE- 8.1

VALENCE BAND OFFSETS FOR ZnS/ZnSe (110) SUPERLATTICE IN FREE STANDING GEOMETRY.

S. No.	% DISPLACEMENT OF INTERFACE ATOMS **								$\Delta E_{av,v}$ (eV)	ΔE_v (eV)
	Out of the plane				Within the plane					
	ZnSe		**ZnS**		**ZnSe**		**ZnS**			
	Zn	Se	Zn	S	Zn	Se	Zn	S		
1.	0.00	0.00	0.00	0.00	0.00	0.00	0.00	0.00	0.09	0.017
2.	0.64	-0.33	0.73	-0.20	0.00	-0.20	0.67	0.00	0.22	0.150
3.*	**0.96**	**-0.50**	**1.10**	**-0.30**	**0.00**	**-0.30**	**1.01**	**0.00**	**0.27**	**0.198**
4.	1.92	-1.00	2.20	-0.59	0.00	-0.60	2.01	0.00	0.38	0.317

** in terms of bond length

* For minimum emergy configuration.

TABLE - 8.2

% ATOMIC DISPLACEMENTS IN THE VARIOUS LAYERS FOR THE MINIMUM ENERGY FREE STANDING (5+5) ZnSe/ZnS (110) SUPERLATTICE. THE LABELING OF LAYERS HAS BEEN SHOWN IN FIG. 8.1

S.No.	LAYERS OF	ATOM	ATOMIC DISPLACEMENT *		
			X	Y	Z
1		Zn (0)	0.0000	0.0000	0.0000
2		Se (0)	0.0000	0.0000	0.0000
3	ZnSe	Zn (1)	0.0000	0.0000	0.0000
4		Se (1)	0.0000	0.0000	0.0000
5		Zn (2)	0.0029	0.0029	0.0000
6	Interface atoms	Se (2)	-0.0015	-0.0015	-0.0013
7		Zn (C)	0.0034	0.0034	0.0044
8		S (C)	-0.0009	-0.0009	0.0000
9		Zn (B)	0.0000	0.0000	0.0000
10	ZnS	S (B)	0.0000	0.0000	0.0000
11		Zn (A)	0.0000	0.0000	0.0000
12		S (A)	0.0000	0.0000	0.0000

* The atomic displacements are expressed in terms of the in-plane lattice constant ($a_{||}$)

FIG. 8.4 Valence band states and their averaged ones on the two sides of the ZnS / ZnSe (110) interface with atomic relaxation for minimum energy configurations for (a) the free standing geometry (b) ZnSe as substrate and (c) ZnS as substrate.

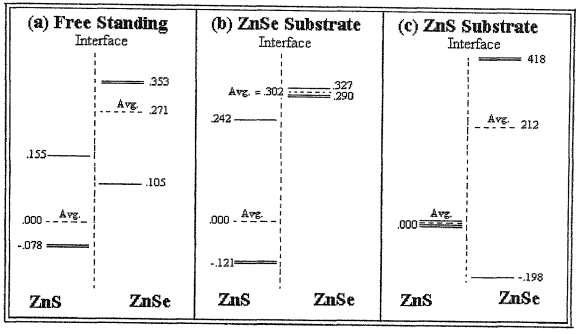
(a) Free Standing
Interface
.353
Avg.
.271
.155
.105
.000
Avg.
-.078
ZnS
ZnSe
(b) ZnSe Substrate
Interface
Avg. = .302
.327
.290
.242
.000
Avg.
-.121
ZnS
ZnSe
(c) ZnS Substrate
Interface
418
Avg.
212
Avg.
.000
-.198
ZnS
ZnSe

For the various magnitudes of the atomic displacements, the calculated valence band offsets (VBO) are depicted in Table 8.1. We observe that the value of the offset increases with the magnitude of the atomic displacements and also this increase is non-linear. The variation in the VBO is quite large which shows very strong sensitivity of the offset on the quite small atomic displacements. The superlattice total energy is seen to show its minimum value for a particular configuration of atoms. The actual atomic displacements for the minimum energy configuration are depicted in Table 8.2.

The Zn atoms of the interface ZnS layer move away from the interface whereas the interface S atoms move towards the interface. On the other hand, the interface Zn atoms of the ZnSe layer move to-wards the interface and the Se atoms away from the interface.

For the minimum energy configurations, we show the positions of the states at the valence band maximum for ZnS and ZnSe on the two sides of the interfaces in the various geometries in Fig. 8.4. The value of the VBO in the equilibrium position of the relaxed atoms is 0.27 eV. This value is nearly half of the value of $\Delta E_{v,av}$ equal to 0.52 eV seen for the ZnS/ZnSe (100) superlattice. One may thus note a very strong sensitivity of the valence band offsets on very small relaxations of atoms in these superlattices. The maximum atomic displacements in the equilibrium configuration are less than 1.1% of the bond length.

(iii) *Interface States* :

The interface states have been obtained for the minimum energy strained ZnS/ZnSe superlattice with atomic relaxation. For a magnitude probability of eigen vector equal to 0.09 or more on the interface layer and for a decay factor of 0.20 i.e. , the states for which the probability of one type of atoms decrease by 20% or more as one move away from the interface, are shown in Fig. 8.5. The planer Brillouin zone for the (110) interface is shown as insert in Fig. 8.5. The interface states arising from all the four types of atoms are shown in this figure, where we

have also included the band structures for the pure ZnS and ZnSe superlattices. The dispersion curves for ZnS and ZnSe are shown as crosses and open circle, respectively whereas the interface states are shown by the big solid circles. These states may be characterized as localized or resonance states depending on their location with respect to the bulk bands of ZnS and ZnSe. Most of the states are bulk like in one of the host compounds but die out when they cross the interface and enter the other host lattice.

It is significant to note that no interface states appears in the energy gap common to the constituent host lattices, a finding obtained earlier [109] after performing a simple calculation using the cluster Bethe lattice.

In order to see the behaviour of the wave functions of the interface states, we investigate the magnitudes of various orbitals associated with the interface states in these different energy regions. There appear interface s-p states just below the top of the valence band of the ZnS-ZnSe superlattice decaying both into the ZnS and ZnSe layers. Interface resonance states are observed in the neighbourhood of the valence band edge right upto -6.5 eV. The interface states and the bulk ZnS and ZnSe states are too crowded to give any clear picture in the energy range -5.5 to -6.9 eV. The interface states lying in the energy region -13.5 to -12.0 eV originate from the s-states of Se and S.

Almost, all the interface states decay on both sides of the interface. As typical cases we depict the variation of the probability of all the eigenvectors for some interface states on different types of atoms lying on the various layers for free standing geometry without atomic relaxation in Fig. 8.6. In the low energy region around -13.0 eV, interface states (E = -13.27eV) which reside mainly on Se and S atoms show a decaying behaviour on both sides of the interface. For the interface states lying just below the top of the valence band (E = -0.224eV), the contributions of the states are seen both on the cation Zn and anion Se, S atoms. In the conduction band region (E = 2.69 eV), the eigenvectors have dominant contributions on the Zn atoms.

The above calculation for the interface states has been performed without considering atomic relaxation arising from the formation of the interface. Inclusion of the atomic relaxation by different overall magnitudes shift the location of these interface states. It results in the high sensitivity of the values of the valence offsets on the magnitudes of the atomic displacements in the interfacial region.

8.3(b) ZnSe substrate *ZnS/ZnSe(110) superlattice :*

For this superlattice, the ZnS compound is assumed to be deposited on the ZnSe substrate so that the value of the lattice constant parallel to the interface is equal to that of the host ZnSe i.e., $a_{||} = 5.59$ Å . The two separate calculations for finding the energy minimum of the 10 layer unit cell give the interlayer spacing as $0.2400\sqrt{2}$ and $0.2275\sqrt{2}$ (in the units of $a_{||}$) for ZnSe and ZnS, respectively. A value of 0.24 smaller than the experimental value of 0.25 for the interlayer spacing in ZnSe is the result of the occurrence of the energy minimum for the bulk ZnSe at somewhat smaller lattice volume. The separation between the two layers forming the interface is chosen as an average of the interlayer separations of the two constituent layer sets and is equal to $0.234\sqrt{2}$.

Self-consistent calculations reveal that the forces on the atoms are quite similar to those seen for the free-standing geometry both qualitatively and quantitatively. Similar to the free standing case, the atoms are relaxed in the direction of the forces experienced by them and self-consistent calculations were performed.

The calculated values of the VBO'S are presented in Table 8.3. In general, the magnitude of $\Delta E_{v,av}$ are greater then those for ΔE_v and are quite non-linear similar to the free-standing geometry. A perusal of Table 8.3 shows that for the two cases i.e., for no atomic relaxation and for very small atomic relaxation, E_v is negative which means that the split state(s) at the top of the valence band of ZnS is lying higher than that of ZnSe. The variation in the values of VBO'S is quite large and is strongly sensitive to the atomic displacements.

The total energy is minimum again for about a maximum displacement of 1.83% of atoms lying at the interface. The valence band offset for the minimum configuration is 0.302 eV as depicted in Table 8.3. The values of the VBO'S are slightly higher than those seen for the free-standing geometry.

8.3(c) ZnS substrate *ZnS/ZnSe(110) superlattice :*

For the deposition of the ZnSe (strained) on the ZnS substrate (unstrained) $a_{||}$ = 5.34 Å . The interlayer spacing in minimum energy configuration is equal to $0.25\sqrt{2}$ for the ZnS layers and 0.265 for the ZnSe layers in terms of the planar lattice constant $a_{||}$ = 5.34 Å.

The calculated values of the VBO's are included in Table 8.4. In contrast to other geometries the values of for $\Delta E_{v,av}$ are now smaller then the corresponding ΔE_v 's. The energy of the superlattice supercell is seems to be minimum for a smaller atomic relaxation of interface atoms i.e., about half as compared to other geometries and the value of the band offset $\Delta E_{v,av}$ is equal to 0.21 eV. which is lower compared to the other geometries.

On making a comparison of our results with those obtained by *Christensen et al* [99-100], who have made calculations only for the ZnSe substrate and ZnS substrate geometries using Keating model. For ZnSe substrate, our value for $\Delta E_{av,v}$ = 0.302 obtained for the minimum energy configuration is quite near to their value of 0.32 eV. However, our value of band offset for the top valence state ΔE_v (= 0.086 eV) is much lower than their value of 0.30 eV. For the ZnS substrate geometry our calculated value of 0.21 eV for the energy minimized configuration is slightly higher than their value of 0.19 eV. The values for ΔE_v are 0.42 eV and 0.54 eV in our and their calculations, respectively.

The values of the valance band offsets calculated for the ZnS / ZnSe (110) and ZnS / ZnSe (001) superlattices in various geometries are seen to be different. The Zn^* S bond lengths vary in the various geometries. The values of the band offsets increases with the planar lattice constant of the various geometries as has been observed earlier [92] for the (001) heterojunctions. For the (110) interfaces, the ZnS bond lengths are nearly equal to 2.42 Å. whereas for (100) interface, this bond length is about 2.31 Å. One thus, observes that the valence band offset increases with the shortening of ZnS bond length. The same is true for the different geometries of the ZnS/ZnSe (100) interface, where the band offset increases with decrease in the bond length of ZnS lying at the interface. In the above calculation spin - orbit effects have not been included. The contribution of this effect will not be more than 0.1 eV.

TABLE 8.3

VALENCE BAND OFFSETS FOR ZnS/ZnSe (110) SUPERLATTICE HAVING ZnSe AS SUBSTRATE.

S. No.	% DISPLACEMENT OF INTERFACE ATOMS **								$\Delta E_{av,v}$ (eV)	ΔE_v (eV)
	Out of the plane				Within the plane					
	ZnSe		ZnS		ZnSe		ZnS			
	Zn	Se	Zn	S	Zn	Se	Zn	S		
1.	0.00	0.0	0.00	0.00	0.00	0.00	0.00	0.00	0.075	-0.141
2.	0.71	-0.19	0.76	-0.12	-0.20	-0.91	0.32	-0.27	0.199	-0.018
3.*	1.41	-0.37	1.53	-0.25	-0.40	-1.83	0.64	-0.55	0.302	0.086
4.	2.12	-0.56	2.29	-0.37	-0.59	-2.74	0.96	-0.82	0.428	0.211

** in terms of bond length

* For minimum energy configuration

TABLE 8.4

VALENCE BAND OFFSETS FOR ZnS/ZnSe (110) SUPERLATTICE HAVING ZnS AS SUBSTRATE.

S. No.	% DISPLACEMENT OF INTERFACE ATOMS **								$\Delta E_{av,v}$ (eV)	ΔE_v (eV)
	Out of the plane				**Within the plane**					
	ZnSe		ZnS		ZnSe		ZnS			
	Zn	Se	Zn	S	Zn	Se	Zn	S		
1.	0.00	0.00	0.00	0.00	0.00	0.00	0.00	0.00	0.17	0.38
2.*	**-0.39**	**0.34**	**-0.43**	**0.10**	**0.14**	**0.00**	**1.06**	**0.00**	**0.21**	**0.42**
3.	-0.78	0.69	-0.85	0.20	0.28	0.00	2.13	0.00	0.26	0.46
4.	-1.18	1.03	-1.27	0.30	0.42	0.00	3.19	0.00	0.31	0.51

** in terms of bond length

* For minimum emergy configuration.

FIG. 8.5 Band structure for bulk ZnS and ZnSe alongwith interface states of the ZnSe:ZnS (110) superlattice in free standing geometry with atomic relaxation in the minimum energy configuration.

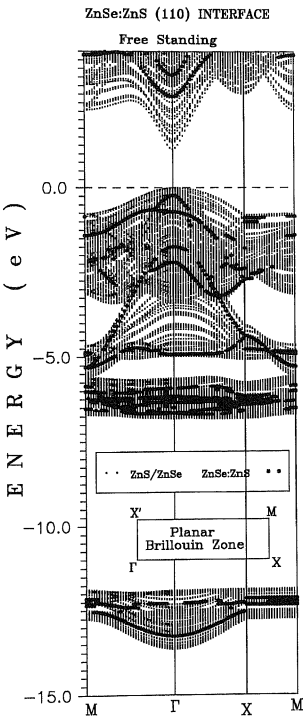
ZnSe:ZnS (110) INTERFACE
Free Standing
ENERGY (eV)
0.0
−5.0
−10.0
−15.0
ZnS/ZnSe
ZnSe:ZnS
X'
M
Planar
Brillouin Zone
Γ
X
M
Γ
X
M

FIG. 8.6 Variation of probability of all the eigen vectors on atoms lying on the various layers of the ZnSe:ZnS interface in free-standing geometry without atomic relaxation . The indexes 'C' and '2' denote the atoms of the layers forming the interface.

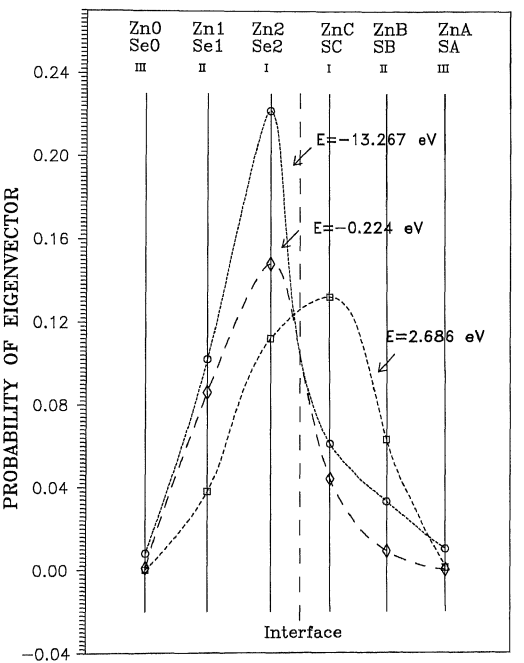
Zn0
Se0
III
Zn1
Se1
II
Zn2
Se2
I
ZnC
SC
I
ZnB
SB
II
ZnA
SA
III
0.24
0.20
0.16
0.12
0.08
0.04
0.00
−0.04
PROBABILITY OF EIGENVECTOR
E=−13.267 eV
E=−0.224 eV
E=2.686 eV
Interface

Chapter-IX

GaN/SiC (001) 2x2 SUPERLATTICES

GaN/SiC (001) 2x2 SUPERLATTICES

9.1 INTRODUCTION :

In recent years, III-V nitrides (GaN and AlN) have been seen to be useful for the development of high temperature, high frequency and high power microelectronic applications. Also, the light emitting diodes (LED) and lasers in the upper part of the visible spectrum i.e., in the blue and the ultraviolet (UV) region may also be developed by these materials. Infact, GaN has already been used for the development of LEDs in blue and UV regions. For future applications, one need to have a suitable lattice matched substrate to have pseudomorphic and defect-free heteroepitaxial growth of GaN. Currently, the usage of sapphire as a substrate is quite common. However, there is a huge lattice mismatch between GaN and sapphire substrate of the order of 14% . SiC is considered to be a promising candidate as substrate because there is a relatively low lattice mismatch between SiC and GaN (≈ 3.5 %). Further, SiC and the nitrides exhibit very similar thermal expansion and also similar structural modifications. Thus, SiC is a very promising substrate for nitrides.

Epitaxial growth has been observed both on the cubic 3C β-SiC and the hexagonal 6H-SiC. The equilibrium bulk phase of nitrides possess wurtzite structure . Recently , the zinc blende phase of GaN on the (001) surface of the cubic SiC has been observed. The zinc blende phase may have superior electrical properties because GaN of zinc blende type is considered better suited for p- or n-type doping because its wurtzite structure presents high n-type background carrier concentration which arises from the occurrence of native defects attributed to nitrogen vacancies [110,111].

Earlier, semiempirical tight-binding calculations [20] have been performed for the unreconstructed hexagonal GaN/SiC (0001) interfaces and also for the reconstructed polar GaN/SiC (001) interfaces [21]. First-principles calculation for the total energy has been performed by *Capaz et al* [112] for the unreconstructed p (1x1) GaN films on hexagonal SiC (0001) substrate. The stability and the electronic structure of the reconstructed zinc blende (001) surfaces has been studied by *Stadele et al* [29] by using a pseudopotential method.

Our group is involved in the study of the structural behaviour and the electronic properties of the heterojunctions by employing a first principles, self-consistent, FP-LMTO method, using density functional theory in LDA [113-114].

The advantage of a LMTO calculation over the linear augumented plane wave (LAPW) and pseudopotential calculations lies in its much less computational efforts enabling one to treat much more complex systems which are many times not accessible by other methods. As pointed out by *Stadele et al* [29], pseudopotential calculations for nitrides are very demanding computationally since carbon and nitrogen have no core p – states and consequently possess strongly localized p–state pseudo-wavefunctions requiring large energy cutoffs.

We perform a calculation for the polar heterojunction formed between the cubic III-V SiC (001) substrate and the strained zinc blende III-V GaN. In practice, usually an interdiffusion of atoms may occur across the polar interface for reducing their energies as will be discussed later. We therefore, consider the intermixed, reconstructed c(2x2) and fully relaxed geometries. The atomic relaxation in the neighbourhood of the interface is quite significant for GaN/SiC interface, which, in turn, affect considerably its electronic properties like band-offsets. We have not considered the spin-orbit interaction in the calculation as its effects on the band offsets for these systems have been seen to be less than 0.01 eV [29].

9.2 CALCULATION:

We employ a relatively large supercell of 16 layers (8 each for SiC and GaN slabs). The chosen LMTO basis functions are Ga (4s,4p,3d), N (2s,2p,3d), Si (3s,3p,3d) and C (2s,2p,3d). The empty space in the lattice was filled by empty spheres and a set of appropriate (spd) states was chosen for them.

For the pure bulk systems, the crystal energy shows minimum in the case of SiC for a value of the lattice parameter a = 4.35 Å (a_{exp} = 4.35 Å) and in GaN, a = 4.50 Å (a_{exp} = 4.50 Å). We observe an excellent reproduction of the experimental data for the lattice parameters by the LMTO method.

The fundamental gap for the pure SiC and the pure GaN are calculated to be 1.36 and 1.75 eV, respectively as compared to the experimental values [110] of 2.2 and 3.4 eV, respectively. The widths of the valence bands for SiC and GaN are approximately -15.4 eV and - 16.3 eV, respectively. The ionic gap for the ionic III-V compound GaN is 4.78 eV in contrast to a value of 2.43 eV for the covalent SiC compound.

In SiC, the VBM is comprised of the hybridized states with dominant contribution from C-p orbitals whereas the states lying at the conduction band minimum (CBM) have dominant contribution from Si-p orbitals. In GaN, the VBM is comprised mainly of N-p orbitals and the CBM of the Ga-s orbitals. The-core Ga-3d states appear near the bottom of the valence band at about -14.0 eV. These states however, have been observed at much lower energies in photoemission measurement [15].

FIG.9.1(a)	Atoms of GaN/ SiC (001) C (2 x2) interface containing Si (50%) and Ga (50%) in mixed interface layer normal to [1 $\bar{1}$ 0] direction
(b)	Atoms of GaN/SiC (001) C (2 x2) interface containing N (50%) and C (50%) in mixed interface layer normal to [1 $\bar{1}$ 0] direction

(a) Mixed [Si, Ga] Interface

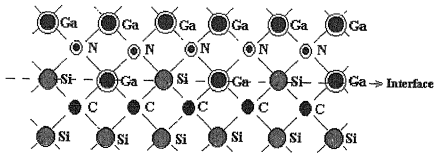

(b) Mixed [C, N] Interface

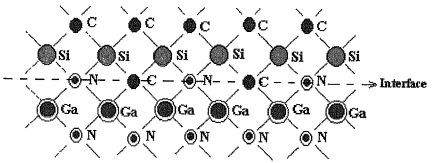

9.3 RESULTS

9.3(a) Bulk Slabs:

We have determined the appropriate minimum energy interlayer separation each for the bulk SiC and GaN compounds. For the bulk slabs, a p(1x1) geometry has been considered . The calculations have been performed for the SiC substrate geometry for which the in - plane lattice constant is 4.35 Å . For the pure GaN slab, for the in-plane lattice constant $a_{||}$ = 4.35 Å an interlayer separation of 0.27 is obtained in contrast to the normal interlayer separation of 0.25 in units of the lattice constant .

9.3(b) Interfaces:

The abrupt polar interfaces are in general energetically unstable and lead to the interdiffusion of atoms across the interface [115, 116]. In the unreconstructed p(1x1) geometry, we observe a highly charged interface. In the formation of the abrupt interface between the two quite different valent compounds such as IV-IV SiC and III-V GaN, one sees the occurrence of under- saturated or over-saturated bonds at the interface, arising from the tetravalent Si and C atoms and the respective trivalent and pentavalent N and Ga atoms. For example, in the case of interface formed by N and Si atoms, we observe the occurrence of oversaturated donor bonds at the interface with more than two electrons, and the interface is negatively charged. On the other hand, in the interface formed by Ga and C ions, the bonds are undersaturated and are called acceptor bonds which contain less than two electrons. The interface is now positively charged. The above mentioned p(1x1) charged interfaces would be energetically unstable [115-120] and will reconstruct so as to become neutral ones on average [121-125]. In order to achieve this neutrality at the interface one should have as many donor bonds as the acceptor bonds. The simplest resulting interface would be a reconstructed c(2x2) one . This interface layer will now contain equal numbers of cations [C, N] or the anions [Si, Ga]. We present the geometries of the mixed [Si, Ga] and [C, N]

interfaces normal to the ($1\bar{1}0$) direction in Fig. 9.1 where the atoms in the various layers in the neighbourhood of the mixed Si-Ga interface are shown in Fig. 9.1(a) and that for the C-N interface are depicted in Fig. 9.1(b). The two basis vectors in the (xy) plane are (110) & ($1\bar{1}0$) and there are two atoms in the planar unit cell.

9.3(c) Mixed [Si, Ga] Interface:

The electronic structure for [Si, Ga] mixed (001) interface is presented in Fig 9.2. The overall electronic structure for the two mixed [Si, Ga] and [C, N] interfaces are very much similar. The semiconducting nature of the constituent compounds is retained in the heterojunction or superlattice.

In Fig. 9.2, we include also the interface states which are characterized by their decay either on both the sides of the interface or on one side only (on moving away from the interface). The probability amplitude and its rate of decay for each interface may, in general, be different. We select only those interface states for which the magnitude of the probability amplitude of the wavefunction is ≥ 0.25 and it decreases by 19% or more on every atom as one moves away from the interface.

Near the bottom of the valence band at $\sim$ -16.0 eV, there appear interface states having dominant contributions from Si - orbitals and these states decay only to-wards the SiC layers. The interface states appearing at the lower end of the ionic gap are comprised mainly of the Ga-orbitals and these states decay to-wards the GaN layers. The interface states at the upper edge of the ionic gap have dominant contribution from the Si-orbitals. The states at VBM originate mainly from the Ga – orbitals.

9.3(d) Valence Band Offsets:

We allow the relaxation of all the atoms lying in the various layers of the heterojunctions on the atoms by different magnitudes and performed the self-

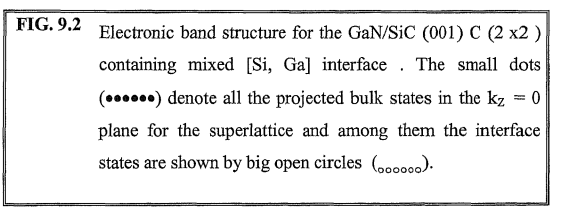

FIG. 9.2 Electronic band structure for the GaN/SiC (001) C (2 x2) containing mixed [Si, Ga] interface . The small dots (••••••) denote all the projected bulk states in the $k_z = 0$ plane for the superlattice and among them the interface states are shown by big open circles ($_{oooooo}$).

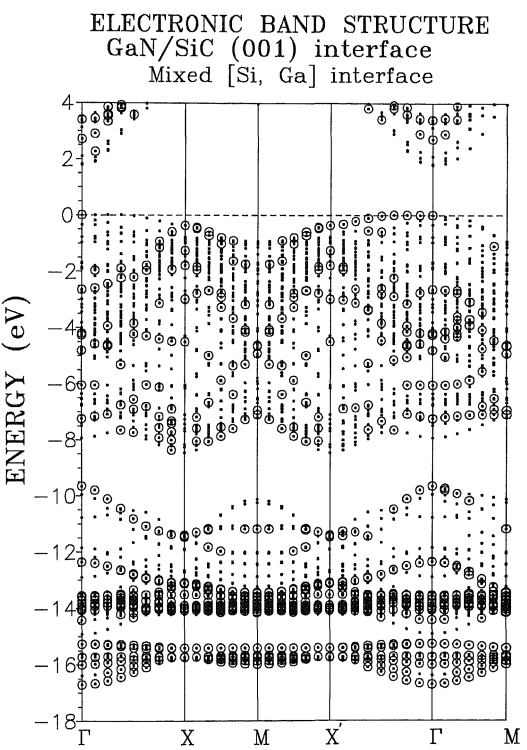
ELECTRONIC BAND STRUCTURE
GaN/SiC (001) interface
Mixed [Si, Ga] interface
ENERGY (eV)
4
2
0
−2
−4
−6
−8
−10
−12
−14
−16
−18
Γ
X
M
X′
Γ
M

Table 9.1 :

Variation of Band-offset with the relaxation of all the atoms lying in all the layers of the supercell for the reconstructed c[2x2] GaN/SiC (001) superlattice containing mixed (Si, Ga) interface having SiC as substrate. For brevity, the changes in bondlengths of the atoms lying in the interfacial neighbourhood normal to the layers have been shown here. There are changes within the plane also but they have not been shown here.

S.NO.	FOR SI (50%) AND GA (50%) MIXED INTERFACE			
	Change in bond length (%) Normal to layers		Band-offset (eV)	
	SiC	GaN	$\Delta E_{v,avg}$	ΔE_{v}
1.	0.00	0.00	1.34	1.13
.2.	-0.77	3.41	1.21	1.00
3.	-1.48	6.63	1.07	0.86
*4.	-1.84	8.16	1.01	0.79
5.	-2.17	9.67	0.93	0.72

* Minimum energy Configuration

consistent calculations for the determination of the lattice energy & the valence band offset for GaN/SiC interface. It may be noted that these atomic displacements, in general, lie both within & perpendicular to the planes. In order to see the variation of the lattice energy & the valence band offset with the magnitudes of the atomic displacements, we performed five different calculations for different magnitudes of atomic displacements. We have computed the changes in the lengths of SiC and GaN bonds for atoms lying in three layers near the interface for each calculation.

For brevity in Table - 9.1, we present only the changes in the interatomic bond lengths lying at the interface for each set of atomic displacements and the calculated values for the two types of VBO's for each set. The actual atomic displacements have not been shown to avoid complexity and only the changes in the lengths of the SiC and GaN bonds lying at the interface are depicted. The new positions of the interface layer atoms are depicted in terms of the changes in the interfacial SiC and GaN bond lengths projected in the [001] direction. The minimum energy of the superlattice has been seen for set no. 4 as shown in Table 9.1.

A perusal of Table -9.1 reveals that the values of $\Delta E_{v,avg}$ are, in general, greater than the corresponding ΔE_v. Further, the band-offsets decrease with the contraction of the SiC bond length and elongation of the GaN bond length. The GaN bond length changes are quite large i.e., they are about four times larger as compared to SiC bond length. The VBO's are affected significantly by atomic relaxation. For example, for an elongation of GaN bond by about 8% and contraction of SiC bond by about 2%, the VBO changes by about 25%.

The minimum energy for the superlattice is obtained for 1.84 % contraction of SiC interface bond and 8.16 % elongation of GaN interface bond. The values of the band-offsets $\Delta E_{v,avg}$ and (ΔE_v) are 1.01 and 1.34 eV for the relaxed surface and are 0.79 and 1.13 eV for the unrelaxed interface. The band-offset for the [Si,Ga] interface in the minimum energy configuration is shown in Fig. 9.4. *Stadele et al*

[29] have obtained a value of 1.4 (1.1) eV for VBO for the relaxed (unrelaxed) (Si, Ga) interface. Our values are lower .

9.3(e) Mixed [C, N] Interface :

The electronic structure for the carbon and nitrogen mixed interface [C, N] of the GaN/SiC (001) system is shown in Fig. 9.3, where the interface states are also depicted. Near VBM, the interface states are composed of the hybridized orbitals of C and N and so are the states lying at the bottom of the valence band. The states in the upper part of the valence band are dominated by the hybridized C and N- orbitals. In the energy region – 10.0 to –14.5 eV, the interface states originate mainly from the C-orbitals. There are dominant contributions from the N-s orbitals near –14.0 eV.

Calculations similar to the [Si, Ga] interface were performed for four different sets of displacements of atoms lying in all the layers of the supercell . The valence band offsets are presented in Table – 9.2. Again, the VBO's vary with the relaxation of atoms. Also, the values of $\Delta E_{v,avg}$ are greater than the corresponding ΔE_v . However, the variation of VBO's with the changes in the SiC and GaN bond lengths are opposite to what has been seen earlier for the mixed [Si, Ga] interface. For the [C, N] mixed interface, the VBO's increase with increase in GaN bond length and decrease in the SiC bond length. The changes in VBO's with bond length changes are now quite enhanced for the [C, N] interface in contrast to the [Si, Ga] interface. For elongation of GaN bond by 8.81% and contraction of SiC bond by –2.39%, the changes in VBO's are about 95%. VBO's change very significantly even for quite small changes in the bond lengths at the interface. The minimum energy for the superlattice is obtained for a contraction of SiC bond by – 0.60% and an elongation of GaN bond by 2.35% and the corresponding values of VBO's are 0.29 eV for $\Delta E_{v,avg}$ and 0.07 eV for ΔE_v , respectively. These values are depicted in Fig. 9.4.

The present value of 0.29 eV lies on the lower energy side as compared to the value of 0.5 eV obtained by *Stadele et al* for the relaxed [C,N] interface. The

present calculation is better than that of *Stadele et al* [29] in some aspects . Firstly, the present results have been obtained after a much reduced computational effort as compared to that of *Stadele et al.* Secondly, the Ga 3d core satates have been considered in the present calculation in a quite natural manner in contrast to the pseudopotential calculation of *Stadele et al* where special care had to be taken . There are some contradictions in the statements made by *Stadele et al* in their paper, e.g., whereas on page 6916 of ref. 29 ; for n=m=7, they quote the values of band-offsets as 1.8 and 0.8 eV for the [Si, Ga] and [C, N] interfaces, respectively, in their Table 9.3, quite different values i.e., 1.4 and 0.5 eV. are quoted.

There is an important difference in the procedures adopted in the present calculation and in that of *Stadele* in the determination of the valence band-offsets. The VBO may be split into two parts : ΔV and ΔE_{BS} . ΔV is the asymptotic difference between the electrostatic (Hartree plus ionic) potential $V(r)$ in the superlattice far from the interface. In the calculation of the first part ΔV, *Stadele* has averaged the electrostatic potentials far from the interface in the superlattice and has determined the difference in them. On the other hand, in the present calculation, we adopt a different procedure. We first carry over the charge distributions and the other data of the deep atoms in the superlattice to the bulk SiC and GaN lattices and calculate the bulk band structures and, in turn, ΔE_{BS} . We also determine the averaged shift in the electrostatic potentials between the bulk calculation and that in the superlattice for each compound and the difference in these averaged electrostatic potentials is named as ΔV to be added to ΔE_{BS}.

The second term $\Delta E_{BS} = E_V(SiC) - \Delta E_V(GaN)$ which is the difference between the eigenvalues of the top of the valence band in the two bulk materials, has been obtained by *Stadele* by performing bulk band structure calculations for SiC and GaN, respectively without giving any details of the procedure. In the present work, in the calculation of ΔE_{BS} , as described above, the charge distributions and the other data of the deep atoms obtained for the superlattice are carried over to the bulk calculations for SiC and GaN . The above mentioned difference in the procedures may be crucial.

The calculations for the valence band-offsets and the interface states were performed after increasing the number of selected k– points. The results remain unaffected by an increase in the number of k – points..

We are not aware of any experimental result for VBO obtained directly in cubic GaN/SiC system. However, an estimated experimental value of 1.2 eV has been reported by *Wang et al* [126] for GaN/SiC system after analyzing the results of the measurements of Schottky barrier heights.

Table 9.2 :

Variation of Band-offset with the relaxation of all the atoms lying in all the layers of the supercell for the reconstructed c[2x2] GaN/SiC (001) superlattice containing mixed (C,N) interface having SiC as substrate. For brevity, the changes in bondlengths of the atoms lying in the interfacial neighbourhood normal to the layers have been shown here. There are changes within the plane also but they have not been shown here.

S.NO.	FOR C (50%) AND N (50%) MIXED INTERFACE			
	Change in bond length (%) Normal to layers		**Band-offset** (eV)	
	SiC	**GaN**	$\Delta E_{v,avg}$	ΔE_{v}
1.	0.00	0.00	0.03	-0.18
*2.	-0.60	2.35	0.29	0.07
3.	-1.19	4.61	0.52	0.30
4	-2.39	8.81	0.95	0.73

* Minimum energy Configuration

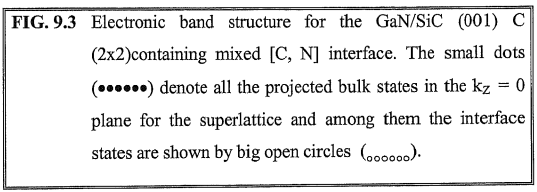

FIG. 9.3 Electronic band structure for the GaN/SiC (001) C (2x2)containing mixed [C, N] interface. The small dots (••••••) denote all the projected bulk states in the $k_Z = 0$ plane for the superlattice and among them the interface states are shown by big open circles ($_{oooooo}$).

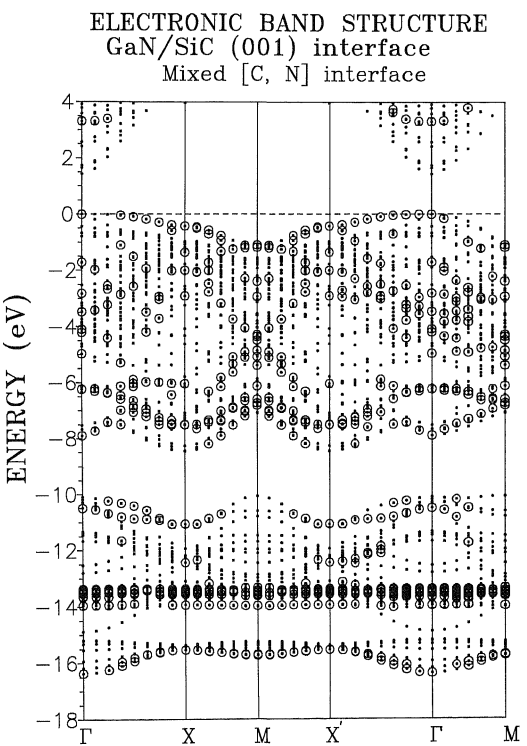
ELECTRONIC BAND STRUCTURE
GaN/SiC (001) interface
Mixed [C, N] interface
ENERGY (eV)
4
2
0
−2
−4
−6
−8
−10
−12
−14
−16
−18
Γ
X
M
X′
Γ
M

FIG. 9.4 Band-offsets for the two types of GaN/SiC (001) C (2x2) interfaces.

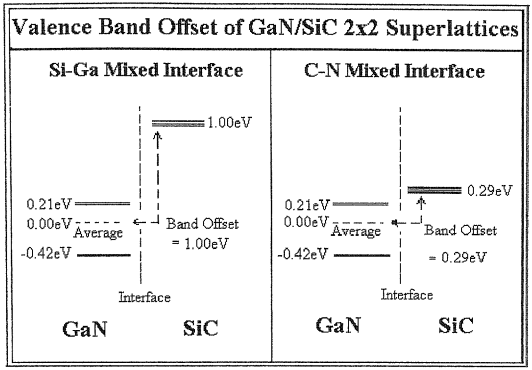
Valence Band Offset of GaN/SiC 2x2 Superlattices
Si-Ga Mixed Interface
1.00eV
0.21eV
0.00eV
Average
-0.42eV
Band Offset
= 1.00eV
Interface
GaN
SiC
C-N Mixed Interface
0.29eV
0.21eV
0.00eV
Average
-0.42eV
Band Offset
= 0.29eV
Interface
GaN
SiC

Chapter-X

CONCLUSIONS

CONCLUSIONS

In the present investigations, a first-principles full potential self-consistent LMTO method has been employed to study the III-V semiconductor alloys and the various types of superlattices containing interfaces of the III-V, II-VI and IV-IV compound semiconductors. The main predictions may be summarized as follows:

10.1 SEMICONDUCTING ALLOYS:

1. In general the calculated lattice parameters for the studied alloys show either linear or non-linear variation with the concentrations of the constituents in the ordered or random configurations. In the case of the ordered alloys, both the N-based Ga(Al)$As_{1-x}N_x$ systems, reveal a non-linear variation of the lattice parameter with concentration x. On the contrary, the $Ga_{1-x}Al_xAs$ alloy shows a linear variation.

   An universal behaviour is observed for all the studied alloys having random configuration of atoms, where a non-linear variation in the lattice constant has been observed.

2. In N- based alloys, there appears a strong hybridization of N-s states with the Ga(Al) (s,p) and As(s,p) states which lie in the neighbourhood of the bottom of the conduction band. It results in the descending of these conduction states into the fundamental gap filling it either partially or completely.

   Normally, one expects, to observe a linear variation in the energy band gap with the concentration of cations or anions in the mixture of semiconducting alloys. In $GaAs_{1-x}N_x$ alloys, where the band gaps for GaAs and GaN are 1.52 eV and 3.3 eV respectively, a replacement of As –atom should incur a blue shift of the photoluminescence edge.

The present calculations reveal that there is a large variation in the calculated band gap with the concentration variations and we observe bowing in the gap. The reduced value of the band gap is smaller than those of the constituent pure semiconductors. In $AlAs_{1-x}N_x$ alloy, a small value of fundamental gap is observed for x = 0.125.

In $GaAs_{1-x}N_x$ alloy, a severe reduction in the gap is observed. A near closure of the fundamental energy gap is observed for a N atomic concentration range of x = 0.125 to 0.625. Inclusion of many body effects such as GW approximation may open the gap by ~ 0.7 – 0.9 eV making these alloys as narrow gap semiconductors in the N - concentration range of 0.125 – 0.625. This effect has been confirmed in the photoluminescence experiment where a red-shift has been observed [46].

3. GaAs and AlAs in pure form are direct and indirect semiconductors, respectively. A replacement of Ga-atom by Al-atom in $Ga_{1-x}Al_xAs$ alloy, changes the nature of the lowest lying conduction states. A direct to indirect band gap crossover has been seen for the semiconducting III-V Ga_{1-x} Al_x As alloys at the concentration x = 0.375. Some band gap bowing has also been observed for both the direct and indirect band gaps. The predicted value of crossover is very near to the measured value of x = 0.35 [79]. The calculated direct and indirect band gaps for the ordered alloys are in excellent agreement with the photoluminescence and absorption data . The present results support towards the occurrence of the ordered structures in the various samples grown up in the various measurements.

4. Both the AlAs and AlN are indirect band gap semiconductors. One expects, the alloy $AlAs_{1-x}N_x$ to show always an indirect band gap on the replacement of As atom by N-atom. Our investigations predict a new behaviour. We observe a crossover from indirect to direct band gap approximately for $x \geq 0.02$ and from direct to indirect gap again for $x \geq 0.56$.

10.2 SUPERLATTICES:

1. Our results show that the model theories used for estimating the values of the valence band offsets are expected to be inadequate as they are based on the use of the bulk like properties of the constituent materials forming the interface.

2. We predict a strong sensitivity of the valence band offsets on the small atomic displacements.

3. There appear a number of interface states of localized and resonance types which may be responsible for the sensitivity of the band offsets on the atomic positions.

4. For GaAs/GaN (001) interface, the valence band offset increases (decreases) with decrease (increase) in the GaN (GaAs) bond length. The calculated values of the band offsets ranging from 1.32 eV to 1.86 eV for the GaAs substrate and the free standing geometries, respectively are quite close to the experimental value of 1.7 - 1.8 eV reported by *Ding et al* [91].

5. In the case of ZnS/ZnSe (110) superlattice :

   (i) For free standing geometry, the value of valence band offset $\Delta E_{av,v}$ and ΔE_v in the equilibrium position of the relaxed atoms are 0.27 eV and 0.198 eV, respectively. The maximum atomic displacements in the equilibrium configuration are less than 1.1% of the bond length.

   (ii) For ZnSe substrate, the presently calculated value for $\Delta E_{av,v} = 0.302$ eV obtained for the minimum energy configuration is quite near to value of *Christensen et al* [99-100] which is equal to 0.32 eV. However, our value of band offset for the top valence state ΔE_v (= 0.086 eV) is much lower than his value of 0.30 eV.

(iii) For the ZnS substrate geometry, our calculated value of 0.21 eV for the energy-minimized configuration is slightly higher than their value of 0.19 eV. Our value for ΔE_V is 0.42 eV as compared to a value of 0.54 eV calculated by *Christensen et al.*[99-100]. Unfortunately, no experimental data is available for comparison.

6. For the polar GaN/SiC (001) (2X2) superlattices in the minimum energy configurations, the values of VBO's for the [Si, Ga] interface are $\Delta E_{v,avg}$ = 1.01eV and ΔE_v = 0.79 eV and that for the [C, N] interface, $\Delta E_{v,avg}$ =0.29 eV and ΔE_v = 0.07 eV, respectively. The presently predicted values are on low energy side as compared to those of the earlier pseudopotential calculation of *Stadele et al.*[29]. Our calculated values of the valence band offsets for the mixed [Si,Ga] interface are quite near to the estimated experimental value 1.2 eV of *Wang et al*[126]. Unfortunately, again no experimental data is available for comparison.

REFERENCES

REFERENCES

1. M. Cardona and N.E. Christensen, J. Vac. Sci. Technol. B6, 1285, 1988.
2. R. L. Anderson, Solid state Electron 5, 341, 1962.
3. W. A. Harrison and J. Tersoff, J. Vac. Sci. Technol. B4, 1068, 1986.
4. D. W. Niles and G. Margaritondo in proceedings of the 19th Internationa Conference on the Physics of semiconductor, edited by O. Engström (Worl Scientific, Singapore, 1987) p.187: D. Niles and G. Margaritondo Phys. Rev. B3 2923, 1986; D. W. Niles, Ming Tang, H. Höchst and G. Margaritondo, J. Vac. Sc Technol. A5, 2057, 1987.
5. A. D. Katnani and G. Margaritondo Phys. Rev. B28, 1944, 1983.
6. R. Dingle, Festkorperprobleme, Advances in solid state Physics (Pergamor Brownschweig) vol. 15, p. 21; R. Dingle, W. Wiegmann and C. H. Henry Phy Rev. Lett. 33, 827, 1974.
7. J. R. Waldrop S. P. Kowalczyk, R. W. Grant, E. A. Krant and D. L. Miller, J. Va Sci. Technol. 19, 573, 1981.
8. R. C. Miller D. A. Kleinman and A. C. Gossard Phys. Rev. B29, 7085, 1984.
9. R. C. Miller, A. C. Gossard and D. A. Kleinman and O. Munteanu, Phys. Rev. B2 3470, 1984.
10. P. Dawson G. Duggan, H. I. Ralph, K. Woodbridge and G. W. Hooft Superlattice and Microstructure 1, 231, 1985.
11. W. G. Wilke and K. Horn, J. Vac. Sci. Tech. B6, 1211, 1988.
12. W. G. Wilke, R. Seedorf and K. Horn, preprint.
13. J. Chen, J. R. Sites, I. L. Spain, M. J. Hafich, G. Y. Robinson, Appl. Phys. Lett. 5 744, 1991.
14. M. Leroux, M. L. Fille, B. Gil, J. P. Landesman and J. C. Garcia, Phys. Rev. B4 6465, 1993.
15. S. A. Ding, G. Neuhold, J. H. Weaver, P. Haberle, K. Horn, O. Brandt, H. Yang, K Ploog, J. Vac. Sci. Technol. A 14(3), 1996.
16. G. Martin, S. Strite, A. Bolchkarev, A. Agrawal, A. Rockett, H. Morkoc, W. R. I Lambrecht and B. Segall, Appl. Phys. Lett. 65, 610, 1994.
17. Z. Q. He, X. M. Ding, X. Y. Hou and X. Wang, Appl. Phys. Lett. 64, 315, 1994.
18. N. Kuwano et al. Jpn. J. Appl. Phys. 33, 18, 1994.
19. K. Nath and A. B. Anderson, Phys. Rev. B40, 7916, 1989.
20. S. Y. Ren and J. D. Dow, appl. Phys. Lett. 69, 251, 1996.

21. L. K. Teles, L. M. R. Scolfaro, R. Enderlein, J. R. Leite, A. Josiek, D. Schikora and K. Lischka, J. Appl. Phys. 80, 6322, 1996.

22. G. C. Osbourn and D. L. Smith, Phys. Rev. B19, 2124, 1978.

23. K. Kunc and R. M. Martin, Phys. Rev. B24, 3445, 1981.

24. C. G. Van de Wall, R. M. Martin, Phys. Rev. B35, 8154, 1987.

25. T. Nakayama and H. Kamimura, J. of the Physics Society of Japan, 54, 4726, 1985.

26. N. E. Christensen Phys. Rev. B47, 4528, 1988.

27. E. A. Albanesi, W. R. L. Lambrecht and B. Segall, J. Vac. Sci. Tech. B12, 2470, 1994.

28. A. Continenza and S. Massidda, Phys. Rev. B50, 11949, 1994.

29. M. Städele, J. A. Majewski and P. Vogl, Phys. Rev. B56, 6911, 1997.

30. A. F. Wright and J. S. Nelson, Phys. Rev. B50, 2159, 1994.

31. J. A. Majewski, M. Städele and P. Vogl, MRS Internet J. Nitride Semicond. Res. 1, 30, 1996.

32. N. E. Christensen and I. Gorezyca, Phys. Rev. B50, 4397, 1994.

33. K. Kim, W. R. L. Lambrecht and B. Segall, Phys. Rev. B50, 1502, 1994.

34. A. Rubio, J. L. Corkill, M. L. Cohen, E. L. Shirley and S. G. Louie, Phys. Rev. B48, 11810, 1993.

35. M. Palummo, L. Reining, R. W. Godby, C. M. Bertoni and N. Bornsen, Europhys. Lett. 26, 607, 1994.

36. W. R. L. Lambrecht, B. Segall J. Rife, W. R. Hunter and D. K. Wickenden, Phys. Rev. B51, 13516, 1995.

37. E. A. Albanesi, W. R. L. Lambrecht and B. Segall, Phys. Rev. B48, 17841, 1993.

38. P. E. Van Camp, V. E. Van Doren and J. T. Devreese, Phys. Rev. B44, 9056, 1994.

39. M. Suzuki, T. Uenoyama and A. Yanase, Phys. Rev. B52, 8132, 1995.

40. K. Kim, W. R. L. Lambrecht and B. Segall, Phys. Rev. B53, 16310, 1996.

41. Su-Huai Wei and Alex Zunger, Appl. Phys. Lett. 69, 2719, 1996.

42. A. Rubio, J. L. Corkill and M. L. Cohen, Phys. Rev. B49, 1952, 1994.

43. S. H. Ke, M. C. Huang and R. Z. Wang, Solid State Commun. 89, 105, 1994.

44. Jörg Neugebauer and Chris G. Van de Walle, Phys. Rev. B51, 10568, 1995.

45. Angel Rubio and Marvin L. Cohen, Phys. Rev. B51, 4343,1995.

46. M. Weyers, M. Sato and H. Ando, Jpn. J. Appl. Phys. 31, 853, 1992.

47. W. Kohn and L. J. Sham, Phys. Rev. 140, A 1133-8,1965.

48. N. D. Lang, Solid State Phys. 28, 225-300, 1973.

49. P. Hohenberg W. Kohn, Phys. Rev. 136, B 864-71, 1964.

50. O. Gunnarsson, J. Harris and R. O. Jones, Phys. Rev. B15, 3027, 1977.

51. N. D. Lang and L. J. Sham, Solid State Commun. 17, 581, 1975.

52. D. C. Langreth and J. P. Perdew, Phys. Rev. B15, 2884, 1977.

53. J. P. Perdew and M. Levy, Phys. Rev. Lett. 51, 1884, 1983.

54. L. J. Sham and M. Schluter, Phys. Rev. Lett. 51, 1888, 1983.

55. R. O. Jones, O. Gunnarson, Rev. Mod. Phys. 61, 689, 1989.

56. R. M. Dreizler, E. K. U. Gross, Density Functional Theory, Springer, Berlin, 1990.

57. R. G. Parr, W. Yang, Density Functional Theory of Atoms and Molecules, Oxford University Press, New York, 1989.

58. M. S. Hyberstsen and S. G. Louie, Phys. Rev. B34, 5390, 1986.

59. O. K. Andersen, Phys. Rev. B12, 3060, 1975.

60. H. L. Skriver, The LMTO Method (Springer, Heidelberg) 1983.

61. L. Bellaiche, S. H. Wei and A. Zunger, Phys. Rev B54, 17568, 1996.

62. L. Hedin and B. I. Lundqvist, J. Phys. C: Solid State Phys. 4 , 2063, 1971.

63. X. Zhu and S. G. Louie, Phys. Rev. B 43, 14142. 1991.

64. Numerical Data and Functional Relationships in Science and Technology edited by K H Hellwege Landolt-Bornstein New Series Group III vol. 17 Pt. a (Springer, New york, 1982).

65. S. J. Jenkins G. P. Srivastava and J. C. Inkson J. Phys. C: Solid State Phys. 6, 8781, 1994.

66. T. Lei, T. D. Moustakas, R. J. Graham Y. He and S. J. Berkowitz, J. Appl. Phys. 71, 4933, 1992 and references therein.

67. J. M. Sanchez and D. de Fontaine, Structure and Bonding in Crystals vol 2, ed M O'keefe and A. Navrotsky (New York: Academic) p 117, 1981.

68. J. M. Sanchez, F. Ducastell and D. Gratias, Physica A 128, 334, 1984.

69. G. P. Srivastava, J. L. Martins and A. Zunger, Phys. Rev. B31, 2561, 1985.

70. Bal K. Agrawal S. Agrawal P. S. Yadav and S. Kumar, J. Phys. Condens. Matter 9, 1763, 1997.

71. M. Paisley Z. Sitar, J. B. Posthill and R. F. Davis, J. Vac. Sci. Technol. A7, 701, 1989; Z. Sitar et al., J. Mater. Sci. Lett., 11, 261, 1992.

72. W. A. Harrison, Phys. Rev. B31, 2121, 1985.

73. S. Yoshida, S. Misawa and S. Gonda, J. Appl. Phys. 53, 6844 1982.

74. R. M. Wentzcowich, M. L. Cohen and P. K. Lam, Phys. Rev. B36, 6058, 1987.

75. M. Ueno, A. Onodera, O. Shimomuna and K. Takemura, Phys. Rev. B45, 10123 1992.

76. R. W. Wycoff, Crystal Structures, 2nd edn., vol 1 (New York : Wiley-Interscience).

77. CRC Handbook of Chemistry and Physics 70th Ed. 1989-90.

78. B. Perry and R. F. Rutz, Appl. Phys. Lett. 33, 319, 1978.

79. B . Monemar, K. K. Shih and G. D. Pettit , J. Appl. Phys., 47, 2604, 1976.

80. G. Torres-Delgado, R. Castanedo-Perez, P. Diaz-Arencibia, J. L. Orozco- Vilchis, M. Murillio-Lara, A. Serra-Jones, J. Appl. Phys. 78, 5090, 1995.

81. C. Tejedor, F. Flores and E. Louis, J. Phys C 10, 2163, 1977.

82. C. Tejedor, F. Flores and E. Louis, J Phys, C 12, 731, 1979.

83. J. Tersoff, Phys. Rev. Lett., 52, 465, 1984.

84. J. Tersoff, Phys. Rev., B30 , 4874, 1984.

85. M. Cardona and N. E. Christensen, Phys. Rev. B31, 879, 1985.

86. S. H. Wei and A. Zunger, Phys. Rev. Lett 59, 144, 1987.

87. M. Jaros, A. Zoryk and D. Ninno, Phys. Rev B35, 1987.

88. C. G. Van de Welle and R. M. Martin, J. Vac. Sci. Technol. B4, 1055, 1986.

89. C. G. Van de Welle and R. M. Martin, Phys. Rev. B34, 5621, 1986.

90. W. Monch, Semiconductor Surfaces and Interfaces 2nd Ed.; Springer Series in Surface Science; Springer Verlag, Berlin vol 26, 1995.

91. S. A. Ding, S. R. Barman, K. Horn, H. Yang, B. Yang, O. Brandt and K. Ploog, Appl. Phys. Lett. 70(18), 2407, 1997.

92. M. Methfessel, B. K. Agrawal and M. Scheffler, unpublished.

93. M. Methfessel, Phys. Rev. B38, 1556, 1988 .

94. M. Methfessel, C. O. Rodriguez and O. K. Anderson, Phy. Rev. B40, 2009, 1989.

95. Bal K. Agrawal and Savitri Agrawal Phys. Rev. B45, 8321, 1992.

96. Bal K. Agrawal and Savitri Agrawal, Phys. Rev. B52, 12556, 1995.

97. Bal K. Agrawal and Savitri Agrawal, Physica C, 233, 8, 1994.

98. Bal K. Agrawal and Savitri Agrawal, Physica C, 234, 29, 1994.

99. N. E. Christensen, Phys. Rev. B37, 4528, 1998.

100. N. E. Christensen and I. Gorczyca, Phys. Rev. B44, 1707, 1991.

101. Bal K. Agrawal P. S. Yadav, Rekha Srivastava and S. Agrawal, J. Phys. Condens. Matter 10, 4597, 1998.

102. L. Bellaiche, S. H. Wei and A. Zunger, Appl. Phy. Letts., 70 ,3558, (1997); ibid 72, 2011, 1998.

103. T. Yokagawa, M. Ogura and T. Kajiwara, Appl. Phys. Lett. 49, 1702, 1986.

104. K. Shahzad, D. J. Olego and C. G. Van de Walle, Phys. Rev. B38, 1417, 1988.

105. W. R. L. Lambrecht, B. Segall and O.K. Anderson; Phys. Rev. B41 , 2813 and 2832, 1990.

106. S. Wei and A. Zunger, J. Appl. Phys. 78, 3846, 1995.

107. National Conference on Advances in Condensed Matter Physics, Pondicherry, 1998.

108. Bal K. Agrawal, P. S. Yadav and Savitri Agrawal, Phys. Rev. B50, 14881, 1994.

109. Bal K. Agrawal, Phys. Rev. B23, 2995, 1981.

110. H. Morkoc, S. Strite, G. B. Gao, M. E. Lin, B. Sverdlov and M. Burns, J. Appl. Phys. 76, 1363, 1994.

111. S. Strite and H. Morkoc, J. Vac. Sci. Technol. B10, 1237, 1992.

112. R. B. Capaz, H. Lim, and J. D. Joannopoulos, Phys. Rev. B51, 17 755, 1995.

113. Bal K. Agrawal and Savitri Agrawal, Surface Science, 424, 232, 1999.

114. Bal K. Agrawal and Savitri Agrawal, Surface Science, 431, 84, 1999.

115. W. A. Harrison, E. A. Kraut, J. R. Waldrop and R. W. Grant, Phys. Rev. B18, 4402, 1978.

116. R. M. Martin, J. Vac. Sci. Technol. B17, 978, 1980.

117. G. Bratina, L. Vanzetti, L. Sorba, G. Biasiol, A. Franciosi, M. Peressi and S. Baroni, Phys. Rev. B50, 11723, 1994.

118. R. Nicolini, L. Vanzetti, G. Mula, G. Bratina, L. Sorba, A. Franciosi, M. Peressi, S. Baroni,R. Resta, A. Baldereschi, J. E. Angelo and W. W. Gerberich, Phys. Rev. Lett. 72, 294, 1994.

119. R. G. Dandera, S. Froyen and A. Zunger, Phys. Rev. B42, 3213, 1990.

120. A. Kley and J. Neugebauer, Phys. Rev. B50, 8616, 1994.

121. F. A. Ponce, M. A. O'Keefe and E. C. Nelson, Philos. Mag. A74, 777, 1996.

122. F. A. Ponce, B. S. Krusor, J. S. Major, Jr. W. E. Plano and D. F. Welch, Appl. Phys. Lett. 67, 410, 1995.

123. F. A. Ponce, C. G. Van de Walle and J. E. Northrup, Phys. Rev. B53, 7473, 1996.

124. W. C. Hughes, W. H. Rowland, Jr., M. A. L. Johnson, S. Fujita, J. W. Cook, Jr., J. F. Schetzina, J. Ren and J. A. Edmond, J. Vac. Sci. Technol. B13, 1571, 1995.

125. O. Brandt, H. Yang, B. Jenichen, Y. Suzuki, L. Daweritz and K. H. Ploog, Phys. Rev. B52, 2253, 1995.

126. M. W. Wang, J. M. McCaldin, J. F. Swenberg, T. C. McGill and R. J. Hauenstein, Appl. Phys. Lett., 66,1974, 1995.

Published Research Papers

J Phys.. Condens Matter 10 (1998) 4597–4607. Printed in the UK PII: S0953-8984(98)90486-6

Ab initio study of anomalous band-gap bowing in $GaAs_{1-x}N_x$ alloys

Bal K Agrawal, P S Yadav, Rekha Srivastava and Savitri Agrawal
Physics Department, Allahabad University, Allahabad 211002, India

Received 7 January 1998

Abstract. A full potential self-consistent linear muffin-tin orbital method in the local density approximation (LDA) has been employed to investigate the electronic structure of the 14 ordered $GaAs_{1-x}N_x$ alloys with x = 0.0, 0.037, 0.074, 0.111, 0.125, 0.25, 0.375, 0.407, 0.50, 0.625, 0.75, 0.875, 0.963 and 1.0. The lattice parameter is seen to have a non-linear variation with the concentration of the constituent atoms. In LDA, a near closure of the fundamental energy gap appears in the concentration range 12.5–62.5% of N atoms. A strong hybridization of N s states with the Ga (s, p) and As (s, p) states is seen at the bottom of the conduction band and these states descend into the fundamental gap, filling it either partially or completely. The band gap for the random alloys also shows an anomalous bowing.

1. Introduction

Great interest has been shown in the study of the electronic properties of III–V semiconducting alloys because of their important applications in optoelectronic devices and other technological applications.

GaAs, which has a comparatively smaller band gap, plays an important role in the semiconductor industry. The alloys of III–V elements which possess wide energy gaps are important for the development of the optoelectronic devices in the high frequency region. In the case of $GaAs_{1-x}N_x$ alloys, one expects to observe a variation of band gap from a value of 1.52 eV (GaAs) to a value of 3.3 eV (GaN). Thus a blue shift of the photoluminescence edge should have been observed experimentally with the addition of N atoms. On the contrary, a red shift of the photoluminescence edge has been observed in these alloys (Weyers *et al* 1992). In the alloys such as $Al_xGa_{1-x}N$, where the lattice mismatch between the end components is about 2.9%, one observes a dominant role played by the cations in determining the electronic structure and the band gaps. On the other hand, in the $GaAs_{1-x}N_x$ alloys, the lattice mismatch is as large as 20% and the effects of various anion component concentrations are seen to be anomalous.

Compound semiconductor alloys of the type $A_xB_{1-x}C$ are often considered to consist of a regular arrangement of A and B atoms on an fcc sublattice. However, real alloys may, in general, be random. Deviations from randomness have been observed, such as phase separation, i.e., formation of distinct AC and BC rich phases. Another case of deviation is the occurrence of order seen in both types of alloy, $A_xB_{1-x}C$ and $AB_{1-x}C_x$. In the extreme case of perfect order, one may observe alternating layers of pure AC and pure BC in cation variant systems $A_xB_{1-x}C$ or AB and AC pure layers in the anion variant systems $AB_{1-x}C_x$.

In an earlier paper (Agrawal *et al* 1997), we reported the results for the electronic structure of a first-principles self-consistent full potential linear muffin-tin orbital (LMTO)

0953-8984/98/214597+11$19.50 © 1998 IOP Publishing Ltd

calculation of the cation dominated $Ga_{1-x}Al_xN$ alloys and observed quite a little bowing in the fundamental energy gap. We extend our studies to $GaAs_{1-x}N_x$ alloys in the present article. The electronic structure of the 14 ordered systems $GaAs_{1-x}N_x$ for $x = 0$, 0.037, 0.074, 0.111, 0.125, 0.25, 0.375, 0.407, 0.50, 0.625, 0.75, 0.875, 0.963 and 1.0 have been investigated. In the local density approximation, we observe a near closure of the band gap in the concentration range $x = 0.125$–0.625 of the N atoms. This creates the possibility of the fabrication of III–V light emitting devices covering the whole optical region. Earlier, Rubio and Cohen (1995) employed a pseudo-potential theory in the local density approximation to obtain a gap of 0.06 eV for one case only, i.e., 25% concentration of N atoms. They have also performed a quasi-particle study and observed an opening of the band gap in the LDA by about 0.7 eV.

Bellaiche *et al* (1996) have discussed the electronic properties of some ordered alloys and quasirandom structures of Ga–As–N alloys by using local empirical pseudopotentials in the plane-wave pseudopotential approach. A fitting with the GW band structures, experimental band gaps and LDA deformation potentials was adopted to obtain the atomic potentials. For each composition, results were averaged over a few randomly selected configurations. They considered a bimodal distribution of bond lengths.

In contrast to Bellaiche *et al* (1996), we have investigated the electronic structure of the ordered and the random $GaAs_{1-x}N_x$ alloys by using a fully *ab initio* LMTO method without adopting any fitting procedure. Although we have adopted a unimodal distribution of bond lengths, in the majority of our calculations, the effects of bimodal distribution have been studied in a typical case and the results are not seen to be affected significantly.

In the present study, the full potential LMTO method has been used to investigate the electronic properties of the ordered $GaAs_{1-x}N_x$ alloys. For detailed information on the method used, we refer to our earlier paper (Agrawal *et al* 1997). The calculated results for the electronic structure, total density of states and band-gap bowing are shown in section 2. The main conclusions are contained in section 3.

2. Calculation and results

The lattice is a face centred cubic one. A unit cell containing eight molecular units (16 atoms) has been employed for the different crystal structures of $Ga_8As_{8-n}N_n$ alloys for $n = 0$–8. For low concentrations of N or As atoms, i.e., for $x = 0.037$, 0.074, 0.111, 0.407 and 0.963, a bigger unit cell or supercell containing 27 molecular units (54 atoms) has been employed.

The non-overlapping radii of muffin-tin spheres are chosen to be 2.17, 2.15 and 1.43 au for Ga, As and N, respectively. We use muffin-tin orbitals (MTOs) of 4s, 4p, 3d (4d) type for Ga (As) atoms and the 2s and 2p type MTOs for N. In a separate calculation, we have also considered Ga 4d states instead of Ga 3d states as valence states at several N concentrations. However, the results are not significantly changed except for a small change in the magnitude of the band gap.

For the calculation of the charge density and the potential, the LMTO envelopes are expanded in terms of the Hankel functions having the spherical harmonic components $l \leqslant 4$. Three values, -0.01, -1.0 and -2.3 Ryd for the decay factor in the Hankel functions are used in the construction of the muffin-tin orbitals for real atoms. In the interstitial region two values, -0.01 and -1.0 Ryd of the decay factor have been employed. Each supercell contains an equal number of real atomic muffin-tin spheres (MTSs) and empty MTSs. The scalar relativistic effects have been considered in all the calculations. For the exchange–correlation potential, the parametrization of Hedin and Lundqvist (1971) has been chosen.

In the present method, the wave functions of the core electrons of the atoms are relaxed, and in the self-consistent calculation in each iteration the core electron charge density is recalculated.

A deficiency of the local density theory is that the calculated value of the fundamental energy gap is about 50% of the experimental one. This originates from the fact that the excitation energies of these systems are not given by eigenvalues of the Kohn–Sham equations (Perdew and Levy 1983, Sham and Schluter 1983). The quasi-particle energies and wide band gaps have been calculated in the so-called GW approximation of the electron self-energies Σ. This self-energy is seen to be a non-local energy dependent effective potential. This is beyond the scope of the present work.

For the different structures of the ordered $GaAs_{1-x}N_x$ alloys, the lattice parameters have been calculated by minimizing the crystal energy in our calculation. We compare these calculated lattice parameters with the available experimental values and the other calculated values in table 1. The variation is shown in figure 1. The variation is seen to be a nonlinear one. The departure from linearity is appreciable. The present calculated value for GaN is in excellent agreement with the experiment, whereas for GaAs the lattice parameter is seen to be well within 2% of the experimental value. Our calculated values are quite close to those reported for some alloys by other workers but are somewhat on the higher side. The discrepancy may arise because of the use of correlation schemes by other workers which are different from the present one.

Table 1. Variation of lattice constant with concentration of the constituent atoms in the ordered $GaAs_{1-x}N_x$ structures. All values are measured in Å.

System (x)	Present	Other calc.	Expt
0.000	5.55	5.61[a]	5.65[b]
0.125	5.46		
0.250	5.36	5.30[c]	
0.375	5 26		
0.500	5.14	5 12[c]	
0.625	4.95		
0.750	4.83		
0.875	4.66		
1.000	4.50	4.42[d], 4.48[e], 4.30[f]	4.50[g]

[a] Model dielectric function, Zhu and Louie 1991.
[b] *Landolt–Börnstein* 1982.
[c] Pseudopotential, Rubio and Cohen 1995.
[d] Pseudopotential, Rubio *et al* 1993.
[e] LMTO–ASA, Albanesi *et al* 1993.
[f] Pseudopotential, Jenkins *et al* 1994.
[g] Optical absorption, Lei *et al* 1992.

In all future calculations, the above calculated lattice parameters have been used. Further, for every ordered structure the bond lengths for the Ga–As and the Ga–N bonds are taken to be the same, i.e., we assume a unimodal distribution of bond lengths. The effect of a bimodal distribution of bond lengths is investigated in the later part of this article.

2.1. Ordered structures

The crystal lattices for all the considered ordered alloys have the zinc blende structure. In figures 2 and 3, the electronic structure is depicted for the 16- and 54-atom supercells,

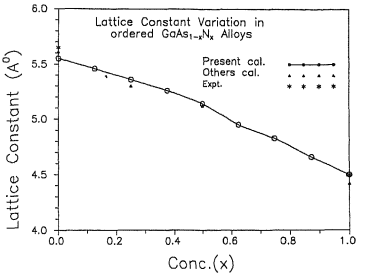

Figure 1. Lattice constant variation in the ordered $GaAs_{1-x}N_x$ alloys. Experimental data are taken from *Landolt–Bornstein* (1982) and Lei *et al* (1992). The results of other calculations are taken from Zhu and Louie (1991), Rubio and Cohen (1995) and Rubio *et al* (1993).

respectively. For brevity, we have not included the band structures for $x = 0.625$ and 0.875 in figure 2. The lengths of the primitive lattice vectors for the 16- and 54-atom supercell are, respectively, doubled and tripled as compared to those of the two-atom unit cell. This results in zone folding. Also, the number of branches increase according to the larger number of molecular units in the supercell. In figures 2 and 3, the dispersion curves are shown only in the vicinity of the fundamental energy gap. The origin of energy is chosen at the top of the valence band for each ordered alloy.

For the end component ordered structure, Ga_8As_8, the point group symmetry is T_d and the symmetry points of the bcc Brillouin zone are W (0.5, 0.25, 0), L (0.25, 0.25, 0.25), Γ (0, 0, 0), X (0.5, 0, 0) and K (0.375, 0.375, 0). A set of 19 special k-points is selected in the irreducible part of the Brillouin zone for achieving self-consistent results. The energy gap is a direct one equal to 0.61 eV. The states just above the bottom of the conduction band correspond to the X-point of the Brillouin zone for the two-atom unit cell. This happens because of the zone folding. The valence band maximum (VBM) is composed of As p-like states whereas the conduction band minimum (CBM) is composed of the s-like orbitals mainly of Ga having some contribution from As. It may be noted that the value of energy gap for this ordered structure in the GW approximation is 1.3 eV (Rubio and Cohen 1995).

For the most dilute ordered structure $Ga_{27}As_{26}N$ (3.7% of N), the point group symmetry is again T_d. The N atoms lying in the adjacent 54-atom supercells are sixth neighbours among themselves. The calculated electron structure in the neighbourhood of the energy gap is shown in figure 3. The band gap is 0.44 eV. The valence band maximum is comprised of almost all the p orbitals of the three constituent atoms N, Ga and As but the main contributions are from the N and As atoms. On the other hand, the main contributors to the CBM are the antibonding mixed states of N (s), Ga (s, p) and As (s, p) orbitals. For all the other alloy systems the main contributors are the s-like orbitals of N and Ga atoms with some contribution from the As (s) orbitals.

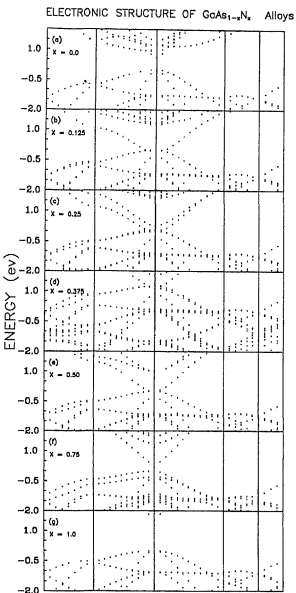

Figure 2. Electronic dispersion curves for the ordered $GaAs_{1-x}N_x$ alloys (a) $x = 0.00$, (b) $x = 0.125$, (c) $x = 0.25$, (d) $x = 0.375$, (e) $x = 0.50$, (f) $x = 0.75$ and (g) $x = 1.0$. The origin of energy has been chosen at the valence band maximum.

For the next dilute ordered structure $Ga_{27}As_{25}N_2$ (7.4% of N), two atomic configurations having different point group symmetries C_{2v} and C_{3v} were considered. In the C_{2v} symmetric configuration two N atoms are next nearest neighbours among themselves, whereas in the C_{3v} point group configuration two N atoms are fourth neighbours among themselves. For the C_{2v} and C_{3v} point group symmetries, the magnitudes of the band gap are seen to be different, i.e., 0.283 and 0.350 eV, respectively. The variation of gap is seen to be small

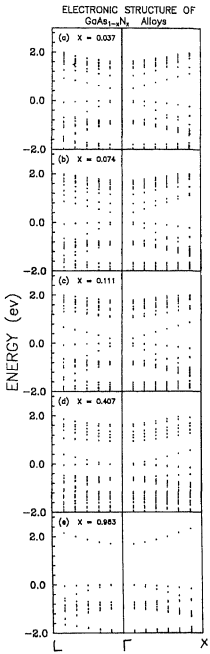

Figure 3. Electronic dispersion curves for the ordered $GaAs_{1-x}N_x$ alloys (a) $x = 0.037$, (b) $x = 0.074$, (c) $x = 0.111$, (d) $x = 0.407$ and (e) $x = 0.963$. The origin of energy has been chosen at the valence band maximum.

for the two different locations of the two N atoms in the supercell. For brevity, we do not include the results obtained for C_{3v} symmetry in the presentation of the results.

In the $Ga_{27}As_{24}N_3$ ordered structure, the three N atoms are second neighbours among

themselves and the point group symmetry is C_{3v}. The magnitude of energy gap decreases to 0.11 eV. The orbital composition of the valence band maximum and that of the conduction band minimum are similar to the above discussed ordered alloys.

For the ordered $GaAs_{0.875}N_{0.125}$ system, the symmetry is T_d. There is one N atom in the 16-atom supercell and the N atoms of the two adjacent supercells are fourth neighbours among themselves. A remarkable observation is that the band gap vanishes at this small concentration of N atoms. In the LDA, the ordered alloy becomes metallic (zero band gap) at $x = 0.125$. The hybridized s orbitals of all the atoms fill the energy gap completely. In fact, at the Γ-point where the closure of the gap is seen, the states at the VBM are comprised of mixed As (p) and N (p) orbitals. Also, the charge inside the MT sphere of N has increased. One observes a localization of charge on the N atom.

For $x = 0.25$, again two different configurations of N atoms have been chosen. In C_{2v} symmetry two N atoms are next nearest neighbours among themselves, whereas in C_{3v} symmetry the nearest two N atoms are seen to be the third neighbours among themselves. For the C_{2v} and C_{3v} point group symmetries, the band gap is seen to be 0.064 and 0.0 eV, respectively. However, we have not included the results obtained for the C_{3v} symmetry in table 2. The present value, 0.064 eV, for the energy gap obtained for C_{2v} point group symmetry is in agreement with the value of 0.06 eV reported by Rubio and Cohen (1995). The inclusion of the many body effects such as considered in the GW approximation may reveal a finite energy gap instead of the closure of the gap. Rubio and Cohen have calculated the GW value as 0.7 eV. The charge inside the MT sphere of N increases further.

For $x = 0.375$, the three N atoms are next nearest neighbours among themselves and the point group symmetry is C_{3v}. The lowest conduction states enter the valence band and the band gap is zero. The MT sphere for the N atom acquires more charge.

For the next ordered structure, the $Ga_{27}As_{16}N_{11}$ supercell, the point group symmetry is chosen to be C_{3v}. There are two sets of clusters of N atoms out of the total of 11 N atoms. A cluster of four atoms is far separated from another set of seven atoms. The N atoms are second neighbours among themselves in each set. The minimum separation between the N atoms in one set and the other set is equivalent to a separation between fourth neighbours. The seven atoms lying in the second set form a centred hexagon normal to the $\langle 111 \rangle$ axis. The calculated energy gap is zero and one observes a closure of the gap.

For the $GaAs_{0.50}N_{0.50}$ ordered alloy, again the two atomic configurations having different point group symmetries T_d and C_{2v} were considered. For C_{2v} symmetry, the nearest N atoms lie in the second neighbouring lattice positions. For the T_d and C_{2v} point group symmetries, the magnitudes of the band gap are 0.00 and 0.16 eV, respectively. Rubio and Cohen (1995) have obtained a band gap of 0.4 eV without including Ga 3d states in their calculation. Their reported GW value is 1.0 eV. We do not present the results obtained for the C_{2v} symmetry in table 2. The charge in the MT sphere of N is large.

For $x = 0.625$, the point group symmetry is C_{3v}. The band gap is seen to be 0.011 eV.

For the $GaAs_{0.25}N_{0.75}$ ordered alloy ($x = 0.75$), the point group symmetry is C_{2v}. The dispersion curves are similar to those of $GaAs_{0.50}N_{0.50}$ alloy except that the direct band gap is 0.34 eV. The ionic gap is wide (-8 to -11 eV).

For an alloy containing 12.5% of As atoms, i.e., $GaAs_{0.125}N_{0.875}$, the point group symmetry is T_d in a 16-atom supercell. The band gap is seen to be 1.12 eV.

At the other end of the alloy system, for one As atom in the 54-atom supercell ($Ga_{27}AsN_{26}$) the point group symmetry is T_d. The electronic structure is depicted in figure 3(e). The band gap is smaller than that of the pure GaN lattice and is equal to 1.66 eV.

For the Ga_8N_8 ordered structure, the other end component of the alloys, the direct band

gap is 1.90 eV. The point group symmetry is T_d. The states lying just above the bottom of the conduction band correspond to the X-point of the Brillouin zone seen in the two-atom unit cell of GaN. The VBM originates from the N (p) states and the CBM from the antibonding mixed s-like states of N and Ga. This somewhat lower value of band gap in comparison to other results (Rubio *et al* 1993, Albanesi *et al* 1993, Jenkins *et al* 1994) may arise because of the use of different exchange–correlation potentials by other workers.

One observes an accumulation of charge or more localized charge around the N atoms in the concentration range $x = 0.111$–0.625. The N atoms behave in a more atomic way. The resulting fall in the potential energy leads to the lowering of N 2s states in the fundamental energy gap, filling it partially or completely. A similar conclusion has been drawn by Rubio and Cohen (1995).

In order to see the effects of a bimodal distribution of bond lengths on the electronic structure as a typical case we perform a separate calculation for the ordered Ga_8As_7N alloy. In this alloy the bond length for each GaAs and GaN bond is same and is equal to 2.38 Å in a unimodal distribution of bond lengths. In order to see the effect of the variation of bond length we have chosen a value of 2.02 Å for all the four neighbouring GaN bonds around the central N atom, keeping the bond lengths of the GaAs bonds equal to 2.38 Å. The band gap is seen to be 0.035 eV against a zero value obtained for a Ga–N bond length of 2.38 Å. Thus, the zero band gap seen in a finite concentration range of N does not seem to be affected significantly in a bimodal distribution of bond lengths.

Table 2. Band-gap variation in the ordered $GaAs_{1-x}N_x$ structures All energies are measured in eV

		Other calc.		
System (x)	Present	LDA	GW	Expt
0 000	0 61	0.60[a]	1.3[c]	1.52[b]
0.037	0.44			
0.074	0.28			
0.111	0.11			
0.125	0.00			
0 250	0.064	0.06[e]	0.7[e]	
0.375	0 00			
0.407	0.00			
0 500	0.00	0.40[e]	1.0[e]	
0 625	0.011			
0.750	0.34			
0.875	1.12			
0 963	1.66			
1.000	1 90	2.10[d], 1.97[e], 2 32[f]	3.1[d].	3 20[g], 3 30[h], 3 52[i], 3 4[j]

[a] Model dielectric function, Zhu and Louie 1991.
[b] Pseudopotential or quasi-particle energy, Rubio and Cohen (1995).
[c] *Landolt–Börnstein* 1982.
[d] Pseudopotential, Rubio *et al* 1993.
[e] LMTO–ASA, Albanesi *et al* 1993.
[f] Pseudopotential, Jenkins *et al* 1994.
[g] Optical absorption, Lei *et al* 1992.
[h] Photoluminescence and cathodoluminescence, Paisley *et al* 1989, Sitar *et al* 1992.
[i] Cathodoluminescence at 53 K on epitaxial films, Harrison 1985.
[j] Optical absorption, Yoshida *et al* 1982.

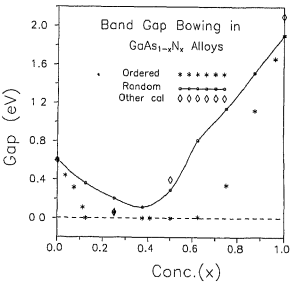

Figure 4. Variation of band gap with the concentration x for the ordered and random $GaAs_{1-x}N_x$ alloys. The results of other calculations are taken from Zhu and Louie (1991), Rubio and Cohen (1995) and Rubio *et al* (1993).

The direct band gap energy of the $GaAs_{1-x}N_x$ ordered alloys, for $x = 0.0$, 0.037, 0.074, 0.111, 0.125, 0.25, 0.375, 0.407, 0.50, 0.625, 0.75, 0.875, 0.963 and 1.0 is presented in table 2. A closure of gap is observed from $x = 0.125$ to 0.625. The calculated band gaps are compared with the available experimental data for $x = 0.0$ and 1.0 and the other calculated values available for $x = 0.0$, 0.25, 0.50 and 1.0. The variation of band gap energy with concentration x of N atoms is shown in figure 4.

Weyers *et al* have obtained an empirical linear relationship for the measured change in energy gap of $GaAs_{1-x}N_x$ alloys up to 1.5% of N atoms. In the present calculation, the lowest concentration of N atoms is 3.7%. Assuming the Weyers *et al* relationship to be true for 3.7% of N atoms, the extrapolated decrease in bandgap for $x = 0.037$ is 0.44 eV. This denotes a change of about 30%.

In the present calculation the calculated decrease in the band gap is about 28%, which is in very good agreement with the experiment.

2.2. *Random alloys*

In general, one may not expect the occurrence of a particular ordered structure. A more probable situation is the occurrence of a number of various different local atomic configurations in different parts of an alloy. The alloy may be a disordered one depending upon the growth conditions. The properties of the disordered alloy may be simulated by considering the statistical mechanical distributions of the ordered structures. A cluster expansion method has been adopted (Sanchez and de Fontaine 1981, Sanchez *et al* 1984, Srivastava *et al* 1985) in the past for obtaining such a statistical mechanical description. It has been suggested that the coefficient of the cluster expansion method may be obtained by a first principles calculation of a set of ordered structures. This method which was first used for binary alloys can be extended to the ternary alloy in the case where the disorder is

assumed to occur only on one type of site, say anion or cation as is the case for the presently discussed $AB_{1-x}C_x$ alloys. One simplifies the calculation by truncating the cluster expansion at the level of nearest neighbour interactions. For a tetrahedron structure one studies the five basic structures corresponding to the nearest neighbour tetrahedron $B_{4-n}C_n$ ($n = 0$–4). The statistical mechanical property of the alloys may be considered as the property seen for the random alloys Any statistical property $F(x)$ at a particular concentration x may be expanded as

$$F(x) = \sum_n P_n(x) F_n \tag{1}$$

where F_n is the property for the anion tetrahedron and $P_n(x)$ is the probability of the occurrence of cluster $B_{4-n}C_n$.

The probability of each cluster which is in general temperature dependent should be obtained at any given temperature by minimizing the free energy with respect to the probability $P_n(x, T)$. However, we assume here a temperature independent random distribution function for the probability given by

$$P_n(x) = \binom{4}{n} x^n (1-x)^{4-n}. \tag{2}$$

A similar calculation has been done by earlier workers (Srivastava *et al* 1985, Albanesi *et al* 1993, Agrawal *et al* 1997). This is obviously a first approximation and may be expected to be valid for the case of frozen-in disorder of the gas or liquid phase from which the solid solutions are quenched.

Using (1) we have calculated the band gap for the random alloys at different concentrations of N and have included the results in figure 4. One observes a very large bowing in the energy gap curve with a minimum value of 0.114 eV at $x = 0.375$.

Our results compare very well with those obtained by Bellaiche *et al* (1996) for electronic structure. Similar to them, we observe a weak localization of the conduction band minimum wavefunctions around N atoms in the N impurity region (dilute N alloys) and a strong localization of valence band maximum wavefunctions around As atoms in the As impurity region (N dominated alloys). For some of their 'special quasirandom structures' which are different from our fixed zinc blende structures, they obtain a negative band gap in contrast to our zero band gap. These authors have obtained a minimum value of band gap equal to 0.4 eV for $x = 0.50$ random alloy in contrast to our value of 0.3 eV for the random alloy obtained here without using any fitting procedure.

3. Conclusions

The first principles full potential self-consistent linear muffin-tin orbital (LMTO) method has been employed to understand the electronic properties of 14 ordered and random $GaAs_{1-x}N_x$ alloys. The calculated lattice constant shows quite a non-linear behaviour. A large band-gap bowing is observed. A near closure of the fundamental energy gap is observed for an N atomic concentration range of $x = 0.125$–0.625. Inclusion of many body effects such as the GW approximation may open the gap by ~0.7–0.9 eV, making these alloys narrow gap materials in the N concentration range of 0.125–0.625. This closure of gap arises because of the descending of the s-like states of N hybridized with those of Ga and As atoms. The results are in agreement with those of other calculations.

Acknowledgments

The authors are thankful to the University Grants Commission, New Delhi and the Department of Science and Technology, New Delhi for financial assistance.

References

Agrawal Bal K, Agrawal S, Yadav P S and Kumar S 1997 *J. Phys.: Condens. Matter* **9** 1763
Albanesi E A, Lambrecht W R L and Segall B 1993 *Phys. Rev.* B **48** 17 841
Bellaiche L, Wei S H and Zunger A 1996 *Phys. Rev* B **54** 17 568
Harrison W A 1985 *Phys. Rev.* B **31** 2121
Hedin L and Lundqvist B I 1971 *J. Phys. C: Solid State Phys.* **4** 2063
Jenkins S J, Srivastava G P and Inkson J C 1994 *J. Phys. C. Solid State Phys.* **6** 8781
Landolt–Börnstein New Series 1982 Group III vol 17, ed K H Hellwege (New York: Springer)
Lei T, Moustakas T D, Graham R J, He Y and Berkowitz S J 1992 *J. Appl Phys.* **71** 4833 and references therein
Paisley M, Sitar Z, Posthill J B and Davis R F 1989 *J. Vac Sci. Technol.* A **7** 701
Perdew J P and Levy M 1983 *Phys. Rev. Lett* **51** 1884
Rubio A and Cohen M L 1995 *Phys. Rev.* B **51** 4343
Rubio A, Corkill J L, Cohen M L, Shirley E L and Louie S G 1993 *Phys Rev.* B **48** 11 810
Sanchez J M and de Fontaine D 1981 *Structure and Bonding in Crystals* vol 2, ed M O'Keefe and A Navrotsky (New York: Academic) p 117
Sanchez J M, Ducastell F and Gratias D 1984 *Physica* A **128** 334
Sham L J and Schluter M 1983 *Phys. Rev. Lett* **51** 1888
Sitar Z *et al* 1992 *J. Mater. Sci Lett.* **11** 261
Srivastava G P, Martins J L and Zunger A 1985 *Phys. Rev.* B **31** 2561
Weyers M, Sato M and Ando H 1992 *Japan. J. Appl. Phys.* **31** L853
Yoshida S, Misawa S and Gonda S 1982 *J. Appl. Phys* **53** 6844
Zhu X and Louie S G 1991 *Phys. Rev.* B **43** 14 142

PERGAMON

Solid State Communications 109 (1999) 383–388

solid state communications

Anomalous band gap bowing in $AlAs_{1-x}N_x$ alloys

R. Srivastava, B.K. Agrawal, P.S. Yadav

Physics Department, Allahabad University, Allahabad 211002, India

Received 10 July 1998; received in revised form 19 October 1998; accepted 18 November 1998 by S. Ushioda

Abstract

We have employed a first principle self consistent linear muffin tin orbital method in the local density approximation to calculate the electronic structure of the nine $AlAs_{1-x}N_x$ alloys with $x = 0.0, 0.125, 0.25, 0.375, 0.50, 0.625, 0.75, 0.875$ and 1.0. The lattice parameter shows a non linear behaviour with the concentration of N-atoms. A quite smaller gap appears in the neighbourhood of $x = 0.125$ concentration of N-atoms. The state lying at the CBM, which is composed of N-s, Al(s,p), As-s descends into the fundamental gap filling it partially. For the random alloys the band gap also shows anomalous bowing. © 1999 Published by Elsevier Science Ltd

Keywords: A. Semiconductors, D. Optical properties, D. Electronic band structure

1. Introduction

The semiconducting alloys of III–V elements have drawn much attention from experimental and theoretical workers in recent years towards the study of their electronic and physical properties because of their potential applications in opto-electronic devices [1-3]. These alloys exhibit very interesting electronic properties such as variation or lowering of energy band gap, etc. Normally, the energy band gap variation is seen to be linear in III–V semiconducting alloys in which the concentration of cation component is varied as reported in $Ga_{1-x}Al_xN$ alloys [4-5]. But, on the other hand, in some III–V alloys when the concentration of anion component is varied, the band gap reduces to a very small value or some times to zero (i.e. metallic behaviour) as has been seen in $GaAs_{1-x}N_x$ alloys at low concentrations. Thus these mixed group V alloys such as $Al(Ga)As_{1-x}N_x$ can in principle allow one to close the band gap between the nitrides and the arsenides and will enable the fabrication of III–V light emitting devices covering the entire visible spectrum.

The III–V nitride semiconductors are potentially useful as high frequency,microwave and short-wavelength electroluminescent devices. The specific role of nitrogen is in the formation of short bonds which leads to smaller lattice constants than for other III–V semiconductors. At ambient conditions the AlN crystallizes in the hexagonal wurtzite structure, but the zinc blende structure is only slightly higher in energy [6]. These nitride compounds undergo a structural phase transformation to rocksalt structure under high pressure such as 12.9 GPa for AlN [7]. Very few ab initio calculations of the electronic and physical properties of group III nitrides, arsenides and their alloys have been reported in the literature. Christensen and Gorczyca [8] have investigated the optical and structural properties of III–V nitrides by means of band structure and total energy calculations.

Experimental results for the electronic properties and the microscopic parameters of AlN and

0038-1098/99/$ - see front matter © 1999 Published by Elsevier Science Ltd
PII. S0038-1098(98)00577-8

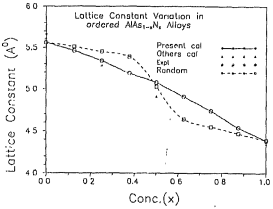

Fig. 1. Lattice constant variation in the ordered and random $AlAs_{1-x}N_x$ alloys.

$AlAs_{1-x}N_x$ alloys have been scarce as a result of difficulties in growing high quality single crystals. More experimental work is required on these compounds to understand the various physical properties. Rubio and cohen [1] have performed a pseudopotential and quasiparticle study of the ordered $AlAs_{1-x}N_x$ alloys.

In an earlier article, we investigated the structural and electronic properties of the $GaAs_{1-x}N_x$ alloys [9]. In the present article, we investigate the electronic structure of ordered $AlAs_{1-x}N_x$ alloys by employing a full potential self consistent linear muffin tin orbital (LMTO) method. For the details of the method the readers are refered to our earlier articles [5,9]. The calculated results for electronic structure and band gap energies are presented in Section 2. Section 3 contains the main conclusions.

2. Calculation and results

For the calculation of electronic properties of ordered $AlAs_{1-x}N_x$ alloys, a unit cell having eight molecular units has been considered. The calculations for nine ordered systems of $AlAs_{1-x}N_x$ alloys ($x = 0.0$, 0.125, 0.25, 0.375, 0.50, 0.625, 0.75, 0.875 and 1.0) have been performed.

The radii of non overlapping spheres drawn around each real and empty atom are properly chosen for each value of concentration (x) except for nitrogen atom for which the radius of atomic sphere is chosen to be the same and equal to 1.43 a.u. The radius of atomic sphere Al atom is varied from 2.30 to 1.92 a.u. The radius of As atomic sphere varies from 2.26 to 1.88 a.u. Al ($3s,3p,3d$), As ($4s,4p,4d$) and N ($2s,2p$) states are considered as valence states.

In the computation of potential and charge density, linear muffin tin orbital envelopes have been expanded in terms of Hankel functions having the spherical harmonic components $l \leq 4$. Three values -0.01, -1.0 and -2.3 Ry for the decay factor in the Hankel functions are used in the construction of the muffin tin orbitals for real atoms. In the interstitial region two values -0.01 and -1.0 Ry of the decay factor have been employed. Each supercell contains an equal number of the real atomic muffin tin spheres (MTS) and the empty MTSs. The scalar relativistic effects have been considered in all the calculations. For the exchange correlation potential, the parametrization of Hedin and Lundqvist [10] has been chosen. In the present method, the wave functions of the core electrons of the atoms are relaxed and in the self consistent calculation in each iteration, the core electron charge density is recalculated.

A deficiency of the local density theory is that the calculated value of the fundamental energy gap is about 50% of the experimental one. This originates from the fact that the excitation energies of these systems are not given by eigenvalues of the Kohn–Sham equations in Refs. [11,12]. The quasi-particle energies and wide band gaps have been calculated in the so-called GW approximation of the electron self-energies Σ. This self energy is seen to be a non-local energy dependent effective potential. This is beyond the scope of present work.

2.1. Ordered structures

The lattice parameters for different values of x in ordered $AlAs_{1-x}N_x$ alloys have been calculated by obtaining the minimum energy for each system and are plotted in Fig. 1. The calculated values are compared with other calculations and also with experimental values (see Table 1). The calculated values of lattice parameters for $x = 0$ and 1 are very close to the available experimental values. The variation of lattice parameter with x is seen to be non-linear. Our values are slightly on the higher side

Table 1
Variation of lattice constant with concentration of the constituent atoms in the ordered $AlAs_{1-x}N_x$ structures. All values are measured in A^0

System (x)	Present	Other Cal	Expt.
0.000	5.56	5.61 [16]	5.66 [17]
0.125	5.46		
0.250	5.34	5.28 [1]	
0.375	5.19		✓
0.500	5.08	4.91 [1]	
0.625	4.91		
0.750	4.74		
0.875	4.54		
1.000	4.39	4.35 [1,18]	4.37 [19]

than those reported by Rubio and Cohen for some structures.

The electronic structure for nine systems of ordered $AlAs_{1-x}N_x$ alloys ($x = 0.0, 0.125, 0.25, 0.375, 0.50, 0.625, 0.75, 0.875$ and 1.0) have been calculated. The zinc blende structure has been considered for all the crystal lattices. The size of the primitive lattice vectors for the 16-atom supercell is doubled which results into the zone-folding. The number of branches increase corresponding to eight molecular units. The calculated electronic dispersion curves are presented in Fig. 2. The symmetry points are W (0.50, 0.25, 0), L (0.25, 0.25, 0.25), Γ (0, 0, 0,), X (0.50, 0, 0) and K (0.375, 0.375, 0). In all the electron dispersion curves, the Fermi-level has been taken at zero electron volt.

For Al_8As_8 ordered system, the point group symmetry is T_d. The calculations were performed for 2-selected k-points in the irreducible part of Brillouin zone for achieving self consistent results. The energy gap is indirect and is equal to 1.21 eV. The main contributors to the valence band maximum (VBM) are As-p with some Al-p like states. On the other hand conduction ban minimum (CBM) is comprised of mainly Al-p and some As-p like states.

For the dilute ordered Al $As_{0.875}N_{0.125}$ alloy, the point group symmetry is T_d. There is one N-atom in the 16-atom supercell and the N-atoms of the two adjacent supercells are fourth neighbours among themselves. The direct band gap is 0.59 eV. The lowest conduction state originating from the hybridization of s-orbitals of all the constituent atoms descends into the band gap of the AlAs. The remarkable observation is that the Al_8As_8 compound becomes a direct band gap material at a small value of $x = 0.125$.

For $x = 0.25$, the point group symmetry is C_{2v}. In this structure two N-atoms are next nearest neighbours among themselves. The band gap becomes a direct one and is equal to 0.77 eV. The VBM is composed of p-like state of As, Al and N atoms. On the other hand, the main contibutors to the CBM are Al(s,p), N-s and As-s like states.

For the $AlAs_{0.625}N_{0.375}$ ordered alloy, the point group symmetry is C_{3v}. The three N-atoms are next nearest neighbours among themselves. The direct band gap is 1.066 eV. For $x = 0.50$, the point group symmetry is T_d. The direct band gap is equal to 1.25 eV. For the $AlAs_{0.375}N_{0.625}$ ordered alloy, the point group symmetry is C_{2v}. The band gap changes to indirect one and is equal to 1.09 eV. For $x = 0.75$, $AlAs_{0.25}N_{0.75}$ ordered alloy, the point group symmetry is C_{2v}. The indirect band gap is 1.31 eV. For the $AlAs_{0.125}N_{0.875}$ ordered alloy, the point group symmetry is T_d. The indirect band gap is 2.13 eV.

For the end component, Al_8N_8 ordered structure the point group symmetry is T_d. The indirect energy gap is 3.35 eV.

There is a localization of charge on the N-atoms and the charge within the muffin tin spheres increases with the N-concentration.

The variation of the direct and indirect band gap energies with x (concentration of N-atoms) for nine ordered systems $AlAs_{1-x}N_x$ are presented in Table 2 and Fig. 3. One observes that there is a crossover from indirect to direct band gap energy approximately at $x = 0.02$ and the alloys becomes direct up to $x \approx 0.56$. The alloys at high concentration ($x > 0.56$) again returns to an indirect one.

On making comparison with the calculation of Rubio and Cohen our values for the direct and indirect band gaps, for the end components, AlAs and AlN, are quite close to (Table 2) their values. However, for the alloys, there are quite large differences. For $x = 0.25$, our value (0.77 eV) is higher than their values (0.45 eV), whereas reverse is the case for the indirect band gap. For $x = 0.50$ the present value (1.25 eV) is quite close to their value (1.13 eV). However, our indirect gap 3.92 eV is much higher than their corresponding value of 0.76 eV. Thus this alloy is direct bank gap in our calculation in contrast to Rubio and Cohen who have seen it as an indirect band gap

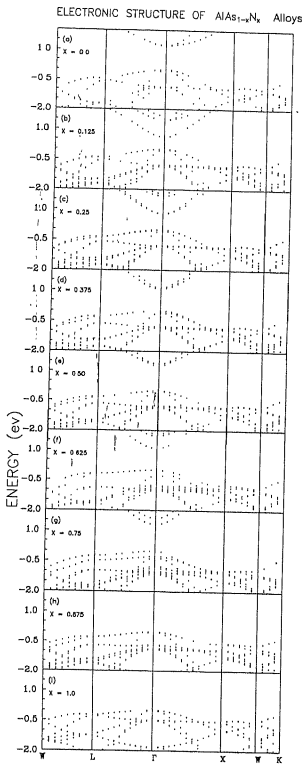
ELECTRONIC STRUCTURE OF AlAs1−xNx Alloys
(a) x = 0.0
(b) x = 0.125
(c) x = 0.25
(d) x = 0.375
(e) x = 0.50
(f) x = 0.625
(g) x = 0.75
(h) x = 0.875
(i) x = 1.0
ENERGY (ev)
1.0
−0.5
−2.0
W
L
Γ
X
W
K

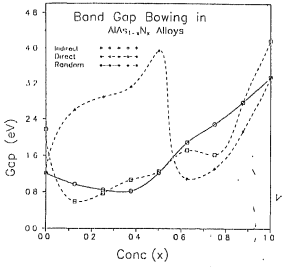

Fig. 3. Variation of band gap with the concentration x for the ordered and random $AlAs_{1-x}N_x$ alloys.

material in their pseudopotential calculation. It may be noted that Rubio and Cohen has employed a pseudopotential calculation for a smaller unit cell containing 8 atoms.

2.2. *Random alloys*

The properties of the disordered alloys can be obtained by considering the statistical mechanical distribution of the ordered structures. For obtaining such a statistical mechanical properties a cluster expansion method has been used [13–15]. In this method it has been suggested that the coefficients of the cluster expansion may be derived by a first-principles calculation of a set of ordered compounds. The method which was primarily used for the binary alloys can be applied to the ternary alloys in the case where the disorder is assumed to occur only on one type of site, say anion or cation as is the case for the presently discussed $AB_{1-x}C_x$ alloys. The problem further simplifies by truncating the cluster expansion at the level of the nearest neighbour interactions. For a tetrahedron structure one studies the five basic structures corresponding to the nearest neighbour tetrahedron $B_{4-n}C_n$ ($n = 0$–4). The statistical mechanical property of the alloys may be considered as the property seen for the random alloys. Any statistical property $F(x)$ at a particular concentration x may be expanded as

$$F(x) = \sum_n P_n(x) F_n$$

where F_n is the property for anion tetrahedron and $P_n(x)$ is the probability of the occurence of cluster $B_{4-n}C_n$.

The probability of each cluster which is in general temperature dependent should be obtained at any given temperature by minimizing the free energy with respect to the probability $P_n(x,T)$. However, we assume here a temperature independent random distribution function for the probability given by

$$P_n(x) = \binom{4}{n} x^n (1-x)^{4-n}$$

This is obviously a first approximation and may be expected to be valid for the case of frozen-in disorder of the gas or liquid phase from which the solid solutions are quenched.

We have first calculated the lattice constant for random alloys using the above theory and results are presented in Fig. 1. We find that the lattice constant for random alloys have greater (less) than that of the ordered alloys for $x < 0.50$ (> 0.50).

For the random alloys the calculation has been made by taking the smaller value of band gaps (direct or indirect) for each alloy. There is a large band gap bowing in the energy gap curve with a minimum value of 0.82 eV at $x = 0.375$.

3. Conclusion

The first principles full potential self consistent linear muffin tin orbital method has been employed to investigate the electronic properties of nine ordered and random $AlAs_{1-x}N_x$ alloys. The calculated lattice constant for ordered alloys shows a non linear

Fig. 2. Electronic dispersion curves for the ordered $AlAs_{1-x}N_x$ alloys (a) $x = 0.00$, (b) $x = 0.125$, (c) $x = 0.25$, (d) $x = 0.375$, (e) $x = 0.50$, (f) $x = 0.75$, (g) $x = 0.875$ and (h) $x = 1.0$.

Table 2
Band Gap Variation in the ordered $AlAs_{1-x}N_x$ structures. All energies are measured in eV

System (x)	Present indirect	Calculation Direct	Others indirect	Calculation Direct	Expt.
0.000	1.21	2.17	1.33 [16]	2.07 [16]	2.3 [20]
0.125	2.61	0.59			
0.250	2.89	0.77	3.47 [1]	0.45 [1]	
0.375	3.12	1.066			
0.500	3.92	1.25	0.76 [1]	1.13 [1]	
0.625	1.09	1.72			
0.750	1.31	1.62			
0.875	2.13	2.77			
1.000	3.35	4.18	3.2 [1]	4.2 [1]	6.1 [4], 6.28 [21]

behaviour. A smaller fundamental gap is observed for $x = 0.125$, because of the descending of the s-like states of N hybridized with those of Al and As atoms. We observe a crossover from indirect to direct band gap approximately at $x = 0.02$ and the alloys becomes indirect again at $x \approx 0.56$. For random alloys also, a large band gap bowing is observed.

Acknowledgements

The authors are thankful to the University Grants Commission, New Delhi, and the Department of Science and Technology, New Delhi, for financial assistance.

References

[1] A. Rubio, M.L. Cohen, Phys. Rev. B51 (1995) 4343.
[2] A. Rubio, J.L. Corkill, E.L. Shirely, S.G. Louie, Phys. Rev. B48 (1993) 11810.
[3] K. Kim, W.R.L. Lambrecht, B. Segall, Phys. Rev. B53 (1996) 16310
[4] S. Yoshida, S. Misawa, S. Gonda, J. Appl. Phys. 53 (1982) 6844.
[5] B K Agrawal, S. Agrawal, P.S. Yadav, S. Kumar, J. Phys. Condens. Matter 9 (1997) 1763.
[6] R.M. Wentzcowich, M.L. Cohen, P.K. Lam, Phys. Rev. B36 (1987) 6058.
[7] M Ueno, A. Onodera, O. Shimomuna, K. Takemura, Phys. Rev. B45 (1992) 10123.
[8] N.E. Christensen, I Gorczyca, Phys. Rev. B50 (1994) 4397.
[9] B K Agrawal, P.S. Yadav, Rekha Srivastava, S. Agrawal, J. Phys. Conden. Matt. 10 (1998) 4597.
[10] L Hedin, B.I. Lundqvist, J. Phys. C:Solid State Physics 4 (1971) 2063.
[11] J.P Perdew, M. Levy, Phys. Rev. Lett. 51 (1983) 1884.
[12] L.J. Sham, M. Schulter Phys. Rev. Lett. 51 (1983) 1888.
[13] J.M. Sanchez, D. de Fontain, in: M. O'Keefe, A. Navrotsky (Eds.), Structure and Bonding in Crystals, vol. 2, Academic, New York, 1981, pp. 117.
[14] J.M. Sanchez, F. Ducastell, D. Gratias, Physica A 128 (1984) 334.
[15] G.P. Srivastava, J.L. Martins, A. Zunger, Phys. Rev. B31 (1985) 2561.
[16] X. Zhu, S.G. Louie, Phys. Rev. B43 (1991) 14142.
[17] K.H. Hellwege, Landolt-Bornstein (Eds.), Numerical Data and Functional Relationship in Science and Technology, 17A, Springer, New York, 1982 New Series, Group III.
[18] E.A. Albanesi, W.R.L. Lambrecht, B. Segall, Phys. Rev. B48 (1993) 17841.
[19] R.W. Wycoff, Crystal Structures 2nd ed., vol. 1, Wiley-Interscience, New York, 1964.
[20] CRC Handbook of Chemistry and Physics 70th ed. CRC Press Inc, Boca Raton, Fl, 1989–90.
[21] B. Perry, R.F. Rutz, Appl. Phys. Lett. 33 (1978) 319.

PERGAMON

Solid State Communications 118 (2001) 479–484

solid state communications

www.elsevier.com/locate/ssc

A first-principles study of structural and electronic properties of $Ga_{1-x}Al_xAs$ alloys

Rekha Srivastava[a,*], P.S. Yadav[a], Savitri Agrawal[a], B.K. Agrawal[a], S. Kumar[b]

[a]*Department of Physics, Allahabad University, Allahabad 211002, India*
[b]*Department of Physics, M.J.P. Rohilkhand University, Bareilly 243006, India*

Received 15 June 2000; received in revised form 15 January 2001; accepted 6 February 2001 by S. Ushioda, received in final form by the Publisher 20 April 2001

Abstract

A first principles full potential self-consistent linear muffin tin orbital (FPLMTO) method alongwith density functional theory in the local approximation has been employed to investigate the structural and electronic properties of seven $Ga_{1-x}Al_xAs$ alloys in their ordered and random configurations. A linear (non-linear) variation of the lattice constant with the concentrations of the constituent atoms is seen for the ordered (random) structures. A direct to indirect band gap crossover takes place for $x = 0.375$. Also, a band gap bowing below and above the crossover for both the direct and indirect band gaps is seen. The direct and indirect band gaps obtained for the ordered structures are in very good agreement with the photoluminescence and absorption data available. Our results support the occurrence of the well ordered structures in the alloys. © 2001 Elsevier Science Ltd. All rights reserved.

PACS: 61.66.Dk; 61.72.Ss; 78.55.−m

Keywords: A. Semiconductors; A. Heterojunctions; C. Impurities in semiconductors

1. Introduction

There has been tremendous interest in the development of opto-electronic devices, especially for obtaining solar cells, light emitting diodes (LEDs) and laser devices. GaAs, which has a comparatively smaller band gap, plays an important role in the semiconductor industry. The fact that GaAs is a direct band gap semiconductor makes it very useful for electro-optical devices. The almost perfect lattice match when combined with $Ga_{1-x}Al_xAs$ makes it possible to use $Ga_{1-x}Al_xAs$/GaAs heterojunctions and superlattices as light emitting devices like LEDs, photo-detectors, semiconductor lasers, etc. They find applications in high-mobility transistors and in microelectronics.

Earlier, we have performed an ab initio study of the structural and electronic properties of the $(Ga, Al)As_{1-x}N_x$ alloys [1,2]. In the present article, we extend our study towards the structural and electronic properties of $Ga_{1-x}Al_xAs$ alloys. For the details of the method, we refer to our earlier papers [1–3]. Section 2 contains the details of the calculations and results. The conclusions are contained in Section 3.

2. Calculations and results

We employ a unit cell containing eight molecular units for the different crystal structures of $Ga_{8-n}Al_nAs_8$ alloys for $n = 0 - 8$. The scalar relativistic effects have been considered in all the calculations. For the exchange correlation potential, the parametrization of Hedin and Lundqvist [4] has been chosen.

2.1. Ordered structures

In choosing these different possible atomic configurations, it has been kept in mind that the point group symmetry of the unit cell should be at least C_{2v}. The lattice parameter for each system has been calculated by minimizing the crystal energy. The calculated lattice parameters for the ordered and the random alloys are compared with the results of other calculations [5] and the available experimental data [6] in

* Corresponding author.

0038-1098/01/$ - see front matter © 2001 Elsevier Science Ltd. All rights reserved.
PII: S0038-1098(01)00051-5

Table 1
Variation of the lattice constant with the concentrations of the constituent atoms in the $Ga_{1-x}Al_xAs$ structures (all values are measured in Å)

System (x)	Present calculations		Other calculations	Experimental
	Ordered	Random		
0.000	5.554	5.554	5.61[a]	5.65[b]
0.125	5.556	5.556		
0.250	5.557	5.556		
0.375	5.558	5.556		
0.500	5.559	5.561		
0.625	5.560	5.562		
0.750	5.562	5.563		
0.875	5.563	5.565		
1.000	5.564	5.564	5.61[a]	5.66[b]

[a] Ref. [5].
[b] Ref. [6].

Table 1. The variation of lattice parameter with concentration x is seen to be linear for the ordered configurations. The lattice parameters of the end components GaAs and AlAs are reproduced in the calculation within 2%.

The electronic structure for all the systems in the neighbourhood of the energy gap is presented in Fig. 1. The symmetry points of the bcc Brillouin zone are $W(0.5, 0.25, 0)$, $L(0.25, 0.25, 0.25)$, $\Gamma(0, 0, 0)$, $X(0.5, 0, 0)$ and $K(0.375, 0.375, 0)$. The length of each primitive lattice vector for the 16-atom supercell is doubled as compared to those of the simple two-atom unit cell. This results in zone-folding. Also, the number of branches increases because of the larger number of molecular units in the supercell. The origin of energy is chosen at the top of the valence band for each alloy.

For Ga_xAs_x, the point group symmetry is T_d. The state at the valence band maximum (VBM) is triplet and originates mainly from the As-p orbitals. The conduction band minimum (CBM) comprises of the s-like orbitals mainly of Ga with some contribution from As. The states just above the bottom of the conduction band at the Γ-point corresponds to the L-point of the Brillouin zone for the two atom unit cell because of the zone-folding. For GaAs, the band gap is direct and is equal to 0.61 eV in local density approximation (LDA). The indirect band gap is 1.07eV. The observation of a smaller energy gap in the local density approximation is an usual phenomenon.

In LDA, one neglects many body effects and the resulting electron self-energies. In fact, the eigenvalues of the Kohn–Sham equations in one-electron theory in the conduction band region are not the excitation energies of the systems [7,8]. There are several methods [9–11] for calculating the electron self-energies. In one of them, namely the GW approximation, the quasi-particle energies have been calculated which lead to wide band gaps somewhat nearer to the experimental values. In the GW approximation [12], the value of the direct band gap is obtained as 1.3 eV, which is again underestimated by 0.22 eV as compared to the experimental value of 1.52 eV.

In some semiconductors like Si, a consideration of the first-order effects of the many body interactions has shown that the resulting self-energy correction (SEC) in the fundamental energy gap is quite stationary. This prompted us to choose a constant value for SEC for each alloy to obtain realistic values for the band gaps, which may be comparable to the experimental values. In the present case, the experimental data for the indirect band gap is available for the whole concentration range [13], we therefore use this data to obtain the underestimation of the band gap calculated here in LDA for each alloy.

We adopt the following procedure: we first determine the underestimation of the indirect band gap in the case of the end components of the alloys, i.e. GaAs and AlAs. For GaAs and AlAs, the values for indirect band gaps in LDA are 1.07 and 1.21 eV, respectively, whereas the reported experimental values are 2.01 and 2.25 eV, respectively. The many body effects cause, thus, an underestimation of band gap by 0.94 and 1.04 eV, in GaAs and AlAs, respectively, and we adopt these values as SECs for the end components of the alloys. As the values of SEC for the end components are quite near, we assume that for $Ga_{1-x}Al_xAs$ alloys the SEC changes linearly from 0.94 to 1.04 eV for the full concentration range of $x = 0$–1. In our future calculation, we also assume this linear variation of SEC as wave vector-independent. For GaAs, the direct and indirect band gaps after including SEC are 1.55 and 2.01 eV, respectively.

For the most dilute ordered $Ga_{0.875}Al_{0.125}As$ alloy, the point-group symmetry remains T_d as shown in Fig. 1(b). There is one Al atom in the 16-atom supercell and the Al atoms of the two adjacent supercells are fourth neighbours among themselves. The calculated direct and indirect band gaps are 0.70 and 1.09 eV, respectively. For $x \leq 0.375$, the

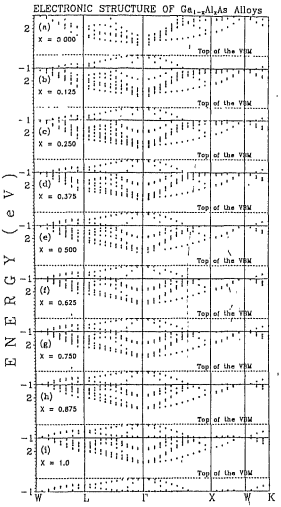

Fig. 1. Electronic dispersion curves for the ordered $Ga_{1-x}Al_xAs$ alloys for (a) $x = 0.00$, (b) $x = 0.125$, (c) $x = 0.25$, (d) $x = 0.375$, (e) $x = 0.50$, (f) $x = 0.625$, (g) $x = 0.75$, (h) $x = 0.875$ and (i) $x = 1.00$

states just above the bottom of the conduction band at the Γ point corresponds to the L-point of the Brillouin zone for the two atom unit cell because of the zone folding and the alloys possess direct band gap. There is splitting of states due to the interaction between the folded states, e.g. interaction between the L- and X-point states. An averaging has been done to determine the energies of the conduction states. At Γ-symmetry point, the VBM is mainly composed of the hybridized As-p and Ga-p like orbitals. The state at CBM is composed of the s-like orbitals of Al and Ga. For $x = 0.125$, the SEC turns out to be 0.95 eV and the self-energy corrected direct and indirect band gaps are 1.65 and 2.04 eV, respectively.

For the next ordered $Ga_{0.75}Al_{0.25}As$ alloy, there are only two possible different configurations which may be considered. They possess C_{3v}- and C_{2v}-symmetries. In both the symmetry configurations, the two Al atoms of the unit cell are the next-nearest neighbours among themselves in C_{2v} symmetry in the same unit cell whereas in C_{3v} symmetry in the adjacent unit cells. The band gap is direct in both the configurations. The values of the direct and indirect band gaps for the C_{3v}-symmetric configuration are somewhat lower than those for the C_{2v}-configuration. The values of band gaps for C_{2v} are 0.79 and 0.97 eV and those for C_{3v} are 0.93 and 1.13 eV, respectively. The states at VBM have contributions mainly from the p-like orbitals of As, whereas the states at CBM again have contributions from s-like orbitals of Ga and Al.

The extrapolated SEC is 0.97 eV and the values of the band gaps after the inclusion of SEC are 1.76 and 1.94 eV for C_{2v}. For C_{3v} configuration, these values are 1.90 and 2.10 eV, respectively. We look for the experimental data in the literature and find the absorption and the photoluminescence data of Monemar et al.[13]. For a sample containing $x = 0.25$, they the values obtained for the direct and indirect band gaps are 1.92 and 2.07 eV, respectively. On making comparison with the present values obtained for C_{2v} and C_{3v} configurations in the until cell, one finds that the experimental values are very close to the presently calculated values obtained for the C_{3v} configuration of atoms in this alloy.

For $x = 0.375$, again there are two possible different atomic configurations having the point group symmetries C_{3v} and C_{2v} as shown in Fig. 1(e) and (f), respectively. In C_{3v} symmetry, the three Al atoms are next-nearest neighbours among themselves whereas in C_{2v}-symmetry, Al atoms are again next-neighbours, but they do not couple to the same As atom, instead form a linear chain. The VBM originates mainly from p-like orbitals of As atoms. The CBM comprises the s-like orbitals of Ga and Al atoms. For $x = 0.375$, the values for the direct and indirect band gaps for the two atomic configurations are quite similar and are 1.1 and 1.02 eV, respectively. The behaviour of the alloy has now changed from a direct to an indirect band gap semiconductor. The SEC is 0.98 eV, making the values of the direct and indirect band gaps as 2.08 and 2.0 eV, respectively.

For the ordered $Ga_{0.50}Al_{0.50}As$ alloy, again there are two possible atomic configurations having point-group symmetries T_d and C_{2v}. In T_d-symmetry, all the four Al atoms in the unit cell couple to the same As atom and are second neighbours among themselves. In the C_{2v}-symmetric configuration, there are two separated sets of two next nearest neighbouring Al atoms which are not coupled to the same As atom. For both symmetries, the values of the band gap are slightly different. The CBM states at the Γ-point are the states of L- and X-points of a two-atom unit cell. The band gap becomes indirect. The VBM is composed of p-like orbitals of As atoms with some contributions from d-orbitals of Al. The CBM comprised s-like states of Al, Ga with some p-like contributions from Al. The SEC is 0.99 eV. The direct

and indirect band gaps after including the SEC are 3.05 and 2.11 eV, respectively.

For $x = 0.625$, similar to the $x = 0.375$ case there are two atomic configurations having the point-group symmetries as C_{2v} and C_{1h}. For all alloys having $x > 0.625$ at the Γ-point of CBM, one finds states appearing at X-point for a two-atom unit cell and the band gap is indirect. For $x = 0.625$, the band gap is equal to 1.16 eV. The direct band gap is 2.09 eV. The VBM is composed of p-like orbitals of As, whereas the CBM is composed of s-like orbitals of As (central atom) and p-like orbitals of second neighbouring As atoms. The SEC is 1.0 eV. Thus, the self energy corrected direct and indirect band gaps are 3.09 and 2.16 eV, respectively.

For the ordered $Ga_{0.25}Al_{0.75}As$ alloy, the two atomic configurations possessing C_{2v} and C_{1h} point-group symmetries were considered. The values for the direct and indirect band gaps are quite similar for C_{2v}- and C_{1h}-symmetric configurations, and are 2.10 and 1.18 eV, respectively. The VBM has contributions mainly from As-p like orbitals. The CBM comprised s–p mixed orbitals of As and Al atoms. The SEC is 1.02 eV and the self energy corrected values are 3.12 and 2.20 eV for the direct and indirect band gaps, respectively.

For $x = 0.875$, the point-group symmetry is T_d. The indirect and direct band gaps are equal to 1.21 and 2.12 eV respectively. The VBM comprised mixed As and Al p-like orbitals. The CBM has contributions mainly from p-like orbitals of Al and As alongwith some contributions from d-orbitals of As. The SEC is 1.03 eV and the self-energy corrected values for the direct and indirect band gaps are 3.15 and 2.24 eV, respectively.

For the other end component ($x = 1.0$) of the alloys, Al_4As_4, the point group symmetry is T_d. The band gap is indirect and is equal to 1.21 eV whereas the direct band gap is 2.17 eV. The VBM is composed of p-like states of As and Al atoms and CBM is composed of p-like orbitals of Al and As and some d-like orbitals of As. The SEC necessary to achieve the experimental value of 2.3 eV for indirect band gap is 1.04 eV and the self-energy corrected value for direct band gap is 3.21 eV.

The total density of states for the ordered $Ga_{1-x}Al_xAs$ alloys for the whole concentration range of Al is shown in Fig. 2. The electronic density of states has been obtained by employing 19 selected k-points in the irreducible part of the Brillouin zone with a Gaussian broadening of 0.015 Ry. The peak at the bottom of the valence band originates from the Ga-3d states.

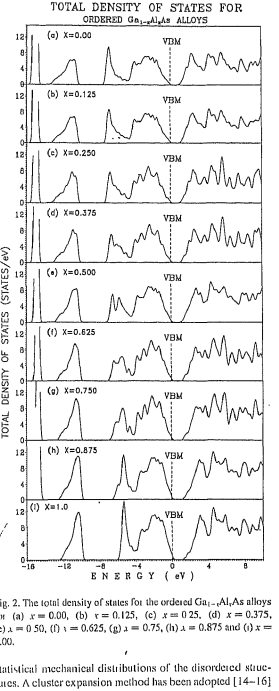

Fig. 2. The total density of states for the ordered $Ga_{1-x}Al_xAs$ alloys for (a) $x = 0.00$, (b) $x = 0.125$, (c) $x = 0.25$, (d) $x = 0.375$, (e) $x = 0.50$, (f) $x = 0.625$, (g) $x = 0.75$, (h) $x = 0.875$ and (i) $x = 1.00$.

2.2. *Random alloys*

In $Ga_{1-x}Al_xAs$ alloys, in some experimentally studied samples one may assume the occurence of the disordered structures mimicking a random atomic configuration. We look into this possibility in this section. The properties of the disordered alloy may be simulated by considering the statistical mechanical distributions of the disordered structures. A cluster expansion method has been adopted [14–16] in the past for obtaining such a statistical mechanical description. It has been suggested that the coefficients of the cluster expansion method may be obtained by a first-principles calculation of a set of ordered structures. This method which was first used for binary alloys can be extended to ternary alloys in case the disorder is assumed to occur only on one type of sites, say anion or cation as is

the case for the presently discussed $A_{1-x}B_xC$ alloys. One simplifies the calculation by truncating the cluster expansion at the level of nearest neighbour interactions. For a tetrahedron structure, one studies the five basic structures corresponding to the nearest neighbour tetrahedron $A_{4-n}B_n$ ($n = 0,4$). The statistical mechanical property of the disordered alloys may be considered as the property valid for the random alloys. Any statistical property $F(x)$ at a particular concentration x may be expanded as

$$F(x) = \sum_n P_n(x) F_n, \tag{1}$$

where $P_n(x)$ is the probability of the occurrence of cluster $A_{1-n}B_n$ and F_n is its property.

The probability of each cluster which is, in general, temperature-dependent should be obtained at any given temperature by minimizing the free energy with respect to the probability $P_n(x,T)$. However, we assume here a temperature-independent random distribution function for the probability given by

$$P_n(x) = \binom{4}{n} x^n (1-x)^{4-n}. \tag{2}$$

A similar calculation has been done by earlier workers [1–3,16,17]. This is obviously a first approximation and may be expected to be valid for the case of frozen-in disorder of the gas or liquid phase from which the solid solutions are quenched. Using Eq. (1), we have calculated the lattice constants and the band gaps for the random alloys at different concentrations of Al which are shown in Tables 1 and 2 (and Fig. 3), respectively.

The calculated lattice constant for the random GaAlAs alloys shows an irregular behaviour with the concentration of Al in contrast to a regular linear behaviour seen earlier for the ordered alloys.

2.3. Band gap

The band gap energies of the ordered and the random $Ga_{1-x}Al_xAs$ alloys after including SEC for different values of x are presented in Table 2 and in Fig. 3. For the random alloys, both the direct and indirect band gaps have been calculated. Delgado et al. [18] have measured the indirect band gap of $Ga_{1-x}Al_xAs$ alloys in the concentration range, $x = 0.48–0.90$ and the direct band gap by observing low-temperature photoluminescence (PL). Their results are also included in Fig. 3. The other data is by Monemar et al. [13] who have measured the band gaps for these alloys; the direct band gap in very small concentration range of $x = 0.24–0.40$ and the indirect gap in the whole concentration range by observing the absorption and PL spectra. The measured values show a quite linear variation of the band gap with x alongwith a very small bowing. The calculated values for both the direct and indirect band gaps also reveal small bowing. A crossover from the direct to indirect band gap is seen below $x = 0.375$ which is quite near the measured value of 0.35. In the concentration range where the experimental data is available, i.e. from $x = 0.24$ to 0.40, the calculated values for the direct band gap for the ordered alloys are in excellent agreement with the measured data. Similarly, the present values obtained for the indirect band gap for the ordered alloys in the full concentration range of

Table 2
Variation of the band gap including SEC in the ordered and the random $Ga_{1-x}Al_xAs$ structures and comparison with the experimental data and other calculations (all energies are measured in eV)

System (x)	Present results with SEC				Other calculations (without SEC)	Experimental	GW
	Ordered structures		Random structures				
	Direct	Indirect	Direct	Indirect			
0.000	1.55	2.01	1.55	2.01	0.60[a] (direct)	1.52[b] (direct) 2.01[c] (indirect)	1.3[d] (direct)
0.125	1.65	2.04	1.61	2.03			
0.250	1.90	2.10	1.70	2.04			
0.375	2.08	2.00	1.80	2.05			
0.500	3.05	2.11	2.50	2.13			
0.625	3.09	2.16	3.14	2.22			
0.750	3.12	2.20	3.16	2.23			
0.875	3.15	2.24	3.18	2.24			
1.000	3.21	2.25	3.21	2.25	2.07[a] (direct) 1.33[a] (indirect)	2.25[b] (indirect)	

[a] Model dielectric function Ref. [5].
[b] Ref. [6].
[c] Ref. [13].
[d] GW approximation, Ref. [12]

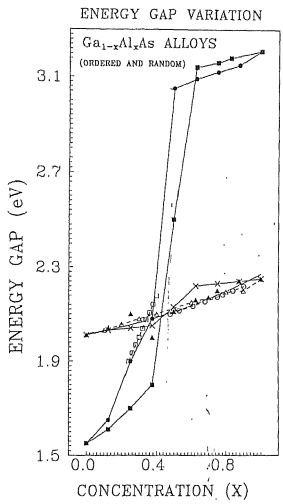

Fig. 3. Variation of energy band gap with concentration x for the direct and indirect gaps for the ordered and random $Ga_{1-x}Al_xAs$ alloys. The continuous curves are the extrapolated curves. The calculated direct and indirect band gaps for the ordered structures are shown by (●) and (▲), respectively. The calculated direct and indirect band gaps for the random alloys are denoted by (■) and (×), respectively. The experimental data for the direct and the indirect band gaps by Monemar et al. [13] are depicted by (□), and (△), respectively. The indirect band gaps measured by Delgado et al. [18] are shown by (○)

$x = 0.0–1.0$ are also in very good agreement with the experimental data. Our results support the occurrence of the ordered structures in the grown up samples studied by different groups.

3. Conclusions

A linear (non-linear) variation of the lattice constant with the concentration of constituent atoms in the ordered (random) alloys has been found. A direct to indirect band gap crossover has been seen for $Ga_{1-x}Al_xAs$ alloys near the concentration $x = 0.375$ alongwith some band gap bowing for both the direct and indirect band gaps. The calculated direct and indirect band gaps for the ordered alloys are in excellent agreement with the PL and absorption data. The present results support the occurrence of ordered structures in different samples grown in various measurements.

Acknowledgements

B.K.A. thanks the Indian National Science Academy.

References

[1] B.K. Agrawal et al. J. Phys. C 10 (1998) 4597.
[2] Rekha Srivastava et al. Solid State Commun. 109 (1999) 383.
[3] B.K. Agrawal et al. J. Phys. C 9 (1997) 1763.
[4] L. Hedin, B.I. Lundqvist, J. Phys. C: Solid State Phys. 4 (1971) 2063.
[5] X. Zhu, S.G. Louie, Phys. Rev. B 43 (1991) 14142
[6] K.H. Hellwege, Landolt-Bornstein (Eds.), Numerical Data New Series, Group III, Vol. 17, Springer, New York, 1982 (Pt. A).
[7] J.P. Perdew, M. Levy, Phys. Rev. Lett. 51 (1983) 1884.
[8] L.J. Sham, M. Schulter, Phys. Rev. Lett. 51 (1983) 1888.
[9] R.O. Jones, O. Gunnarson, Rev. Mod. Phys. 61 (1989) 689.
[10] R.M. Dreizler, E.K.U. Gross, Density Functional Theory, Springer, Berlin, 1990.
[11] R.G. Parr, W. Yang, Density Functional Theory of Atoms and Molecules, Oxford University Press, New York, 1989.
[12] A. Rubio, M.L. Cohen, Phys. Rev. B 51 (1995) 4343.
[13] B. Monemar et al. J. Appl. Phys. 47 (1976) 2604.
[14] J.M. Sanchez, D. de Fontain, in: M. O'Keefe, A. Navrotsky (Eds.), Structure and Bonding in Crystals, Vol. 2, Academic Press, New York, 1981, p. 117.
[15] J.M. Sanchez et al. Physica A 128 (1984) 334.
[16] G.P. Srivastava et al. Phys. Rev. B 31 (1985) 2561.
[17] E.A. Albanesi, Phys. Rev. B 48 (1993) 17841.
[18] G. Torres-Delgado et al. J. Appl. Phys. 78 (1995) 5090.

ELSEVIER

surface science

Surface Science 424 (1999) 232–243

First-principles calculation of valence band offset and the interface states in GaAs/GaN(001) superlattice

Bal K. Agrawal *, Savitri Agrawal, Rekha Srivastava

Physics Department, Allahabad University, Allahabad 211002, India

Received 22 May 1998, accepted for publication 10 December 1998

Abstract

A first-principles scalar relativistic version of full-potential self-consistent linear muffin tin orbital (LMTO) method, together with a density functional theory in local density approximation, has been employed for calculating the electronic structure of the superlattices formed from two different types of semiconductors. In particular, we report here the results for the lattice mismatched GaAs/GaN(001) superlattices. The calculation has been performed for the two strain modes: (i) free-standing interface, where both GaAs and GaN are strained, and (ii) GaN (strained) deposited on the unrestrained GaAs. The calculated band offsets reveal strong sensitivity of the atomic positions in the interfacial region. The valence band offset increases (decreases) with decrease (increase) in GaN (GaAs) bond length. There appear a number of interface states of localized and/or resonance types which may be responsible for the sensitivity of the band offsets on the atomic positions. The calculated band offset ranging from 1.32 eV to 1.86 eV for the GaAs substrate and the free-standing geometries, respectively, are quite close to the experimental value of about 1.7–1.8 eV reported by Ding et al. [12]. © 1999 Elsevier Science B.V. All rights reserved.

Keywords: Ab initio calculations; Density functional calculations; Interface states; Semiconductor–semiconductor interfaces; Superlattices

1. Introduction

In the recent past, first-principles supercell calculations have been reported for the valence band offsets (VBOs) for a number of superlattices [1–10]. In most of the cases [11], the systems considered use the lattice-matched interfaces and the atomic positions in the interfacial region were assumed to retain their perfect three-dimensional lattice structures. This situation may be true for the interfaces formed from chemically similar constituents. However, for interfaces built up from different types of constituent semiconductors, such as having different lattice parameters or chemical atoms (II–VI and III–V compounds), the interfacial atoms may relax and occupy positions different from the perfect lattice ones. This may result in appreciable changes in the values of the valence band offsets.

The III–V GaAs/GaN superlattices which have wide bandgaps are very promising for the development of optoelectronic devices in the visible and ultraviolet regions of the electromagnetic spectrum, with photon energies spread over a wide energy range. Bandgap tuning is possible by forming alloys of the compounds with gaps of desired ranges. Quite recently Ding et al. [12] have measured the valence band discontinuity at a cubic GaN/GaAs(001) heterojunction by using synchrotron radiation photoemission spectroscopy.

* Corresponding author. Fax: +91-532-608316.

0039-6028/99/$ – see front matter © 1999 Elsevier Science B.V. All rights reserved.
PII: S0039-6028(98)00942-X

The lattice parameters of the pure GaAs and GaN differ by 20%. Epitaxial growth of a superlattice with alternating GaAs and GaN layers will contain built-in elastic strain which can be named as strained-layer superlattice. The strain may have two components: hydrostatic and shear. The shear components will lower the symmetry of the system and split the highly degenerate electronic levels which may cause drastic changes in the values of the energy gap. The strain dependence offers a convenient method for optimizing the electronic structure of the superlattices.

Earlier [13], one of the authors (B.K.A.), as a co-author, obtained results for the influence of atomic relaxation in the interfacial region on the valence band offsets for the lattice mismatched ZnS/ZnSe(001) superlattices and the lattice matched II–VI and III–V superlattice ZnTe/GaSb (110). In these calculations, a scalar relativistic version of a full-potential self-consistent linear muffin tin orbital method (LMTO) with the density functional theory (DFT) in local density approximation (LDA) was employed. The results revealed large changes in the values of the valence band offsets caused by atomic relaxations. These calculations have further been extended to ZnSe/ZnS(110) superlattices [14] by our group.

Usually in the application of the standard LMTO method, an atomic sphere approximation (ASA) is used to make it efficient. However, this LMTO–ASA method suffers from several disadvantages. (i) It neglects the symmetry-breaking terms by discarding the non-spherical parts of the electron density. (ii) The method discards the interstitial region by replacing the muffin tin spheres by space filling Wigner spheres. (iii) It uses spherical Hankel functions with vanishing kinetic energy only.

The method has also been utilized for predicting the structural, dynamic and electronic properties of semiconductors [15–17], alloys [18] and the parent high T_c oxide superconductors $CaCuO_2$ [19] and Hg-based superconductors [20,21].

In the present communication, we report the results for the valence band offsets for the GaAs/GaN superstructures with a (001) geometry and also the interface states after determining the atomic relaxations by minimization of the total energy for the supercells of (10+10) layers or (5+5) bilayers. Each bilayer is comprised of one set of cation and anion layers.

The calculations are described in Section 2 and the main results in Section 3. Section 4 contains the main conclusions.

2. Calculations

For the details of the method, we refer to earlier papers [14–21].

2.1. Bulk GaAs and GaN

The local density potential of Hedin and Lundquist [22] has been employed.

The LMTO basis functions for the atoms were chosen as Ga (4s,4p,4d), As (4s,4p,4d) and N (2s,2p,3d). Empty spheres were assumed to be present at the vacant sites and a set of appropriate (spd) states was chosen for them. The core electrons are not frozen but are relaxed in the sense that the core electron charge density is recalculated in each iteration in the self-consistent loop. We have not considered the spin–orbital coupling but have generated the self-consistent supercell potentials by considering the scalar relativistic effects. It has been observed [23,24] that spin–orbit coupling to lowest order splits only the bands and does not change appreciably the relative positions of band centres. The cohesive properties are hardly affected.

The detailed results for the energy variation, the electronic structure, the elastic constants and the frozen phonon frequencies for the bulk GaAs and GaN compounds have been reported elsewhere.

2.2. Superlattices

We have computed the electronic structure of the 20 layer superlattice (each layer contains one atom) by repeating a supercell containing 20 real atoms and 20 empty spheres on a fcc lattice. As a variational basis for solving the Schrödinger equation in the interstitial region two augmental Hankel functions with decay energies -0.01 and -1.0 Ry

have been employed. For the lattice sites occupied by real atoms, three spherical Hankel functions with decay energies -0.01, -1.0 and -2.3 Ry have been considered. In an attempt to reduce the computer time and cope with the available restricted CPU memory, we have confined the LMTOs up to the angular momentum $l=3$.

The lattice mismatch between GaAs and GaN is about 20% and there is a possibility of achieving different types of strained superlattice (SSL) in their growth experiments. We consider the two geometries depending on the lattice constant parallel to the interface: (a) $a_{\parallel}=5.075$ Å ('free-standing' interface) and (b) $a_{\parallel}=5.65$ Å (i.e. GaAs unstrained).

Before assembling the interface, we first performed calculations for the bulk GaAs and GaN compounds separately using the 40 atom supercell, and determined the appropriate minimum energy interlayer distances separately. A value of the lattice constant parallel to the interface $a_{\parallel}$ was chosen in accordance with one of the two above mentioned geometries and the interlayer spacing of the (10+10) layer set was varied. The crystal energy was minimized to obtain an appropriate interlayer spacing to be used later for assembling the heterojunction.

The VBO is defined as the difference $\Delta E_v = E_v^R - E_v^L$ where E_v^L is the valence band maximum (VBM) of the compound on the left side (considered to be lying at lower energy) and E_v^R is the VBM of the compound on the right side of the interface. The valence band maximum for each compound is determined for those layers in the superlattice which lie deep in the layer set of the compound.

The potentials at these middle layers on both sides of the interface should converge with the number of layers chosen in the supercell. This convergence has been tested by us by performing calculations for (7+7) bilayers. The results remain unchanged. Christensen [23,24] has also found that the 5+5 bicells yield almost the same VBO values as the 7+7 bicells.

2.3. Atomic relaxations and valence band offset

In the actual calculation of the valence band offset, for each compound a bulk crystal is generated by repeating the two atom unit cell (containing cation and anion) on a fcc lattice which is later on distorted (if required) to have the appropriate planer lattice constant $a_{\parallel}$ corresponding to the geometry of the superlattice. A normal lattice constant $a_{\perp}$ is obtained by keeping the volume of the unit cell unchanged. The crystal potential of the corresponding middle layer (assumed to be of bulk-like properties) of the 5 bilayer set of the superlattice is taken over to the above bulk crystal. A band structure calculation is then performed for each bulk crystal and the VBM is determined.

In a self-consistent calculation of the interface, the potentials of constituents are adjusted properly to each other and there exists, in general, a relative potential difference between the potentials of the middle layers of the two compounds. This difference in the potentials called the dipole contribution is added to the difference of the VBM obtained above for the bulk.

We determine two types of VBO: (i) an averaged $\Delta E_{v,av}$ which is the difference for the constituent compounds obtained after taking the weighted average of the VBM derived states for a compound split by the shear; and (ii) ΔE_v, equal to the difference in energies of the highest occupied VBM states.

2.4. Interface states

The interface GaAs/GaN represents a two-dimensional defect when one moves from one material to another normal to the interface. The planar defect will thus induce some interface states; resonance and/or localized ones, which would be characterized by the decay of the wavefunction either on both sides of the interface or on one side. The quantities like the valence band offset are not expected to be determined by the averaged bulk properties of the two different materials. It may be noted that all the model theories for estimating the valence band offsets which are based on the bulk properties of the constituents may no longer be true in real systems. A calculation is made for the interface states which are identified by extracting those states for which the values of the eigenvectors decrease away from the interface region.

3. Results

3.1 Free-standing GaAs/GaN(001) superlattice

For the free-standing superlattice, $a_{\parallel}$ = 5.075 Å, for GaAs, the interlayer spacing increases by 0.05 in the units of lattice parameter ($a_{\parallel}$) and in GaN it decreases by 0.065. These spacings have been depicted in Fig. 1a.

3.1.1. Electronic structure

The planer Brillouin zone for the (001) interface is shown in Fig. 1b. The symmetric points are Γ(0,0,0), X(0.5,0.5,0), X'(0.5,−0.5,0) and M(0.5,0,0.5); all of them lie in the K-plane parallel to the interface (001).

The electronic structures for the pure strained GaAs and GaN slabs for the above obtained energy minimized interlayer spacings are depicted

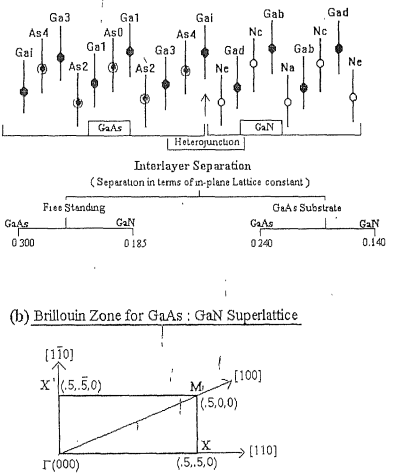

Fig. 1. GaN/GaAs(001) supercell for free-standing and GaAs substrate geometries. Each layer contains one type of ion, cation or anion. All the values of the interlayer spacings are given in terms of the value of the planar lattice constant ($a_{\parallel}$) equal to 5.075 Å for free-standing and equal to 5.65 Å for GaAs substrate geometries. The interlayer spacing for the unrelaxed case is 0.25. The planar Brillouin zone is also included at bottom.

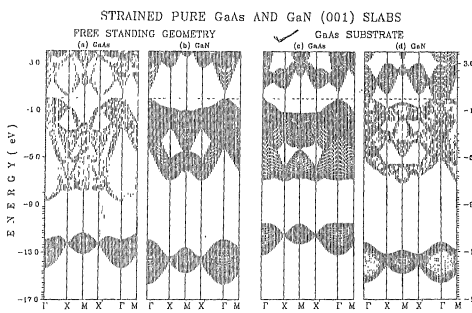

Fig. 2. Electronic structure for the (5 1 5) (001) bilayer slabs of pure (a) GaAs and (b) GaN in the free-standing geometry and for (c) GaAs and (d) GaN for the GaAs substrate geometry.

in Fig. 2a and b, respectively. The total widths of the valence bands are 14.4 and 15.8 eV for GaAs and GaN, respectively. The ionic gap for GaN is much wider (−7 to −12 eV) than GaAs (−8.8 to −11.4 eV). Although the bottom of the conduction band in both the semiconductors descends into the fundamental gap, they retain their semiconducting character; there is no closure of the energy gap. A notable feature in the case of strained GaAs is that the bottom of the conduction band appears now at the symmetry point X, in contrast to the unstrained GaAs where it appears at Γ – as may be seen in Fig. 2c.

In Fig. 3a, we include the electronic structure of the free-standing strained GaN/GaAs(001) superlattice. A comparison with Fig. 2 reveals some notable features. In the heterojunction, there is an overall downward shift of the electronic states in GaN by about 1.6 eV with respect to that of GaAs. The low lying s-like orbital states of GaAs and GaN are almost separated. The total width of the valence band for the heterojunction increases to about 17 eV. The width of the ionic gap is similar to that of pure strained GaAs slab, and the upper part of the ionic gap is composed mainly of the GaAs states. Also, the top of the valence band of the heterojunction originates mainly from the GaAs electron states. On the other hand, the GaN states descend into the fundamental gap, filling it completely and making it metallic. A similar closure of gap in local density approximation has been observed in the ordered $GaAs_{1-x}N_x$ alloys in the concentration range $x = 0.125$ to 0.625 [25,26]. However, the many body effects such as considered in the GW approximation will raise the conduction states and may open the gap. The VBMs, however, will remain unaffected.

3.1.2. Electron density of states

Calculations for the electronic density of states were performed for the GaAs/GaN superlattice without relaxing the atoms of the heterojunction. The total density of states (DOS) is shown in Fig. 4a and the projected electronic density of states at the atoms of the different layers in Fig. 5a. The metallic behaviour of the GaN/GaAs(001) superlattice is evident from Fig. 4, where the fundamental gap contains a small density in the lower part of the gap. A perusal of Fig. 5a reveals that

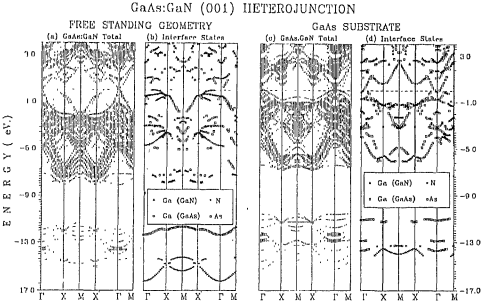

Fig 3 Electronic structure and interface states for the GaN/GaAs(001) superlattice for (i) the free-standing geometry (a and b) and (ii) the GaAs substrate geometry (c and d), respectively

there is enhanced Ga-s induced density at the bottom of the CBM at the interface atom Ga_i. Dominant contributions from the As-p orbitals appear at VBM in the interfacial region. The projected density at the N atoms is quite small in the vicinity of the energy gap. The projected density at the interfacial Ga atom has contributions from the hybridized As-S and the N-s orbitals at the bottom of the valence band.

3.1.3. *Valence band offsets*

We allow all the atoms to relax by different magnitudes in accordance with the calculated forces and perform self-consistent calculations for the relaxed structures. We studied the variation of the total energy and obtained the energy minimum for a slight displacement of the interfacial Ga layer towards the As layer with 0.15% and −0.21% changes in the GaN and GaAs bond lengths, respectively. The calculated values for the two types of VBO as defined earlier are presented in Table 1 for different magnitudes of atomic displacements at the interface. It may be noted that the different magnitudes of atomic displacements give rise to different changes in the GaAs and GaN bond lengths. The values for ΔE_v are larger than those for $\Delta E_{v,av}$. This large difference occurs because of the occurrence of quite large shear strain in the heterojunction which splits the three-fold bulk VBM state significantly. For the minimum energy configuration the two values of band offset are $\Delta E_{v,av}=1.86$ eV and $\Delta E_v=2.72$ eV.

We observe that the value of the offset increases with decrease (increase) in the interface GaN (GaAs) bond length. For a combined change in the bond lengths of GaN and GaAs at the interface by 0.54% and −0.84%, respectively, $\Delta E_{v,av}$ or ΔE_v decreases by 0.11 eV, i.e. by 6%.

In the minimum energy configuration of the relaxed atoms, we depict the levels at the VBM for GaAs and GaN on the two sides of the interface in Fig. 6a. In order to investigate the effect of the interfacial GaN bond length on the valence band offset, we have made a separate calculation. While keeping intact the GaAs bond length in the heterojunction, we shift all the layers lying on the GaN side except the interfacial Ga layer. We find that the VBO increases (decreases) with shortening (lengthening) of the GaN bond length, and these changes are doubled when the

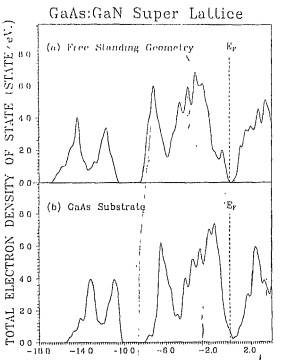

Fig. 4. Total electron density of states for the GaN/GaAs(001) superlattice for (a) the free-standing geometry and (b) the GaAs substrate geometry

changes in both the GaAs and GaN bond lengths are considered.

3.1.4. Interface states

The interface states have been calculated for the minimum energy GaAs/GaN superlattice. The states having magnitude of eigenvector >0.3 on the interface atoms and for a decay factor of 0.10, i.e. the states for which the modulus of the eigenvector of one type of atoms decreases by 10% or more away from the interface, are shown in Fig. 3b, along some symmetric directions in the different energy regions. Most of the states show a bulk-like behaviour in one of the host compounds, but decay on the other side of the interface.

The decay behaviour of some interface states is depicted in Fig. 7a for the free-standing interface. The conduction states in the vicinity of the energy gap originate from the sp-hybridized orbitals of Ga and N atoms and practically do not enter the GaAs layers but decay slowly towards GaN layers. The interface states at and near VBM are the mixed As-p and Ga-p orbitals decaying fast on both sides of the interface. The Ga-p induced interface states appearing in the range -1.0 to -5.0 eV decay only towards the GaAs layers. The interface states lying in the energy region -12.0 to -13.5 eV originate mainly from the As-s and N-s orbitals and decay only towards the GaAs side. The interface states lying at the bottom of the valence band ($E=-16.3$ eV) originate mainly from the N-s orbitals and decay on both sides of the interface.

3.2. GaAs substrate GaN(001) superlattice

Now, the GaN is deposited on the GaAs substrate so that the value of the lattice constan parallel to the interface is equal to that of the hos GaAs, i.e. $a_{||}=5.65$ Å. The two separate calcula tions for finding the energy minimum of the 1(bilayer unit cell each for GaAs and GaN give th interlayer spacings as 0.24 and 0.14 (in the units of $a_{||}$), respectively. A value of 0.24 smaller than the experimental value of 0.25 for the interlayer spacing in GaAs is obtained because of the occurrence of the energy minimum for the bulk GaAs at a smaller lattice volume.

For this geometry, the forces on the atoms are quite similar to those seen for the free-standing geometry, both qualitatively and quantitatively. Similar to the free-standing case, the atoms in the various layers are relaxed in the direction of the forces experienced by them by overall different magnitudes, and self-consistent calculations are performed.

The electronic structure for the unstrained pure GaAs and the strained pure GaN slab is presented in Fig. 2c and d, respectively. The states lying below the ionic gap remain unaffected with a change in the in-plane lattice constant. However, there are notable changes in the upper part of the valence band of the GaN. For a larger value of $a_{||}$, there occur more states in the vicinity of the VBM. Also, the Ga induced states descend into the fundamental gap and enter the valence band.

The electronic structure for the GaN/GaAs

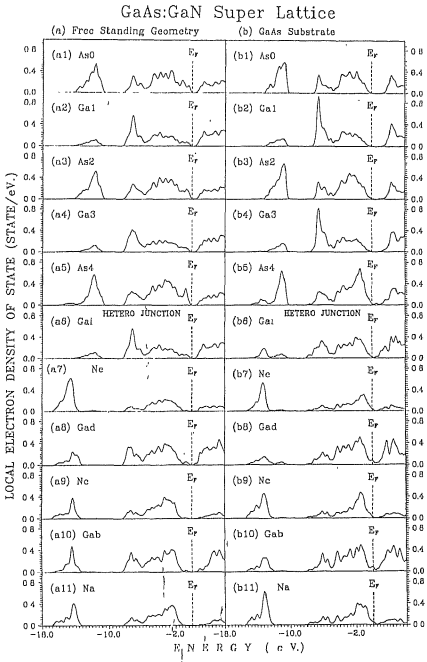

Fig. 8. Projected electron density of states (PDOS) for the cation Ga and anions As and N lying in the different layers of the GaN/GaAs(001) superlattice for (a) the free-standing geometry and (b) the GaAs substrate geometry.

(001) heterojunction in the GaAs substrate geometry is shown in Fig. 3c. The total density of states and the projected ones are presented in Figs 4b and 5b, respectively. The total densities of states for the two different geometries are quite similar. There are states in the fundamental gap region.

Table 1
Valence band offsets (eV) for GaN/GaAs(001) superlattice in free standing geometry for different sets of changes in GaAs and GaN bond lengths

% Change in bond length		Band offsets	
GaAs	GaN	$\Delta E_{v,av}$	ΔE_v
0.84	−0.55	1.98	2.83
0.00	0.00	1.89	2.75
Minimum energy −0.21	0.15	1.86	2.72
of superlattice			
−0.86	0.54	1.78	2.64

The calculated values of the two types of VBO for the various atomic configurations are presented in Table 2. In general, the magnitude of $\Delta E_{v,av}$ is much larger than those of ΔE_v for the GaAs substrate geometry (GSG) in contrast to the free-standing geometry (FSG), where the reverse is true. The values of the two types of VBO for the minimum energy configuration are $\Delta E_{v,av}$ 1.32 eV and ΔE_v −0.67 eV. The variation in the values of VBO is quite large, and is strongly sensitive to the atomic displacements. For 0.199% elongation and 0.442% contraction in the bond lengths of GaN and GaAs, respectively, the VBO decreases by −0.11 eV, i.e. by 8%. For the minimum energy configuration the positions of the energy levels at the interface are shown in Fig. 6b.

The interface states for the GaAs substrate GaN(001) heterojunction have been depicted in Fig. 3d. The interface states are quite similar to those seen for the free-standing geometry. The lowest states decay towards the GaAs side of the interface and are bulk-like in GaN. The interface states near −11 eV decay towards the GaAs layers and practically do not enter the GaN side. The states in the vicinity of the top of the ionic gap originate from Ga-s orbitals and decay towards the GaAs. The states near −3.3 eV arise from the p-orbitals of anions and are bulk-like in GaN and decay towards the GaAs side. In the energy region −1.7 eV the interface states are the mixed s–p orbitals which decay towards the GaN side but remain bulk-like in GaAs layers.

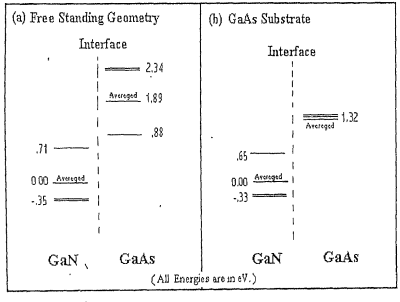

Fig. 6. Energy levels (eV) for GaN and GaAs at the valence band maximum on the two sides of the interface for (a) the free-standing geometry and (b) the GaAs substrate.

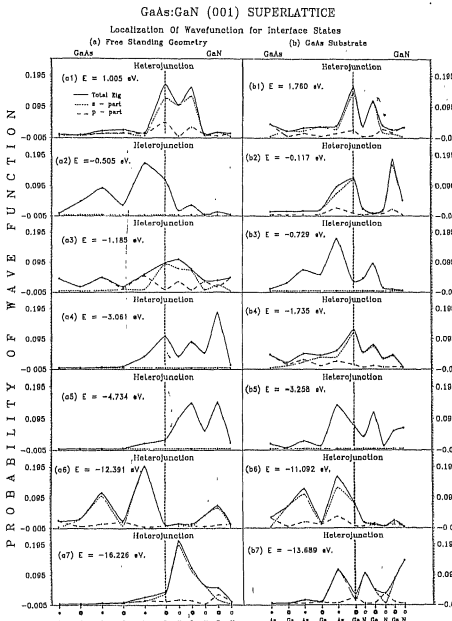

Fig 7 Variation of magnitude of eigenvectors on the atoms lying on the various layers for (a) free-standing geometry and (b) GaAs substrate geometry.

3.2.1. *Effect of atomic relaxation on valence band offsets*

The VBO shows dependence on the position of the interfacial Ga atoms, Ga_i. The interatomic separation within the Ga_i layer is smaller in FSG compared with that of GSG by about 9% and the value of VBO is enhanced by about 40%. In GSG, the in-plane shear strain in GaN layers is about

Table 2
Valence band offset (eV) for GaAs substrate GaN/GaAs(001) superlattice for different sets of changes in GaAs and GaN bond lengths

% Change in bond length		Band offsets	
GaAs	GaN	$\Delta E_{v,s}$	ΔE_{v}
0.446	−0.197	1.36	0.71
0.000	0.000	1.32	0.67
−0.442	0.199	1.21	0.56

Minimum energy of superlattice

46% while the GaAs layers remain unstrained. On the other hand, in FSG the in-plane shear strains are present both in the GaAs and GaN layers to the order of 23%. For contraction within GaAs layers and elongation within GaN layers, the values of VBO are higher. The sheat strains split the three-fold degenerate VBM of the bulk by a magnitude depending on the amount of strain. The values of ΔE_v reveal (Tables 1 and 2) very large changes with strain. These changes become subtle for the weighted average of the split VBM states.

The layers are polar, each layer containing one type of ions. The shift of the interface layer Ga_i towards (away from) the GaAs (GaN) bulk layers decreases the VBOs. Small changes in the bond lengths caused by atomic displacements normal to the layer incur large changes in the values of VBO. The observed changes in VBO are seen to be greater in GSG than in FSG. For 0.2 to 0.4% changes in bond length in GSG, the VBO changes by 8%, whereas for 0.5 to 0.8% changes in bond lengths in FSG, VBO changes by 6% only.

In the experimental measurement where GaN layers were deposited on the GaAs substrate our calculated values of 1.32 eV for the GaAs substrate and 1.86 eV for the free-standing geometry are quite near to the measured volume of 1.7–1.8 eV. The measured sample may have somewhat different atomic configuration from the ideal configuration considered in the present calculation. A change of bond length of the order of 1 to 2% may enhance the VBO by approximately 30–40%. Bellaiche et al. [27,28] after using the LAPW method have reported a value of 2.18 to 2.28 eV for the band offset for relaxed atoms, which is on the higher side.

4. Conclusions

Our results show that the model theories used for estimating the values of the valence offsets are expected to be inadequate as they are based on the use of the bulk-like properties of the constituent materials forming the interface. The presence of interface states is an extra feature in the physical properties of the heterojunction. A strong sensitivity of the valence band offsets on the small atomic displacements is seen in the present calculation. The valence band offset increases (decreases) with decrease (increase) in the GaN (GaAs) bond length. Our calculated values of VBO for the two geometries of the interface are quite close to the experimental value of 1.7–1.8 eV, reported by Ding et al.

Acknowledgements

The work is financially supported by the University Grant Commission, New Delhi and the Department of Science and Technology, New Delhi.

References

[1] C. Tejedor, F. Flores, E. Louis, J. Phys. C 10 (1977) 2163.
[2] C. Tejedor, F. Flores, E. Louis, J. Phys. C 12 (1979) 731.
[3] J. Tersoff, Phys. Rev. Lett. 52 (1984) 465.
[4] J. Tersoff, Phys. Rev. B 30 (1984) 4874.
[5] M. Cardona, N.E. Christensen, Phys. Rev. B 31 (1985) 879.
[6] S.H. Wei, A. Zunger, Phys. Rev. Lett. 59 (1987) 144.
[7] M. Jaros, A. Zoryk, D. Ninno, Phys. Rev. B 35 (1987).
[8] C.G. Van de Walle, R.M. Martin, J. Vac. Sci. Technol. B 4 (1986) 1055.
[9] C.G. Van de Walle, R.M. Martin, Phys. Rev. B 34 (1986) 5621.
[10] C.G. Van de Walle, R.M. Martin, Phys. Rev. B 35 (1987) 8154.
[11] W. Mönch, Semiconductor Surfaces and Interfaces, Springer Series in Surface Science, 2nd edn. Springer, Berlin, 1995.

[12] S A Ding S R Barman, K Horn, H Yang B Yang, O Brandt, K Ploog Appl Phys Lett 70 (18) (1997) 2407
[14] M Methfessel B K Agrawal M Scheffler unpublished results
[14] B K Agrawal, S Agrawal, preprint
[15] M Methfessel, Phys Rev B 38 (1988) 1556
[16] M Methfessel, C O Rodriguez, O K Anderson, Phys Rev B 40 (1989) 2009
[17] B K Agrawal, S Agrawal, Phys Rev B 45 (1992) 8321
[18] B K Agrawal S Agrawal, P S Yadav, S Kumar, J Phys: Condens Matter 9 (1997) 1763
[19] B K Agrawal, S Agrawal, Phys Rev. B 52 (1995) 12556
[20] B K Agrawal, S Agrawal, Physica C 233 (1994) 8
[21] B K Agrawal, S Agrawal, Physica C 234 (1994) 29
[22] L Hedin, B Lundquist, J. Phys C: Solid State Phys. 6 (1994) 8701
[23] N E Christensen, Phys Rev. B 37 (1998) 4528
[24] N E. Christensen, I. Gorczyca, Phys. Rev. B 44 (1991) 1707.
[25] B K. Agrawal, P.S. Yadav, R. Srivastava, S. Agrawal, J Phys Condens Matter 10 (1998) 4597
[26] A. Rubio, M L Cohen, Phys. Rev B 51 (1995) 4343.
[27] L Bellaiche, S H Wei, A. Zunger, Appl. Phys Lett 70 (1997) 3558.
[28] L Bellaiche, S.H Wei, A. Zunger, Appl. Phys Lett. 72 (1998) 2011

ELSEVIER

Surface Science 431 (1999) 84–95

surface science

www.elsevier.nl/locate/susc

Effect of atomic relaxation on the valence band offset and the interface states in ZnS/ZnSe(110) superlattices

Bal K. Agrawal *, Savitri Agrawal, Rekha Srivastava

Physics Department, Allahabad University, Allahabad-211002, India

Received 22 September 1997; accepted for publication 19 February 1999

Abstract

A first principles scalar relativistic version of full potential self-consistent linear muffin tin orbital (LMTO) method, together with a local density functional theory, has been employed for calculating the electronic structure and the atomic structures of the superlattices formed from the two different types of semiconductors. In particular, we report here the results for the lattice mismatched ZnS/ZnSe superlattices in (110) geometry. We have performed the calculations for three strain modes: (i) free-standing interface, where both ZnS and ZnSe are strained; (ii) ZnS (strained) deposited on the unstrained ZnSe; and (iii) ZnSe (strained) deposited on unstrained ZnS. The calculated band offsets reveal strong sensitivity on the atomic positions in the interfacial region and show a non-linear behaviour with respect to the atomic displacements. There appear a number of interface states of localized and resonance types which may be responsible for the sensitivity of the band offsets on the atomic positions. © 1999 Elsevier Science B.V. All rights reserved.

Keywords: Atomic relaxation; Interface states; Valence band offset; ZnS/ZnSe superlattices

1. Introduction

In the recent past, first-principles supercell calculations have been reported for the valence band offsets (VBO) for a number of superlattices [1–10]. In most of the cases, the systems considered use the lattice-matched interfaces and the atomic positions in the interfacial region were assumed to retain their perfect three-dimensional lattice structures. This situation may be true for the interfaces formed from the chemically similar constituents. However, for interfaces built from the different types of constituent semiconductors such as having different lattice parameters or chemical atoms (II–VI and III–V compounds), the interfacial atoms may relax and occupy positions different from the perfect lattice ones. It may result in appreciable changes in the values of the valence band offsets.

The II–VI superlattices which have wide band gaps are very promising for the development of the opto-electronic devices in the visible and the ultraviolet regions of the electromagnetic spectrum with photon energies spread in a wide energy range. Band gap tuning is possible by forming alloys of the compounds with gaps of desired ranges.

Multilayer systems formed from ZnS and ZnSe have been investigated. Multilayer structures containing alternate layers of ZnS_xSe_{1-x} and ZnSe compounds have potential applications in the development of blue-light emitting diodes and blue lasers. The lattice parameters of the pure ZnS and

* Corresponding author. Fax: +91-532-461316.
E-mail address: physics@nde.vsnl.net.in (B.K. Agrawal)

0039-6028/99/$ – see front matter © 1999 Elsevier Science B.V All rights reserved.
PII: S0039-6028(99)00404-5

ZnSe differ by 4.5%. Epitaxial growth of a superlattice with alternating ZnSe and ZnS layers will contain built-in elastic strain which can be named as strained-layer superlattice. Further, a variation of the composition x in the ZnS_xSe_{1-x} alloys allows a chemical tuning of gaps as well as the elastic strain. The strain may have two components: hydrostatic and shear. The shear components will lower the symmetry of the system and split the highly degenerate electronic levels which may cause drastic changes in the values of the energy gap. The above strain dependence on x offers a convenient method for optimizing the electronic structure of the superlattices.

Yokagawa et al. [11] have successfully grown the ZnS/ZnSe strained-layer superlattices by using a low pressure vapor-phase epitaxial method. More recently, Shahzad et al. [12] grew several $ZnSe/ZnS_xSe_{1-x}$ strained layer superlattices (SLSL) by employing molecular-beam epitaxy and performed photoluminescence experiments. For $x=0.19$, they measured the valence band offset (ΔE_v) equal to 0.109 eV. Their prepared structure may be considered approaching to a free standing superlattice.

In an earlier paper [13], one of the co-authors investigated the influence of structural relaxation on the electronic and atomic structures and the valence band offset (VBO) of the semiconductor–semiconductor interfaces; lattice mismatched II–VI ZnS/ZnSe(001) and the lattice matched combination of II–VI and III–V ZnTe/GaSb(110) superlattices. In this calculation, the total energy was minimized for supercells of (3+3) layers and the resulting geometry was transferred to a (5+5) supercell to determine the VBO. In the case of polar Zn/ZnSe interface, the VBO changes significantly, i.e., by about 0.35 eV as the interface layer Zn atom moves from unequal interface ZnS and ZnSe bonds to equal bond lengths. The Zn displacement for the minimum energy superlattice was about 0.8% of the in-plane lattice constant. The change in the averaged VBO with strain is determined entirely by the strain splitting of the valence band maximum. The calculated value of VBO for a particular geometry, i.e., the free-standing one was 0.53 eV which is in an excellent agreement with the extrapolated measured value of 0.52 eV by Shahzad et al. [12].

For the ZnTe/GaSb(110) superlattice, a value of 0.69 eV was obtained for the relaxed geometry in contrast to the measured value of 0.34 eV by Wilke and Horn [14]. The discrepancy may arise because of mixing and segregation at the experimentally studied interface.

Lambrecht et al. [15] have calculated the band offsets for a number of heterojunctions by using a restricted treatment of self consistency in the LMTO method in atomic sphere approximation (ASA). The limitations of ASA are pointed out below. Also, these authors have not investigated the presently discussed ZnS/ZnSe heterojunctions. Further, the effect of the atomic relaxation of the atoms of the different layers on the band offsets, which are investigated in the present work, were not considered by Lambrecht et al.

Calculated results for the effects of the detailed atomic structure on the band offsets of ZnSe/ZnS superlattices have been reported by Christensen and Gorczyca [16,17] (CG) after employing LMTO in ASA. In the ASA scheme, one cannot optimize the lattice structure by minimization of the total energy of the system and, therefore, Christensen [17] used the convenient Keating model for determining the forces and the positions of the relaxed atoms. This method may work well for the superlattices formed from the atoms which are non-ionic like Si and Ge. However, for the superlattices containing the ionic atoms like Zn, Se, S, the above scheme may be questionable. Although in the Keating model, the above work considered the Coulombian interactions to the extent that the elastic properties of the constituent pure ZnS and ZnSe were well reproduced, but the Coulomb effects on the forces caused by the large atomic rearrangements in the interfacial region may not be very well accounted for.

Very recently, Wei and Zunger [18] have calculated band offsets for the chalcopyrites and Zn-based II–VI alloys by using the general potential relativistic all electron linearized augmented plane wave (LAPW) method along with the density functional theory. For the ZnS/ZnSe(001) superlattice they obtained a valence band offset of

0.53 eV, which is equal to the value obtained by us in our earlier [13] calculation.

Recently, the LMTO method has drawn much attention towards its application to the study of the electronic structure of molecules as well as of crystalline solids. The method has several advantages. (i) Only a minimal basis set is required in the method; thus it enables its application to large unit cells with high efficiency. (ii) The method treats all the elements of the periodic table in a similar manner. Thus the atoms with a large number of core states and the metals having prominently d- of f-character can be easily treated. (iii) As the augmentation procedure generates the correct shapes of the wavefunction near the nuclei, it is quite accurate. (iv) The use of atom-centered basis functions belonging to the different values of the angular momentum in the method helps one to have quite a clear physical picture.

Usually in the application of the standard LMTO method, an ASA is used to make it efficient. However, this LMTO–ASA method suffers from several disadvantages. (i) It neglects the symmetry-breaking terms by discarding the non-spherical parts of the electron density. (ii) The method discards interstitial region by replacing the muffin-tin spheres by the space filling Wigner spheres. (iii) It uses spherical Hankel functions with vanishing kinetic energy only.

It has been noted that quite reliable results could be attained by employing a LMTO basis if all the potential terms are determined accurately. For this, the sizes of atomic spheres are shrunk so as to make them non-overlapping. The potential matrix elements are then split into two parts: one contribution coming from the atomic spheres and the other from the complicated interstitial region. The first part, i.e., that from the atomic sphere, is easy to evaluate by expanding it in terms of the usual spherical harmonics. On the other hand, the evaluation of the interstitial contribution is quite difficult and very time consuming if done by standard techniques. Efforts have been made to find an efficient and quick way to determine the interstitial contribution. In the method used in the present work, the interstitial quantities were expanded in terms of the spherical Hankel functions. The involved three-centre integrals were expressed as the linear combination of the two-centre integrals by numerical means. These two-centre integrals involving Hankel functions can easily be evaluated analytically. The method does not employ plane waves and is thus applicable to the periodic as well as the non-periodic systems that so often need to be treated, especially when there occur impurities, defects and lattice distortions or atomic relaxations.

The present LMTO method is seen to produce the electronic structure, cohesive energy, lattice constants, elastic constants, phonon frequencies, mode Gruneneisen and strain parameters for simple systems such as Si, C, etc. [19,20]. Very recently [21], the method has been successfully applied also for the III–V and II–VI semiconducting compounds such as AlAs, CdS, GaSb, ZnSe, ZnTe, ZnS, etc., and their alloys [22]. The method has also been utilized for predicting the structural, dynamical and electronic properties of the parent high T_c oxide superconductors $CaCuO_2$ [23] and Hg-based superconductors [24,25].

In the present communication, we report the results for the valence band offsets for the ZnS/ZnSe superstructures with a different geometry, i.e., (011) and also the interface states after determining the atomic relaxations by the minimization of the total energy for the supercells of (5+5) layers in contrast to our earlier results for the (001) superlattices obtained after minimizing the energy for the supercells of (3+3) layers only. A preliminary account of the work has been reported earlier [26].

The calculations are described in Section 2 and the main results in Section 3. Section 4 contains the main conclusions.

2. Calculations

For the details of the method, we refer to earlier papers [19–22].

2.1. Bulk ZnSe and ZnS

At first the scalar relativistic calculations were performed for the host bulk semiconductors ZnSe and ZnS. The LMTO envelope functions were

formed from the spherical harmonic components with $l \leq 4$ with three decay energies, -0.01, -1.0 and -2.3 Ry for the occupied muffin tin spheres (MTS) of real atoms and with two decay energies -1 and -3 Ry for the empty MTSs lying in the interstitial region. The set for each sphere consisted 50 functions. The local density potential of Hedin and Lundqvist [27] has been used.

The chosen LMTO basis functions in the valence energy region were Zn (4s,4p,3d), Se (4s,4p,4d) and S (3s,3p,3d). In order to account for the influence of semi-core 3d-states in Se, we made a separate calculation and thus a two-panel self-consistent method was employed. Empty spheres were assumed to be present at the vacant sites and a set of appropriate (spd) states were chosen for them. The core electrons are not frozen but are relaxed in the sense that the core electron charge density is recalculated in each iteration in the self-consistent loop. It has been observed [16,17] that spin orbit coupling to lowest order splits only the bands and does not change the relative position of band centres. The cohesion properties are hardly effected.

The energy minimum was seen to appear at the ratio $V_{calc}/V_{exp}=0.98$ for ZnSe ($a=5.59$ Å) and at 0.95 for ZnS ($a=5.34$ Å), which are quite encouraging. The detailed results for the energy variation, the electronic structure, the elastic constants and the frozen phonon frequencies for the bulk ZnSe and ZnS compounds have been reported elsewhere [28].

2.2. Superlattices

We have computed the electronic structure of the ten-layer superlattice by repeating a supercell containing 40 atoms in the supercell; 20 are empty spheres to fill the vacant interstitial space. We have performed a separate calculation for Zn atom, the LMTO basis for the three energies are s p d, s p and s p, respectively, whereas for both the Se and S atoms, the chosen basis are s p d, s p d and s p, respectively. In an attempt to reduce the computer time and cope with the available restricted CPU memory, we have employed the LMTOs only up to $l=3$ in the calculation.

The lattice mismatch between ZnSe and ZnS is about 4.5% and there is a possibility of achieving different types of strained superlattices (SS) in their growth experiments. We have obtained results for the three geometries depending on the lattice constant parallel to the interface (a) $a_{\parallel}=5.59$ Å (i.e., ZnSe unstrained); (b) $a_{\parallel}=5.47$ Å ('free-standing' interface) and (c) $a_{\parallel}=5.34$ Å (ZnS unstrained).

In the present calculation, before assembling the interface, we first perform calculations for the bulk ZnSe and ZnS compounds separately using the 40 atom supercell and determine the appropriate minimum energy interlayer distances for each compound. A value of the lattice constant parallel to the interface, namely the in-plane lattice constant $a_{\parallel}$, is chosen in accordance with one of the above-mentioned three geometries and the interlayer spacing of the (5+5) layer set is varied. The crystal energy is minimized to obtain an appropriate interlayer spacing to be used later for assembling the heterojunction. In the earlier calculation [13], we employed (3+3) supercells for obtaining the interlayer spacings. In the present calculation we employ (5+5) supercells for determining the interlayer spacings.

The valence band offset (VBO) of a superlattice A_L/B_R is defined as the difference $\Delta E_v = E_v^R - E_v^L$, where E_v^L is the valence band maximum (VBM) of the compound A on the left side (considered to be lying at lower energy) and that E_v^R as VBM of the compound B on right side of the interface. The valence band maximum for each compound is determined for layer in the superlattice which lies deep into the layer set of the compound. In the five-layer set, it is third layer lying in the middle.

The potentials at these middle layers on both sides of the interface should converge with the number of layers chosen in the supercell. We have made separate calculations by choosing (7+7) layer supercells and have observed no appreciable changes in the present results. Christensen has also found that the 5+5 cells yield almost the same VBO values as 7+7 cells.

2.3. Atomic relaxations and valence band offsets

In the actual calculation for each compound, a bulk crystal is assembled by repeating a supercell

of ten layers having values for the interlayer spacing and $a_{\parallel}$ equal to those used in the heterojunction. The crystal potential of the corresponding middle layer of the supercell containing the interface is taken over to the bulk crystal as the potential for each layer. A band structure calculation is performed for each bulk crystal and the valence band maximum is determined. We then perform a self-consistent calculation for their assembly and note the forces on each atom observed in the calculation and relax the various atoms in the directions of these observed forces by different magnitudes and perform self-consistent calculations again and study the energy of the superlattice. We obtain minimum energy for a particular configuration of the atomic displacements for a stable superlattice.

The difference in the two values of the valence band maximum for the two compounds is calculated. But this is not the actual valence band offset. The reason is that when we assemble the interface of the two different compounds and perform self-consistent calculation, the potentials are adjusted properly relatively to each other and there exists, in general, a relative potential difference between the potentials of the middle layers of the two compounds. This difference in the potential should be taken care of in obtaining the difference of the VBMs obtained by the bulk calculation to obtain the final value of VBO. In this procedure, the valence band maxima states are thus subjected to strict bulk like boundary conditions.

We determined two values of the valence band offset $\Delta E_{v,av}$ and ΔE_v. Here $\Delta E_{v,av}$ is the difference in the weighted average of the states at the valence band maximum of the constituent compounds. The triply degenerate VBM state of a cubic crystal at Γ-point splits into a doubly degenerates and a singlet states in a tetragonally distorted crystal. The other, ΔE_v, denotes the difference in the energies of the highest occupied states in the two constituent compounds.

2.4. Interface states

For a single interface, the periodic boundary conditions which are applicable to the infinitely extended period structure are valid only to the wave vectors corresponding to the two-dimensional lattice parallel to the interface. The wave vectors normal to the interface are the artifact of the calculation where we are repeating the supercell of ten layers containing the interface in the direction normal to the interface.

The interface ZnS/ZnSe is formed by the two different materials and hence represents a two-dimensional defect when one moves from one material to another normal to the interface. The planar defect will thus induce interface states; resonance and/or localized ones which would be characterized by the decay of the wavefunctions either on both sides of the interface or on one side as one moves away from the interface. Thus quantities like valence band offset which will depend on the behaviour of the wave functions in both constituents are not expected to be determined by the averaged bulk properties of the two constituent materials. It may be noted that all the model theories for estimating the valance band offsets which are based on the bulk properties of the constituents may no longer be true in real system.

3. Results

3.1. Free-standing ZnS/ZnSe(110) superlattice

For the free-standing superlattice, the value of the lattice constant parallel to the interface of the ZnS and ZnSe layers was chosen as the average of the lattice constants of the two host lattices, i.e., $a_{\parallel}=5.47$ Å. For ZnSe, the minimum energy interlayer spacing increases by $0.0075\sqrt{2}$ in the units of planar lattice parameter ($a_{\parallel}$) and for ZnS, it decreases by $0.0125\sqrt{2}$. At the interface, the separation between the ZnSe and ZnS layers was chosen to be the average of the obtained energy minimized interlayer spacing of the two components ZnS and ZnSe. These spacing have been depicted for the free-standing geometry without atomic relaxation in Fig. 1. Here, the atoms of the various layers are numbered 2, 1 and 0 on the ZnSe side and by C, B and A on the ZnS side as one move away from the interface.

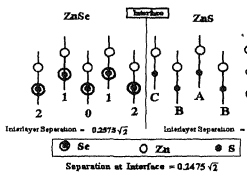

Fig 1 Free-standing ZnS/ZnSe(110), (5+5) supercell. Each layer contains two dissimilar atoms. All the values of the interlayer spacings are given in terms of the value of the lattice constant in the plane which is 5.47 Å here. The interlayer spacing for the unrelaxed case is $0.25\sqrt{2}$ in terms of planer lattice constant

3.1.1. *Electronic density of states*

Calculations were performed for the ZnS/ZnSe superlattice first without relaxation the atoms. The total electronic density of states (DOS) after selecting 18 k-points for the first panel, i.e., after ignoring the density of the quite low-lying 3d states of Se is shown in Fig. 2.

With a motivation to see the variation of local density of states at the atoms of the different layers, we present the local density of states at different atoms for the free-standing geometry without atomic relaxation in Fig. 3. The local density of states at all the atoms Zn, S and Se for the superlattice is seen to be quite similar to their counter-parts in the host compounds. All the atoms possess DOS in the whole energy range of the valence band, i.e. from −14 to 0.0 eV. However, the anions S and Se have dominant contributions of p-states in the upper part of the valence bands and the s-like states around −12 eV. The DOS at the cation Zn in both the host lattices ZnS and ZnSe contains dominant contributions from the d-orbitals in the limited energy range around −6.5 eV. It may be noted that, in general, the overall local density in most of the energy range at each atom is layer-independent, i.e., the magnitudes of local DOS at the interface layers are very much similar to those for the middle layer. However, a close observation of the figures reveals that there are extra states at the interface layer atoms, especially in the lowest energy region.

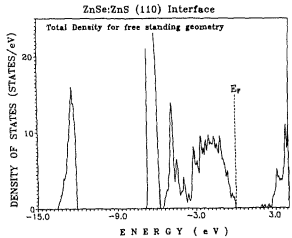

Fig. 2. Total electron-density of states for the ZnS/ZnSe (5+5) superlattice for the free-standing geometry without any atomic relaxation.

3.1.2. *Valence band offsets*

We allow all the atoms of the superlattice to relax by different magnitudes and perform self-consistent calculations for the relaxed structures and obtained the energy minimum.

For the various magnitudes of the atomic displacements, the calculated valence band offsets (VBO) are depicted in Table 1. We observe that the value of the offset increases with the magnitude of the atomic displacement and also that this increase is non-linear. The variation in the VBO is quite large which shows very strong sensitivity of the offset on the quite small atomic displacements. The superlattice total energy is seen to show its minimum value for a particular configuration of atoms. The actual atomic displacements for the minimum energy configuration are depicted in Table 2.

The Zn atoms of the interface ZnS layer move away from the interface, whereas the interface S atoms move towards the interface. On the other hand, the interface Zn atoms of the ZnSe layer move towards the interface and the Se atoms away from the interface.

For the minimum energy configurations, we show the positions of the states at the valence

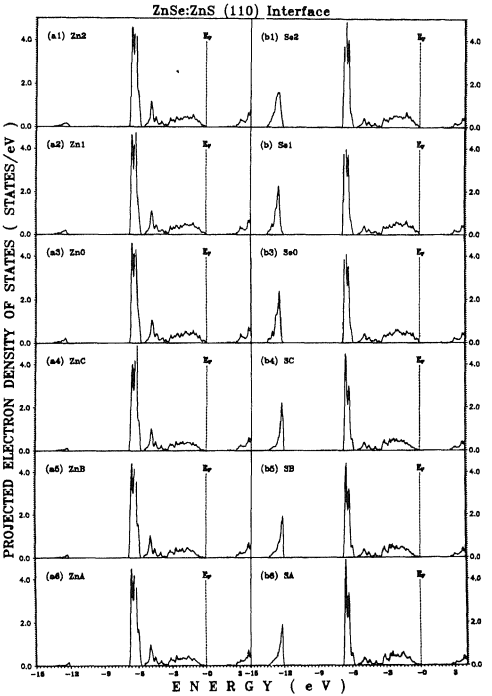

Fig. 3. Projected electron density of states (PDOS) for the cation Zn and anions S and Se lying in the three different ZnS and ZnSe layers for the ZnS/ZnSe(110) superlattice for the free-standing geometry without atomic relaxation. A, B and C for ZnS and 0, 1 and 2 for ZnSe denote, respectively, the middle layer, the next layer and the layer forming the interface.

Table 1
Valence band offsets for ZnS/ZnSe(110) superlattice in free-standing geometry

S. No	% Displacement of interface atoms[a]								$\Delta E_{av,v}$ (eV)	ΔE_v (eV)
	Out of the plane				Within the plane					
	ZnSe		ZnS		ZnSe		ZnS			
	Zn	Se	Zn	S	Zn	Se	Zn	S		
1.	0.00	0.00	0.00	0.00	0.00	0.00	0.00	0.00	0.09	0.017
2.	0.64	−0.33	0.73	−0.20	0.00	−0.20	0.67	0.00	0.22	0.150
3[b]	0.96	−0.50	1.10	−0.30	0.00	−0.30	1.01	0.00	0.27	0.198
4	1.92	−1.00	2.20	−0.59	0.00	−0.60	2.01	0.00	0.38	0.317

[a] In terms of bond length.
[b] For minimum energy configuration.

Table 2
Percent atomic displacements in the various layers for the minimum energy free-standing (5+5) ZnSe/ZnS(110) superlattice[a]

S. No.	Layers of	Atom	Atomic displacement[b]		
			X	Y	Z
1	ZnSe	Zn (0)	0.0000	0.0000	0.0000
2		Se (0)	0.0000	0.0000	0.0000
3		Zn (1)	0.00000	0.0000	0.0000
4		Se (1)	0.0000	0.0000	0.0000
5	Interface atoms	Zn (2)	0.0029	0.0029	0.0000
6		Se (2)	−0.0015	−0.0015	−0.0013
7		Zn (C)	0.0034	0.0034	0.0044
8		S (C)	−0.0009	−0.0009	0.0000
9	ZnS	Zn (B)	0.0000	0.0000	0.0000
10		S (B)	0.0000	0.0000	0.0000
11		Zn (A)	0.0000	0.0000	0.0000
12		S (A)	0.0000	0.0000	0.0000

[a] The labelling of layers is shown in Fig. 1.
[b] The atomic displacements are expressed in terms of the in-plane lattice constant ($a_{\parallel}$).

band maximum for ZnS and ZnSe on the two sides of the interfaces in the various geometries in Fig. 4. The value of the VBO in the equilibrium position of the relaxed atoms is 0.27 eV. This value is nearly half of the value of $\Delta E_{v,av}=0.52$ eV seen for the ZnS/ZnSe(100) superlattice. One may thus note a very strong sensitivity of the valence band offsets on very small relaxations of atoms in these superlattices. The maximum atomic displacements in the equilibrium configuration are less than 1.1% of the bond length.

3.1.3. Interface states

The interface states have been obtained for the minimum energy strained ZnS/ZnSe superlattice with atomic relaxation. For a magnitude probability of eigen vector equal to 0.09 or more on the interface layer and for a decay factor of 0.20, i.e., the states for which the probability of one type of atom decrease by 20% or more as one move away from the interface, are shown in Fig. 5. The planer Brillouin zone for the (110) interface is shown as inset in Fig. 5. The symmetric points are $\Gamma(0,0,0)$, $X(0.5,-0.5,0)$, $X'(0.5,0.5,0)$ and $M(0.5,-0.5,0.5)$ and all of them lie in the k-plane parallel to the interface (110). The interface states arising from all the four types of atoms are shown in this figure, where we have also included the band structures for the pure ZnS and ZnSe superlattices. The dispersion curves for ZnS and ZnSe are shown as crosses and open circle, respectively, whereas the interface states are shown by the big solid circles. These states may be characterized as localized or resonance states depending on their location with respect to the bulk bands of ZnS and ZnSe. Most of the states are bulk like in one of the host compounds, but die out when they cross the interface and enter the other host lattice.

It is significant to note that no interface states appears in the energy gap common to the constituent host lattices, a finding obtained much earlier

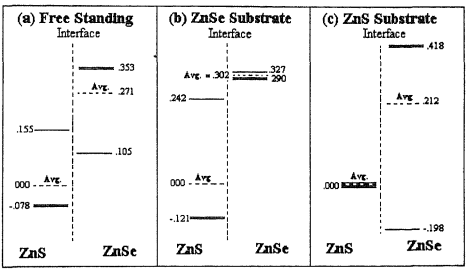

Fig 4. Valence band states and their averaged ones on the two sides of the ZnS/ZnSe(110) interface with atomic relaxation for minimum energy configurations for (a) the free-standing geometry, (b) ZnSe as substrate and (c) ZnS as substrate.

[29] by one of the authors (Agrawal) after performing a simple calculation using the cluster Bethe lattice.

In order to see the behaviour of the wave functions of the interface states, we investigate the magnitudes of various orbitals associated with the interface states in these different energy regions. Interface s–p states appear just below the top of the valence band of the ZnS/ZnSe superlattice, decaying into both the ZnS and ZnSe layers. Interface resonance states are observed in the neighbourhood of the valence band edge right up to -6.5 eV. The interface states and the bulk Zns and ZnSe states are too crowded to give any clear picture in the energy range -5.5 to -6.9 eV. The interface states lying in the energy region -13.5 to -12.0 eV originate from the s-states of Se and S.

Almost all the interface states decay on both sides of the interface. As typical cases, we depict the variation of the probability of all the eigenvectors for some interface states on different types of atoms lying on the various layers for free-standing geometry without atomic relaxation in Fig. 6. In the low energy region around -13.0 eV, interface states ($E=-13.27$ eV) which reside mainly on Se and S atoms show a decaying behaviour on both sides of the interface. For the interface states lying just below the top of the valence band ($E=-0.224$ eV), the contributions of the states are seen both on the cation Zn and anion Se, S atoms. In the conduction band region ($E=2.69$ eV), the eigenvectors have dominant contributions on the Zn atoms.

The above calculation for the interface states has been performed without considering atomic relaxation arising from the formation of the interface. Inclusion of the atomic relaxation by different overall magnitudes shift the location of these interface states. It results in the high sensitivity of the values of the valence offsets on the magnitudes of the atomic displacements in the interfacial region.

3.2. ZnSe substrate ZnS/ZnSe(110) superlattice

For this superlattice, the ZnS compound is assumed to be deposited on the ZnSe substrate so that the value of the lattice constant parallel to the interface is equal to that of the host ZnSe, i.e., $a_{\parallel}=5.59$ Å. The two separate calculations for finding the energy minimum of the ten-layer unit cell give the interlayer spacing as $0.2400\sqrt{2}$ and $0.2275\sqrt{2}$ (in the units of $a_{\parallel}$) for ZnSe and ZnS, respectively. A value of 0.24 smaller than the

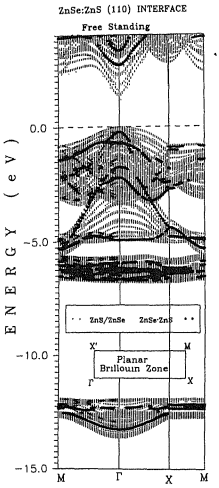

Fig 5 Band structure for bulk ZnS and ZnSe along with interface states of the ZnSe/ZnS(110) superlattice in free-standing geometry with atomic relaxation in the minimum energy configuration.

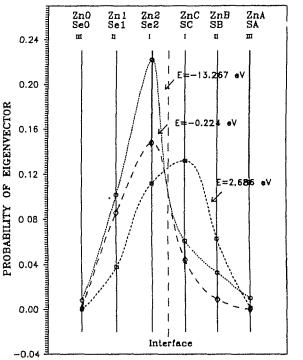

Fig. 6. Variation of probability of all the eigen vectors on atoms lying on the various layers of the ZnSe/ZnS interface in free-standing geometry without atomic relaxation. The indexes 'C' and '2' denote the atoms of the layers forming the interface.

experimental value of 0.25 for the interlayer spacing in ZnSe is the result of the occurrence of the energy minimum for the bulk ZnSe at somewhat smaller lattice volume. The separation between the two layers forming the interface is chosen as an average of the interlayer separations of the two constituent layer sets and is equal to $0.234\sqrt{2}$.

Self-consistent calculations reveal that the forces on the atoms are quite similar to those seen for the free-standing geometry, both qualitatively and quantitatively. Similar to the free-standing case, the atoms are relaxed in the direction of the forces experienced by them and self-consistent calculations were performed.

The calculated values of the VBOs are presented in Table 3. In general, the magnitudes of $\Delta E_{v,av}$ are greater than those for ΔE_v and are quite non-linear, similar to the free-standing geometry. A perusal of Table 3 shows that for the two cases, i.e., for no atomic relaxation and for very small atomic relaxation, E_v is negative which means that the split state(s) at the top of the valence band of ZnS is lying higher than that of ZnSe. The variation in the values of VBOs is quite large and is strongly sensitive to the atomic displacements.

The total energy is minimum again for about a maximum displacement of 1.83% of atoms lying at the interface. The valence band offset for the minimum configuration is 0.302 eV, as depicted in Table 3. The values of the VBOs are slightly higher than those seen for the free-standing geometry.

Table 3
Valence band offsets for ZnS/ZnSe(110) superlattice having ZnSe as substrate

S. No.	% Displacement of interface atoms[a]								$\Delta E_{av,v}$ (eV)	ΔE_v (eV)
	Out of the plane				Within the plane					
	ZnSe		ZnS		ZnSe		ZnS			
	Zn	Se	Zn	S	Zn	Se	Zn	S		
1.	0.00	0.00	0.00	0.00	0.00	0.00	0.00	0.00	0.075	−0.141
2.	0 71	−0.19	0.76	−0.12	−0.20	−0.91	0.32	−0 27	0.199	−0.018
3.[b]	1.41	−0.37	1.53	−0.25	−0 40	−1.83	0.64	−0.55	0 302	0.086
4.	2.12	−0.56	2.29	−0.37	−0.59	−2.74	0.96	−0.82	0.428	0.211

[a] In terms of bond length.
[b] For minimum energy configuration.

3.3. ZnS substrate ZnS/ZnSe(110) superlattice

For the deposition of the ZnSe (strained) on the ZnS substrate (unstrained) $a_{\parallel}=5.34$ Å. The interlayer spacing in minimum energy configuration is equal to $0.25\sqrt{2}$ for the ZnS layers and 0.265 for the ZnSe layers in terms of the planar lattice constant $a_{\parallel}=5.34$ Å.

The calculated values of VBOs are included in Table 4. In contrast to other geometries, the values for $\Delta E_{v,av}$ are now smaller than the corresponding ΔE_v. The energy of the superlattice supercell seems to be minimum for a smaller atomic relaxation of interface atoms, i.e., about half as compared to other geometries and the value of the band offset $\Delta E_{v,av}$ is equal to 0.21 eV, which is lower compared with the other geometries.

We make a comparison of our results with those obtained by Christensen et al. [16,17], who have made calculations only for the ZnSe substrate and ZnS substrate geometries using Keating model. For ZnSe substrate, our value for $\Delta E_{av,v}=0.302$ obtained for the minimum energy configuration is quite near to their value of 0.32 eV. However, our value of band offset for the top valence state ΔE_v (=0.086 eV) is much lower than their value of 0.30 eV. For the ZnS substrate geometry our calculated value of 0.21 eV for the energy minimized configuration is slightly higher than their value of 0.19 eV. The values for ΔE_v are 0.46 eV and 0.54 eV in our calculations and theirs, respectively.

The values of the valence band offsets calculated for the ZnS/ZnSe(110) and ZnS/ZnSe(001) superlattices in various geometries are seen to be

Table 4
Valence band offsets for ZnS/ZnSe(110) superlattice having ZnS as substrate

S No.	% Displacement of interface atoms[a]								$\Delta E_{av,v}$ (eV)	ΔE_v (eV)
	Out of the plane				Within the plane					
	ZnSe		ZnS		ZnSe		ZnS			
	Zn	Se	Zn	S	Zn	Se	Zn	S		
1.	0.00	0.00	0.00	0.00	0.00	0.00	0.00	0.00	0.17	0.38
2.[b]	−0.39	0.34	−0.43	0.10	0.14	0.00	1.06	0.00	0.21	0.42
3.	−0.78	0.69	−0.85	0.20	0.28	0.00	2.13	0.00	0.26	0.46
4.	−1.18	1.03	−1.27	0.30	0.42	0.00	3.19	0.00	0.31	0.51

[a] In terms of bond length.
[b] For minimum energy configuration.

different. The ZnS bond lengths vary in the various geometries. The values of the band offsets increases with the planar lattice constant of the various geometries, as has been observed earlier [13] for the (001) heterojunctions. For the (110) interfaces, the ZnS bond lengths are nearly equal to 2.42 Å, whereas for (100) interface, this bond length is about 2.31 Å. One thus observes that the valence band offset increases with the shortening of ZnS bond length. The same is true for the different geometries of the ZnS/ZnSe(100) interface, where the band offset increases with decrease in the bond length of ZnS lying at the interface. In the above calculation, spin–orbit effects have not been included. The contribution of this effect will not be more than 0.1 eV.

4. Conclusions

Our results show that the model theories used for estimating the values of the valence offsets are expected to be inadequate, as they are based on the use of the bulk-like properties of the constituent compounds forming the interface. The presence of interface states is an extra feature in the physical properties of the heterojunction. Further, the strong sensitivity of the valence band offsets on the small atomic displacements seen earlier for the ZnS/ZnSe (001) interface is also true for the presently discussed ZnS/ZnSe(110) interface. The valence band offset increases with the planer lattice constant in the various geometries of the (110) and (001) quantum wells.

Acknowledgements

The work is financially supported by University Grant Commission, New Delhi and Department of Science and Technology, New Delhi.

References

[1] C. Tejedor, F. Flores, E. Louis, J. Phys. C 10 (1977) 2163.
[2] C. Tejedor, F. Flores, E. Louis, J. Phys. C 12 (1979) 731.
[3] J. Tersoff, Phys. Rev. Lett. 52 (1984) 465.
[4] J. Tersoff, Phys. Rev. B 30 (1984) 4874.
[5] M. Cardona, N.E. Christensen, Phys. Rev. B 31 (1985) 879.
[6] S.H. Wei, A. Zunger, Phys. Rev. Lett. 59 (1987) 144.
[7] M. Jaros, A. Zoryk, D Ninno, Phys. Rev. B 35 (1987) 8277.
[8] C.G. Van de Walle, R.M. Martin, J. Vac. Sci. Technol. B 4 (1986) 1055.
[9] C.G. Van de Walle, R.M. Martin, Phys. Rev. B 34 (1986) 5621.
[10] C.G. Van de Walle, R.M. Martin, Phys. Rev. B 35 (1987) 8154.
[11] T. Yokagawa, M. Ogura, T. Kajiwara, Appl. Phys. Lett. 49 (1986) 1702.
[12] K. Shahzad, D.J. Olego, C.G. Van de Walle, Phys. Rev. B 38 (1988) 1417.
[13] M. Methfessel, B.K. Agrawal, M. Scheffler, unpublished, 1990.
[14] W.G. Wilke, K. Horn, J. Vac. Sci. Technol. B 6 (1988) 1211.
[15] W R.L. Lambrecht, B Segall, O.K. Anderson, Phys. Rev. B 41 (1990) 2813, 2832.
[16] N.E. Christensen, Phys. Rev. B 37 (1988) 4528.
[17] N.E. Christensen, I. Gorczyca, Phys. Rev. B 44 (1991) 1707.
[18] S. Wei, A. Zunger, J. Appl. Phys. 78 (1995) 3846.
[19] M. Methfessel, Phys. Rev. B 38 (1988) 1556.
[20] M. Methfessel, C.O. Rodriguez, O.K. Anderson, Phys. Rev. B 40 (1989) 2009.
[21] B.K. Agrawal, S. Agrawal, Phys. Rev. B 45 (1992) 8321.
[22] B.K. Agrawal, S. Agrawal, P.S. Yadav, S. Kumar, J. Phys.: Condens. Matter 9 (1997) 1763.
[23] B.K. Agrawal, S. Agrawal, Phys. Rev. B 52 (1995) 12556
[24] B.K. Agrawal, S. Agrawal, Physica C 233 (1994) 8
[25] B.K. Agrawal, S. Agrawal, Physica C 234 (1994) 29.
[26] National Conference on Advances in Condensed Matter Physics, Pondicherry, 1998.
[27] L. Hedin, B. Lundqvist, J. Phys. C: Solid State Phys. 6 (1994) 8781.
[28] B.K. Agrawal, P.S. Yadav, S. Agrawal, Phys. Rev. B 50 (1994) 14881.
[29] B.K. Agrawal, Phys. Rev. B 23 (1981) 2995.